Dissertation zur Erlangung des Doktorgrades
der Fakultät für Chemie und Pharmazie
der Ludwig-Maximilians-Universität München

Targeting the ER-Mitochondrial Interface of Cell Death Sensitizes Leukemia Cells Towards Cytostatics

Fabian Koczian
(geb. Bischoff)

aus
Dinkelsbühl, Deutschland

2017

Erklärung

Diese Dissertation wurde im Sinne von § 7 der Promotionsordnung vom 28. November 2011 von Frau Prof. Dr. Angelika M. Vollmar betreut.

Eidesstattliche Versicherung

Diese Dissertation wurde eigenständig und ohne unerlaubte Hilfe erarbeitet.

München, den 13. Juni 2017

_____

Fabian Koczian

Dissertation eingereicht am:	24.04.2017
1. Gutachterin:	Prof. Dr. Angelika M. Vollmar
2. Gutachterin:	Prof. Dr. Irmela Jeremias
Mündliche Prüfung am:	01.06.2017

Projects at a glance

Main project: PS89 – Chapter 1-4

Targeting the ER-Mitochondrial Interface of Cell Death Sensitizes Leukemia Cells Towards Cytostatics

Combination chemotherapy has proved to be a favorable strategy to treat acute leukemias. However, the integration of novel pharmaceutical approaches remains challenging and is associated with a lack of understanding the mechanistic background of successful combination therapies. In the present study, we demonstrate a highly increased response of various acute leukemia cell lines, drug resistant cells and patient derived xenograft (PDX) cells combining cytostatics with the recently introduced protein disulfide isomerase (PDI) inhibitor PS89. In order to elucidate the source of the robust antileukemic effects, we applied activity-based protein profiling. This screening revealed a polypharmacological character of PS89 targeting a network of endoplasmic reticulum (ER) homeostasis proteins. In combination with cytostatics, we show that the strong apoptosis induction is orchestrated by the direct PS89 target B-cell receptor-associated protein 31 (BAP31) which transduces apoptosis signals at the ER-mitochondrial interface. The activation of caspase-8 and cleavage of BAP31 precede a pro-apoptotic crosstalk including ER calcium and reactive oxygen species (ROS) resulting in stimulation of the intrinsic apoptosis pathway. Achieving to tune these amplification loops imparts PS89 the unique ability to sensitize acute leukemia cells at subtoxic concentrations. This uncovers that the ER-mitochondrial 'social network of cell death' can be exploited for synergistic drug combinations.

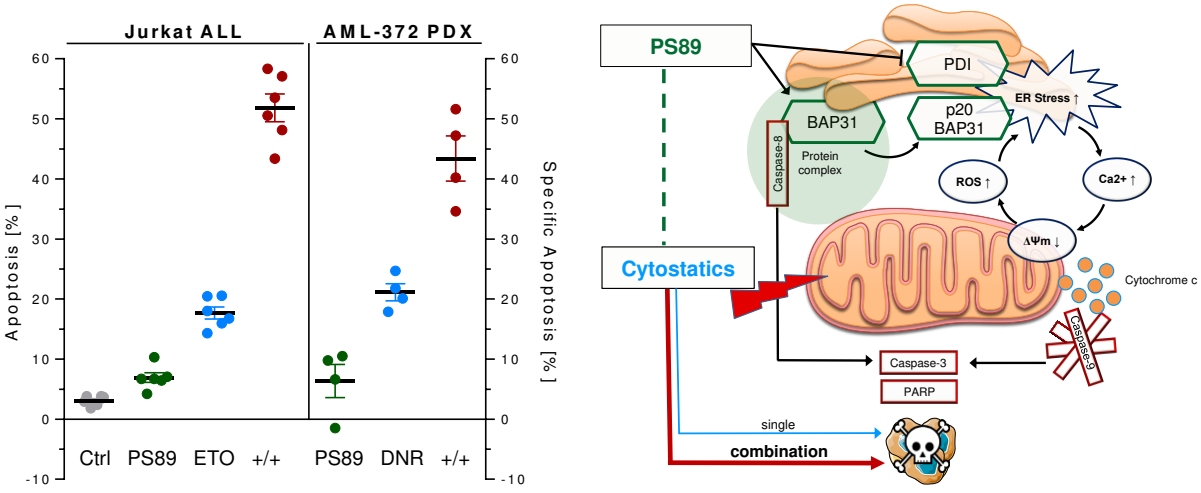

Side project: Vioprolide A – Chapter 5

Anticancer Effects and Transcriptomic Regulation by the Myxobacterial Compound Vioprolide A

Vioprolide A (VioA) is a highly active cyclic peptide isolated from the myxobacterium *Cystobacter violaceus* and was first published in the 1990s. However, it seemed to fall into oblivion as no pharmaceutical studies have been published since then. Here, we point out that VioA deserves much closer attention as low nanomolar concentrations of the compound were able to induce strong apoptotic effects in Jurkat leukemia cells while peripheral bone mononuclear cells (PBMCs) of healthy donors remained unaffected. The versatility of VioA was further demonstrated by an inhibition of proliferation, colony formation as well as migration of T24 bladder carcinoma cells. Moreover, the study outlines pioneer work in VioA signaling with the presentation of a transcriptome screening by massive analysis of cDNA ends (MACE). Both the strong anticancer effects and the initial findings on the transcriptional regulation mediated by VioA finally encourage the exploitation and further development of this exceptionally potent natural compound for chemotherapy.

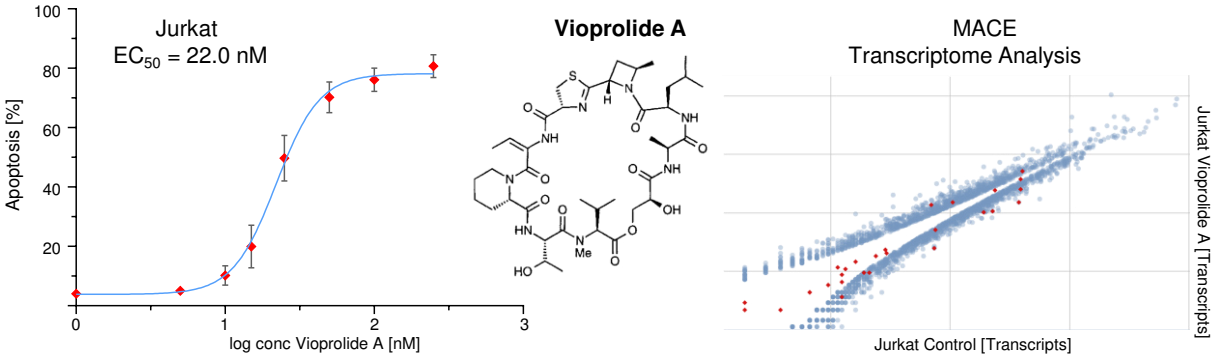

Contribution: P8-D6 – Chapter 6

Antileukemic effects of the dual topoisomerase inhibitor P8-D6

Interference with topoisomerases is an effective strategy for cancer therapy. At the University of Kiel, C. Meier *et al* recently synthesized analogs of naturally occurring benzo[*c*]phenanthridines revealing P8-D6 which is a powerful inducer of apoptosis. This is caused by an equipotent inhibition of topoisomerase I and II activities. In contribution to this project, we highlight the synergistic interaction of P8-D6 with PS89 and its strong antileukemic effects associated with G2 cell cycle arrest and DNA damage in Jurkat cells.

1 Introduction

1.1 Acute Leukemia: Disease and Therapy

1.1.1 Epidemiology and pathobiology

Leukemia is a heterogeneous group of hematologic malignancies characterized by an uncontrolled accumulation of immature white blood cells termed blasts or leukemia cells.[1] In contrast to chronic forms which may persist for years without major signs, acute leukemia progresses rapidly without therapeutic intervention. As functionless blasts displace the normal bone marrow cells, patients develop symptoms such as easy bleeding and fatigue caused by platelet deficiency and anemia. Furthermore, they suffer from a higher susceptibility to infections as a consequence of an inadequate white cell count.[2] The malignant transformation can affect lymphoid and myeloid progenitor cells which defines the main types acute lymphoblastic leukemia (ALL) and acute myeloid leukemia (AML). Both feature distinct disease characteristics and thus require specialized therapeutic management.

ALL is the most common childhood cancer.[3] Based on the US population, the median age at diagnosis is 15 years. Though, the incidence among 1- to 4-years-olds is nearly eight times higher than for young adults 20-24 years and four times higher than for elderly persons 80-84 years.[4] The improved survival of pediatric ALL patients is one of the success stories of cancer research with a 5-year survival rate increasing from 57% (diagnosis 1975-1979) to 90% (diagnosis 2003-2009).[3] However, the percentage of all patients surviving 5 years is 68.1% (Figure 1a) which indicates that a medical need persists especially for adult and relapsed ALL patients.[5] The initial pathogenic events leading to ALL are largely unknown, though several genetic lesions have been identified that favor an unlimited self-renewal capacity and excessive proliferation. For example, over 50% of T-cell ALLs feature activating mutations in the *NOTCH1* gene which encodes a transmembrane receptor that causes oncogenic signaling.[6] Another frequent characteristic of ALL are chromosomal translocations such as *TEL-AML1*, which is the most frequent translocation in childhood B-cell precursor ALL and may serve as a first-hit mutation providing altered self-renewal and survival properties.[7] Though large sets

of data have been generated to date, the challenge persists to translate an increasing understanding of the pathobiology into effective therapies.

In a similar way, this challenge accounts for AML. The evaluation of disease-related factors such as genetic markers is an active field of research and a number of mutations have demonstrated a prognostic value. These include the *NPM1* gene, which is the most frequent mutation in AML, and *FLT3* internal tandem duplications (ITDs) that activate receptor tyrosine kinase signaling.[8] Besides, patient-associated factors including age and comorbidities are predictive for survival. The median age at diagnosis is 67 years and incidence rates have increased since the early 1990s, a trend that will likely continue in ageing societies (Figure 1b, 3.3 cases/100.000 in 1992 vs 4.3/100.000 in 2013). Although long-term survival has improved for younger AML patients,[9] there has been little progress for patients aged >60 years who represent the bulk of AML cases. Thus, today's percentage of all patients surviving 5 years remains low at 26.6% (Figure 1b).

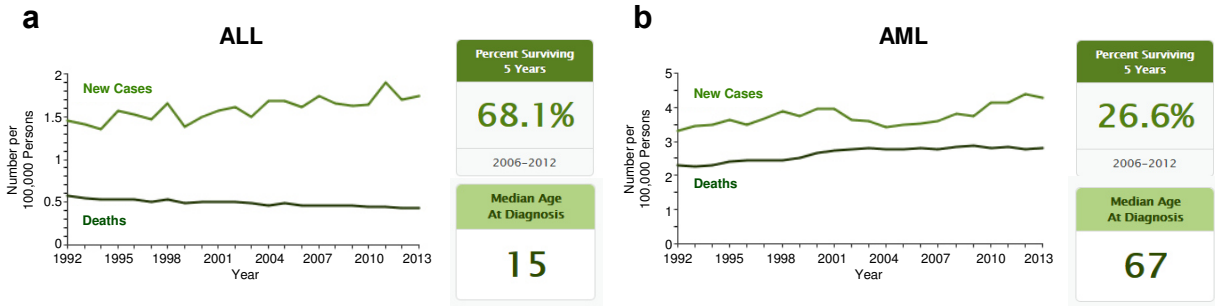

Figure 1 | ALL and AML statistical facts based on the US population. Percentage of new cases and deaths per 100.000 persons over time, 5-year survival of patients diagnosed 2006-2012 and median age at diagnosis (2009-2013). (**a**) ALL and (**b**) AML. Source: SEER Cancer Statistics Review 1975-2013.[4]

1.1.2 Chemotherapy and associated challenges

Five decades after the successful implementation and systematic clinical documentation of drug treatment in acute leukemia,[10] combination chemotherapy has proved to be a favorable strategy in both ALL and AML. Attributed to the fast progression of the disease, immediate induction chemotherapy is essential to reduce the burden of blasts in the bone marrow <5% (complete remission). Commonly, this is followed by a consolidation and / or maintenance phase in order to eradicate remaining leukemia cells and prevent relapse.[8, 11]

In ALL, induction therapy utilizes an arsenal of chemotherapeutic drugs which are adjusted based on the patient's prognostic factors. It includes amongst others the tubulin binder vincristine (VCR), topoisomerase inhibitors such as daunorubicin (DNR) and etoposide (ETO), corticosteroids and the alkylating agent cyclophosphamide.[11, 12] In addition, patients with Philadelphia chromosome positive ALL profit from tyrosine kinase inhibitors such as imatinib.

Similarly, targeted approaches are underway for different types of AML, for example the multi-target protein kinase inhibitor midostaurin for patients with FLT3 mutated AML. This compound is currently investigated in a phase III trial and shows to prolong survival in combination with cytarabine (Ara-C) and DNR,[13, 14] which have remained the primary drugs of AML induction therapy to date. Provided that an intensive chemotherapy is possible, patients commonly receive the so-called 7+3 regimen meaning seven days of Ara-C with three days of an anthracycline. With this strategy, complete remission is achieved in 60-80% of younger adults and in 40-60% of >60 year old patients.[15]

However, the situation persists unsatisfactory especially for patients who relapse or are unable to receive intensive chemotherapy and therefore face very limited options.[15] Besides, chemotherapy regimens of both ALL and AML are accompanied by severe side effects. This toxicity issue is further challenged by the development of leukemic cell resistances that have been demonstrated for several cytostatics including tubulin binders and topoisomerase inhibitors.[16, 17] Thus, there remains a strong need for novel pharmaceutical strategies which will be of great value if they achieve an improvement in the balance of tolerable dosing versus effective cytotoxicity in combination with current standard therapy.[18, 19]

1.2 Targeting ER Homeostasis: a Source for Novel Anticancer Drugs

1.2.1 ER stress and unfolded protein response

As accumulating evidence attributed a pro-tumorigenic role to processes within the endoplasmic reticulum (ER), it yielded increasing attention in the search for novel tumor targets.[20] The ER is the central organelle for calcium storage, protein folding and

maturation. However, multiple stimuli and pathological conditions can alter ER function leading to an imbalance between ER protein load and folding capacity known as ER stress.[21] Aiming to reduce the accumulation of unfolded proteins and restore ER homeostasis, a series of compensatory mechanisms is initiated which constitutes the unfolded protein response (UPR).[22] The master regulator of the UPR is the ER chaperone BIP which is titrated away from the luminal domains of the three sensors IRE1α, ATF6α and PERK by misfolded proteins (Figure 2, left). The following signaling pathways are thoroughly summarized in Figure 2 and commonly aim to stimulate protein folding and attenuate protein synthesis during ER stress conditions. The UPR thus exhibits a cytoprotective function which is physiologically induced as an adaptive response, though frequently activated in cancer cells.[23] However, prolonged and severe UPR activation resulting from unresolved ER stress may lead to apoptotic cell death (Figure 2) and therefore provides an opportunity for pharmaceutical intervention.

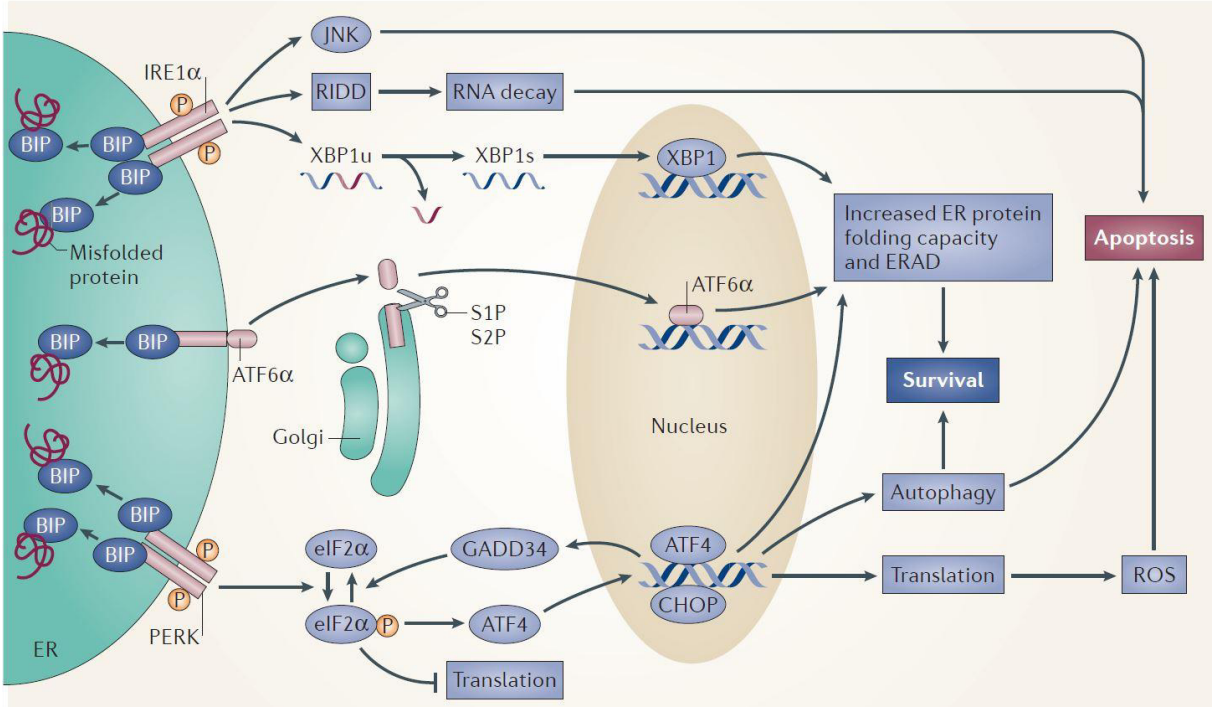

Figure 2 | The unfolded protein response (UPR) signaling pathways. Upon ER stress, unfolded and misfolded proteins bind and sequester immunoglobulin heavy-chain binding protein (BIP), thereby activating the UPR. The UPR comprises 3 parallel signaling branches: PRKR-like ER kinase (PERK)–eukaryotic translation initiation factor 2α (eIF2α), inositol-requiring protein 1α (IRE1α)–X-box binding protein 1 (XBP1) and activating transcription factor 6α (ATF6α). The outcome of UPR activation increases protein folding, transport and ER-associated protein degradation (ERAD), while attenuating protein synthesis. If protein misfolding is not resolved, cells enter apoptosis. CHOP, C/EBP homologous protein; GADD34, growth arrest and DNA damage-inducible protein 34; JNK, JUN N-terminal kinase; P, phosphorylation; RIDD, regulated IRE1-dependent decay; ROS, reactive oxygen species; S1/2P, Site-1/2 protease; XBP1s, transcriptionally active XBP1; XBP1u, unspliced XBP1. Figure and legend adapted from M Wang and RJ Kaufman.[23]

1.2.2 ER-mitochondrial crosstalk in apoptosis signaling

The switch from adaptive to fatal UPR likely depends on the intensity and duration of ER stress, though the underlying mechanisms are incompletely understood.[22, 23] However, an increasing number of studies recently indicated that the communication of ER stress and mitochondrial apoptosis has an essential role for cell fate decision.[24-27] In this conception, bidirectional signaling loops finally result in a significant amplification and are the key to exceed the critical point of no return for apoptosis induction. Besides the pro-apoptotic transcription factor CHOP, ER calcium and mitochondrial ROS, the B-cell receptor-associated protein 31 (BAP31) has been identified as a key communicator in this so-called 'social network of cell death'.[25, 27] BAP31 functions as an ER protein sorting factor in its native state,[28] though has been identified to associate with the mitochondrial protein Fis1 upon apoptotic stimuli. So, this protein complex is able to bridge the ER-mitochondrial interface and serves as a platform for caspase-8 (CASP8) activation.[29] Active caspase-8 in turn is able to cleave BAP31 into p20BAP31 which promotes calcium release from the ER and apoptosis (Figure 3, caspase recognition sites D164 and D238 are outlined).[30, 31]

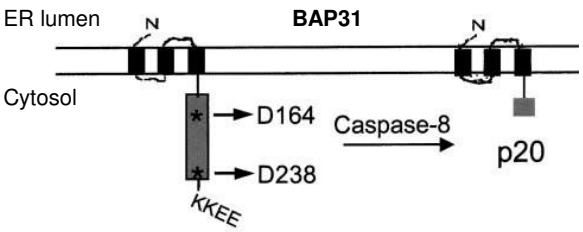

Figure 3 | Schematic representation of the B-cell receptor-associated protein 31 (BAP31). BAP31 contains three ER transmembrane domains and a cytosolic tail (caspase recognition sites are shown) with an ER retrieval sequence (KKEE). Cleavage of the cytosolic tail by caspase-8 leads to the pro-apoptotic p20BAP31 fragment. Figure adapted from Breckenridge *et al*.[31]

Interestingly, a recent report highlighted that BAP31 also transduces apoptotic signals from the ER to mitochondria under ER stress.[32] Consistently, the critical role of the CASP8-BAP31 axis has been demonstrated earlier in ER stress-triggered apoptosis of B-cell lymphocytic leukemia cells.[33] Thus, BAP31 appears to be an important mediator of pro-apoptotic ER stress signaling which finally raises the question if currently developed ER targeting drugs could make use of this route to switch the pro-survival mode of the UPR into apoptosis.

1.2.3 Advances in the development of ER interfering drugs

Motivated by the chance to reverse the UPR pro-survival effects as a novel pharmaceutical strategy, there has been progress in the development of ER interfering drugs in recent years.[20, 23] This was encouraged by the successful clinical application of the proteasome inhibitor bortezomib which functions as an ER stress inducer.[34] In addition, a phase I-II clinical trial lately suggested that childhood relapsed ALL patients profit from bortezomib in combination with chemotherapy.[35] Another promising compound class are inhibitors of the chaperone Heat-shock protein 90 (Hsp90) that are in clinical development against several malignancies including AML and have demonstrated to be a useful co-treatment as well.[36, 37] Finally, several anticancer approaches that directly target ER stress sensors are at preclinical stage, for example inhibitors of PRKR-like ER kinase (PERK) and inositol-requiring protein 1α (IRE1α).[22, 38, 39] Importantly, the key enzyme family for the maintenance of oxidative protein folding in the ER, namely protein disulfide isomerases (PDIs), have also been recognized as druggable targets for cancer therapy. Therefore, an increasing scientific interest evolved for a novel group of substances, the PDI inhibitors.

1.2.4 Therapeutic potential of protein disulfide isomerase inhibitors

The human PDI gene family contains 21 members which facilitate protein folding in the ER through the oxidation, reduction and isomerization of disulfide bonds.[40] Furthermore, several PDIs including the best studied isoform 1 (PDI, gene name *P4HB*) feature chaperone activity.[41] Hence, they are key regulators of ER homeostasis.

As proliferating cancer cells face environmental stress and a global increase in protein synthesis, PDIs are frequently overexpressed and support tumor survival.[20, 42] Though a systematic analysis in leukemia is missing, individual reports have discovered overexpression of several PDI isoforms associated with chemoresistance in ALL and AML cells.[43-45] In addition, a novel role of PDI was identified during the UPR in leukemic cells of AML patients by suppressing myeloid differentiation.[46] Therefore, PDIs became attractive targets in the context of solid tumors as well as hematologic malignancies.

In practice, the therapeutic potential of PDI targeting has been stressed with the introduction of novel inhibitors, the most promising being PACMA31 and CCF642.[47, 48] These compounds in fact showed a strong *in vitro* and *in vivo* activity against ovarian cancer and myeloma cells, respectively. However, their irreversible mode of action is in general pharmacologically less desired and their utility in combination with standard therapy remains obscure. Interesting issues in the development of alternative PDI inhibitors therefore concerned their binding mode as well as their impact in combinatory approaches. These points were particularly respected in the development of the novel PDI inhibitor PS89 and will be addressed in the following section.

1.3 Development and Characterization of PS89

1.3.1 Introduction of a novel compound class: the T8 family

As the starting point of the present study, a compound screening for the chemosensitization towards etoposide-induced cell death revealed the lead structure T8 which was able to induce synergistic apoptosis in various cell lines.[49] Aiming to explore the structure-activity relationship and to increase the potency of the compound, several T8-derviatives, named PS83-PS89, were prepared. Among these, PS89 demonstrated the best sensitizing activity and was therefore subjected to a closer mechanistic investigation.

1.3.2 Inhibition of protein disulfide isomerase

The discovery of the T8 class was accompanied by a proteomic analysis of cellular targets in MDA-MB-231 breast cancer cells which revealed PDI (gene name *P4HB*) as a main target protein. Further investigations demonstrated that especially PS89 was able to inhibit the reductase activity of recombinant PDI (IC_{50} 78 ± 17 µM) and molecular docking studies showed that PS89 binds in close proximity to the catalytic centers of PDI.[49] As illustrated in Figure 4, PS89 in fact shields the two active sites of PDI and their catalytically active cysteines which are responsible for the disulfide exchange reactions (left: active domain a', center: molecular structure of PS89, right: active domain a; cysteines are depicted by yellow dots).

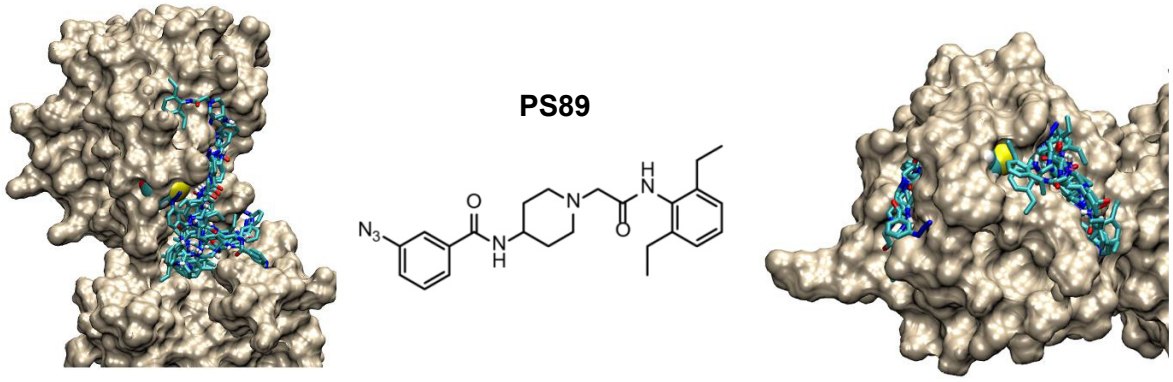

Figure 4 | Molecular docking of PS89 and protein disulfide isomerase (PDI). Collective view of the energetically best 10 structural clusters of PS89 around the catalytic sites of PDI. The active domains a' (left) and a (right) are shown and the catalytic cysteine residues are represented in yellow. Figure adapted from Eirich *et al*.[49]

1.3.3 Significance of PS89 and open issues

In contrast to most of the published PDI inhibitors, PS89 unifies a number of favorable pharmacologic characteristics: first, a suitable druglikeness with satisfaction of the Lipinski rule of five. Second, a reversible mode of action which is generally beneficial in terms of drug surveillance. And finally, an exceptional chemosensitizing character shown by the combination treatment with etoposide which resulted in a highly increased apoptotic response of Jurkat cells.

These suitable properties predestined PS89 not only for further combination therapy studies, but also for a deeper analysis of its interactive signaling. In particular, the last point raised the central question of the present study:

How does PS89 cooperate with cytostatics
to achieve synergistic apoptosis in leukemia cells?

1.4 Aims of the Study

The signaling underlying the chemosensitizing effects of PS89 was of special interest as there is a general agreement that combination therapies benefit from a certain form of crosstalk, but the mechanisms of interaction have only been explored for a few.[50] This coincides with the persisting challenge to integrate novel drugs into acute leukemia therapy. Thus, the agenda broadly aimed to improve the understanding of combination

therapy signaling and finally overcome the lack of response towards available cytostatics in acute leukemia.

The precise goals of the thesis can be summarized as follows:

1. Assessing the potential of PS89 combination therapies in acute leukemia cell lines, drug resistant and patient-derived xenograft (PDX) cells
2. Validating the impact of protein disulfide isomerase (PDI)
   a) as a single target and
   b) in relationship to further PS89 target proteins from a network perspective
3. Investigating the pro-apoptotic function of the novel PS89 target protein B-cell receptor-associated protein 31 (BAP31)
4. Elucidating the interactive apoptosis signaling between PS89 and cytostatics

2 Materials and Methods

2.1 Materials

2.1.1 Cells

2.1.1.1 Cell lines

Cell line	Supplier or academic partner
CCRF-CEM	M. Kavallaris, Sydney, Australia
HEK 293	DSMZ, Braunschweig, Germany
Hela	DSMZ, Braunschweig, Germany
HL-60	ATCC, Manassas, VA, USA
Jurkat WT	P. H. Krammer, Heidelberg, Germany
Jurkat/*neo*	P. H. Krammer, Heidelberg, Germany
Jurkat/*Bcl-2*	P. H. Krammer, Heidelberg, Germany
Jurkat/*Bcl-xL*	P. H. Krammer, Heidelberg, Germany
Jurkat CASP8 -/-	P. H. Krammer, Heidelberg, Germany
VCR-R CEM	M. Kavallaris, Sydney, Australia

Table 1 | List of cell lines

A verification of Jurkat wildtype cells was performed prior to start of the project at the German Collection of Microorganisms and Cell Cultures (DSMZ). Generation and characteristics of genetically modified Jurkat cells has been described previously.[51, 52] Acquirement and profile of vincristine resistance in CEM cells (VCR-R CEM) has been characterized by the group of M. Kavallaris.[53-55]

2.1.1.2 Patient derived xenograft cells

The model of acute leukemia patients' cells growing in mice has been described previously.[56, 57] Patient derived xenograft (PDX) cells were kindly provided by the group of Prof. Dr. Irmela Jeremias (Helmholtz Center, Munich, Germany) after isolation from the bone marrow or spleen of NSG mice. Characteristics of PDX cells used in the present study are summarized in Table 2.

Sample	Type	Subtype	Disease Stage	Sex	Age
ALL-168	ALL	Pre-B ALL	Initial diagnosis	Female	5
ALL-230	ALL	T ALL	Initial diagnosis	Male	4
AML-346	AML	M7	Relapse	Female	1
AML-372	AML	M0	Relapse	Male	42
AML-393	AML	M4	Relapse	Female	47
AML-491	AML	n/a	Relapse	Female	53

Table 2 | Samples and characteristics of patient derived xenograft (PDX) cells. ALL: Acute lymphoblastic leukemia, AML: Acute myeloid leukemia. Subtype classification ALL: according to type of lymphoblast (B cell or T cell) and immunophenotype. AML: according to type of myeloblast based on the French-American-British (FAB) system. n/a: not available.

2.1.1.3 Peripheral blood mononuclear cells

Peripheral blood mononuclear cells (PBMCs) were freshly isolated from blood of healthy donors by gradient centrifugation as described in section 2.3.

2.1.2 Compounds

The study compound PS89 as well as the PS89 photo probe (JP04-042) were synthesized and provided by Prof. Dr. Uli Kazmaier (Saarland University, Saarbrücken, Germany). The structures are shown in Figure 5 and chemical properties of the compound family have been characterized.[49]

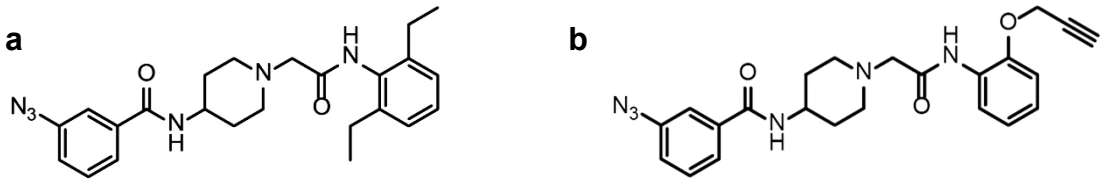

Figure 5 | Chemical structures of study compounds. (**a**) PS89 and (**b**) the PS89 photo probe (JP04-042) modified by an alkyne handle.

The cytostatics etoposide (ETO), daunorubicin (DNR) and vincristine (VCR) were obtained from Sigma Aldrich (St Louis, MO, USA). Cytarabine (Ara-C) was purchased from Merck (Darmstadt, Germany).

2.1.3 Antibodies

Primary antibody	Origin	Supplier
Actin Clone C4	Mouse	Millipore, Darmstadt, Germany
Alexa Fluor 488 IgG_{2b} κ Isotype Control	Mouse	BD, Franklin Lakes, NJ, USA
BAP31 C-15	Goat	Santa Cruz, Dallas, TX, USA

BAP31 B-10	Mouse	Santa Cruz, Dallas, TX, USA
BAP31 HPA003906	Rabbit	Sigma Aldrich, St Louis, MO, USA
Bcl-2 #2872	Rabbit	Cell Signaling, Danvers, MA, USA
Bcl-xL #2762	Rabbit	Cell Signaling, Danvers, MA, USA
Caspase-3, Active C8487	Rabbit	Sigma Aldrich, St Louis, MO, USA
Caspase-8 1C12	Mouse	Cell Signaling, Danvers, MA, USA
Cytochrome c #4272	Rabbit	Cell Signaling, Danvers, MA, USA
PARP #9542	Rabbit	Cell Signaling, Danvers, MA, USA
PE IgG_{2b} κ Isotype Control	Mouse	BD, Franklin Lakes, NJ, USA
PDI C81H6	Rabbit	Cell Signaling, Danvers, MA, USA
VDAC #4866	Rabbit	Cell Signaling, Danvers, MA, USA

Table 3 | List of primary antibodies

Secondary antibody	Origin	Supplier
Anti-goat IgG, HRP 705-035-147	Donkey	Dianova, Hamburg, Germany
Anti-mouse IgG, HRP 7076	Goat	Cell Signaling, Danvers, MA, USA
Anti-mouse IgG, IRDye 800CW	Goat	Li-Cor, Lincoln, NE, USA
Anti-rabbit Alexa 488 A11008	Goat	Thermo Fisher, Waltham, MA, USA
Anti-rabbit IgG, HRP 172-1019	Goat	Bio-Rad, Hercules, CA, USA

Table 4 | List of secondary antibodies

2.1.4 Small interfering RNAs

For gene silencing, ON-TARGETplus SMARTpool small interfering RNA (siRNA) reagents from GE Dharmacon (Lafayette, CO, USA) against human PDI (gene name *P4HB*) and BAP31 (gene name *BCAP31*) were used. ON-TARGETplus non-targeting control siRNA, designated as siCtrl, served as control to determine baseline cellular responses in RNA interference experiments. siRNAs were resuspended according to Dharmacon instructions in 1x siRNA buffer (diluted from Dharmacon 5x siRNA buffer in RNase-free water) to a stock concentration of 20 µM and stored at -20°C.

2.1.5 Plasmid encoding protein disulfide isomerase

Overexpression of PDI (gene name *P4HB*) was performed using pPDI vector kindly provided by W. Ou (Bethesda, MD, USA).[58] The non-coding plasmid pcDNA3.1 (Thermo Fisher, Waltham, MA, USA) served as empty vector control.

2.1.6 Chemicals and reagents

Reagent	Supplier
2,2,2-Trichloroethanol (TCE)	Sigma Aldrich, St Louis, MO, USA
5-TAMRA-Azide	Jena Bioscience, Jena, Germany
µMACS Protein G MicroBeads Kit	Miltenyi Biotech, Bergisch Gladbach, Germany
Ammonium persulfate (APS)	Sigma Aldrich, St Louis, MO, USA
BCA, Uptima BC Assay Kit	Interchim, Montlucon, France
Bovine serum albumin (BSA)	Sigma Aldrich, St Louis, MO, USA
Cal-520, AM	AAT Bioquest, Sunnyvale, CA, USA
Carboxy-H_2DCFDA	Thermo Fisher, Waltham, MA, USA
Cell-Titer Blue (CTB)	Promega, Madison, WI, USA
CompBeads Anti-mouse Ig, κ	BD, Franklin Lakes, NJ, USA
Complete	Roche Diagnostics, Basel, Switzerland
Coumaric acid	Fluka, Buchs, Switzerland
DMEM cell culture medium	PAN Biotech, Aidenbach, Germany
DMSO	AppliChem, Darmstadt, Germany
Fetal calf serum (FCS)	PAA Laboratories, Pasching, Austria
Ficoll-Paque PLUS	GE Healthcare, Chicago, IL, USA
FluorSave Reagent	Merck, Darmstadt, Germany
Formaldehyde 16%, ultrapure	Polysciences, Warrington, PA, USA
FuGene HD	Promega, Fitchburg, WI, USA
GenaxxoFect	Genaxxon, Ulm, Germany
Glycerol	AppliChem, Darmstadt, Germany
Glycine	AppliChem, Darmstadt, Germany
Hoechst 33342	Sigma Aldrich, St Louis, MO, USA
IMDM cell culture medium	Thermo Fisher Gibco, Waltham, MA, USA
JC-1	Enzo, Farmingdale, NY, USA
Luminol	AppliChem, Darmstadt, Germany
Methylcellulose	Sigma Aldrich, St Louis, MO, USA
MTT	Sigma Aldrich, St Louis, MO, USA
Na_2EDTA x 2 H_2O	Sigma Aldrich, St Louis, MO, USA
Na_2-β-glycerophosphate x 5 H_2O	Merck, Darmstadt, Germany
Na_3VO_4	ICN Biomedicals, Aurora, OH, USA
$Na_4P_2O_7$ x 10 H_2O	Sigma Aldrich, St Louis, MO, USA
NaF	Merck, Darmstadt, Germany
Nonfat powdered milk (Blotto)	Carl Roth, Karlsruhe, Germany

PageRuler protein ladder	Thermo Fisher, Waltham, MA, USA
Penicillin-Streptomycin	PAN Biotech, Aidenbach, Germany
PMSF	Sigma Aldrich, St Louis, MO, USA
Rotiphorese Gel 30	Carl Roth, Karlsruhe, Germany
Propidium iodide	Sigma Aldrich, St Louis, MO, USA
Pyronin Y	Sigma Aldrich, St Louis, MO, USA
Pyruvate	Merck, Darmstadt, Germany
Q-VD-OPh	Merck Millipore, Darmstadt, Germany
RPMI 1640 cell culture medium	PAN Biotech, Aidenbach, Germany
siRNA buffer (5x)	GE Dharmacon, Lafayette, CO, USA
Sodium dodecyl sulfate (SDS)	AppliChem, Darmstadt, Germany
TEMED	VWR, Radnor, PA, USA
Triton X-100	Merck, Darmstadt, Germany
Trypsin	PAN Biotech, Aidenbach, Germany
Tween 20	VWR, Radnor, PA, USA
YO-PRO-1	Thermo Fisher, Waltham, MA, USA
Z-IETD-FMK	R&D Systems, Minneapolis, MN, USA

Table 5 | List of dyes, inhibitors, kits and chemicals

All commonly used acids, bases, buffer salts and organic solvents were either purchased from Merck (Darmstadt, Germany) or Sigma-Aldrich (St Louis, MO, USA).

2.1.7 Technical equipment

Device	**Function**	**Manufacturer**
µMACS separator with µColumns	Immunoprecipitation	Miltenyi Biotech, Bergisch Gladbach, Germany
Amersham NC/PVDF (0.2 µM, 0.45 µM)	Blotting membrane	GE Healthcare, Chicago, IL, USA
ChemiDoc Touch	Immunoblot Imaging	Bio-Rad, Hercules, CA, USA
Cell culture flasks, tubes and plates	Disposable cell culture material	Nunc, Thermo Fisher, Waltham, MA, USA
Consort power supply E835	Electrophoresis	Sigma Aldrich, St Louis, MO, USA
Curix 60 with Super RX films	Film processor with X-ray films	Agfa, Cologne, Germany Fujifilm, Tokio, Japan
FACSCanto II	Flow cytometer	BD, Franklin Lakes, NJ, USA
HBT 130-2	Thermoblock	Haep Labor Consult, Bovenden, Germany
HeraCell	Incubator	Heraeus, Hanau, Germany
ibiTreat µ-slide	Microscopy 8-well slide	Ibidi, Planegg, Germany

LU105M camera	Digital camera	Lumenera, Ottawa, Canada
Mikro 22R	Microcentrifuge	Hettich, Tuttlingen, Germany
Mini Protean 3	Electrophoretic transfer	Bio-Rad, Hercules, CA, USA
Odyssey 2.1	Western blot fluorescence imaging	Licor, Lincoln, NE, USA
Olympus CK30	Inverted microscope	Olympus, Tokyo, Japan
Rotina 46R	Centrifuge	Hettich, Tuttlingen, Germany
Tecan Sunrise	Absorbance reader	Tecan, Männedorf, Switzerland
SP8 LSM system	Confocal microscope	Leica, Wetzlar, Germany
SpectraFluor Plus	Fluorescence reader	Tecan, Männedorf, Switzerland
ViCell XR	Cell viability analyzer	Beckman Coulter, Brea, CA, USA

Table 6 | Materials and devices for cell culture and analytics

2.1.8 Software

Software name and version	Supplier
FlowJo v7.6.5	Tree Star, Ashland, OR, USA
GraphPad Prism 7	GraphPad Software, San Diego, CA, USA
Image Lab v5.2	Bio-Rad, Hercules, CA, USA
Leica LAS X	Leica, Wetzlar, Germany
LuCam Capture v6.3.2	Lumenera, Ottawa, Canada
Microsoft Office 2010	Microsoft, Redmont, WA, USA
STRING v10	STRING Consortium, Zurich, Switzerland

Table 7 | Software tools for data interpretation

2.2 Cell Culture

2.2.1 Maintenance of cells

CEM cells were maintained in RPMI 1640 medium with 2 mM glutamine supplemented with 10% (v/v) heat-inactivated fetal calf serum (FCS) and a combination of 100 U/ml penicillin and 100 µg/ml streptomycin (Pen/Strep). Jurkat cells were cultivated in the same medium with additional 1 mM pyruvate. Jurkat medium with 20% FCS instead of 10% FCS was used to cultivate PBMCs and ALL PDX cells. AML PDX cells were maintained in DD medium (StemPro-34 SFM medium with nutrient supplement, Pen/Strep, L-glutamine, 2% (v/v) FCS, 10 ng/mL FLT3L, 10 ng/mL SCF, 10 ng/mL TPO, 10 ng/mL IL3) which was kindly provided by Prof. Dr. Irmela Jeremias (Helmholtz Center, Munich, Germany). HL-60 cells were cultured in IMDM medium supplemented

with 20% FCS and Pen/Strep. HEK293 and Hela cells were maintained in DMEM medium (2 mM glutamine, 4.5 g/l glucose) supplemented with 10% FCS and Pen/Strep.

Cells were cultivated in a humidified incubator at 37°C under a 5% CO_2 atmosphere and typically passaged three times per week. Suspension cell lines were maintained at a cell density between 0.1-1.0 x 10^6 cells/ml. Adherent cells were cultured as monolayers and passaged the latest by reaching 80-90% of confluence. Therefore, cells were rinsed twice with PBS and detached by trypsin/EDTA (Table 8). The enzymatic reaction was stopped by addition of complete growth medium. For all cell lines, the cell density was determined using the cell viability analyzer ViCell XR prior to seeding for experiments or further cultivation.

PBS (pH 7.4)	
NaCl	123.2 mM
Na_2HPO_4	10.4 mM
KH_2PO_4	3.2 mM
H_2O	

Trypsin/EDTA	
Trypsin	0.05% (w/v)
Na_2EDTA	0.02% (w/v)
PBS	

Table 8 | Buffers commonly applied in cell culture

2.2.2 Stimulation with test compounds

Suspension cells were seeded, unless otherwise stated, at 0.2 x 10^6 cells/ml and stimulated after 4 h incubation. HEK and Hela cells were allowed to adhere and therefore typically seeded the day before treatment. DMSO stock solutions of test compounds (PS89, cytostatics and inhibitors) were appropriately pre-diluted in growth medium, so the DMSO concentration did not exceed 0.5% (v/v) in all experiments.

2.2.3 Plasmid and siRNA transfection

For overexpression of PDI, 0.2 x 10^6 HEK cells were seeded per 6-well the day before transfection. The transfection complex was prepared according to manufacturer's instructions and contained 2 µg DNA (pPDI or empty vector pcDNA3.1) and 6 µl FuGene HD reagent per well.

For gene silencing, cells were transfected using the GenaxxoFect One-Step protocol. Representative for one 12-well, 2 µl GenaxxoFect and 1.25 µl siRNA (c = 20 µM) were each diluted in 80 µl of the supplied Dilution Buffer, mixed by rapid pipette action and

incubated for 20-30 min at RT. Cells were freshly detached (if applicable) and resuspended in antibiotic free medium (0.15 x 10^6 cells / ml), mixed gently with the transfection complexes (final V = 1 ml) and transferred to the culture plate. The siRNAs used for transfection experiments are listed in section 2.1.4.

2.2.4 Freezing and thawing of cells

For long-term storage, the cell density was adjusted to 2 x 10^6 cells/ml in growth medium supplemented with 20% FCS, Pen/Strep and 10% DMSO. Aliquots (V = 1.5 ml) were prepared in cryo vials and immediately frozen at -20°C for 24 h, temporary stored at -80°C and finally transferred to liquid nitrogen for long-term storage. For recultivation, frozen cells were thawed in a water bath at 37°C, transferred to 20 ml of growth medium and centrifuged. The DMSO-rich supernatant was discarded and the cell pellet resuspended in culture medium. Cells were subsequently expanded in a 25 cm^2 flask.

2.3 Isolation of Peripheral Blood Mononuclear Cells

Peripheral blood mononuclear cells (PBMCs) were isolated from EDTA-anticoagulated blood of healthy donors (final concentration Na_2EDTA x 2 H_2O 1.5 mg/ml blood) by gradient centrifugation using Ficoll-Paque PLUS according to manufacturer's instructions. Blood was mixed 1:1 (v/v) with balanced salt solution (BSS, Table 9), layered on top of the Ficoll reagent and centrifuged (45 min, 400 g, RT). Cells were collected from the PBMC layer (Figure 6, light grey layer) and washed with BSS (10 min, 100 g, RT) to remove platelets. Cells were finally resuspended in growth medium, seeded and stimulated as previously described (sections 2.2.1 and 2.2.2).

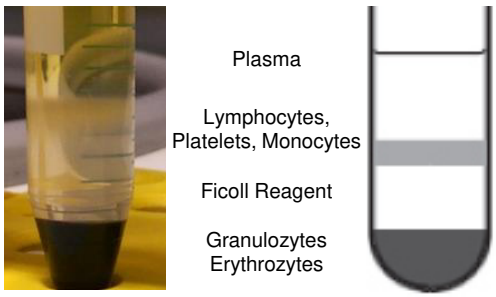

Figure 6 | Cell layers after Ficoll gradient centrifugation

BSS (pH 7.6)	
NaCl	126 mM
$CaCl_2$ x 2 H_20	0.005 mM
$MgCl_2$ x 6 H_20	0.098 mM
KCl	0.54 mM
Tris base	14.5 mM
D-glucose	0.01% (w/v)
H_2O	

Table 9 | Balanced salt solution (BSS)

2.4 Flow Cytometry

2.4.1 Apoptosis and cell cycle analysis

Apoptosis was determined by propidium iodide (PI) staining and flow cytometry according to Nicoletti et al.[59, 60] Therefore, cells were detached (if applicable), washed with ice cold PBS, permeabilized and stained with fluorochrome solution (Table 10). After 30 min incubation at 4°C in the dark, cells were analyzed on a BD FACSCanto II. 10.000 events were measured per sample at Ex 488 nm and Em 585/42 nm. Cell cycle analysis and percentage of apoptotic cells, represented by the subG1 population featuring fragmented or loss of DNA, were determined with FlowJo software.

Fluorochrome solution	
Propidium iodide	50 µg/ml
Sodium citrate	0.1% (w/v)
Triton X-100	0.1% (v/v)
PBS	

Table 10 | Fluorochrome solution

Exceptionally, apoptosis of daunorubicin treated HL-60 cells was determined by YO-PRO-1 nucleic acid stain which selectively passes through the plasma membranes of apoptotic cells. Cells were washed with PBS, stained with YO-PRO-1 solution (c = 1 µM in PBS) and directly analyzed on a BD FACSCanto II (Ex 488 nM, Em 530/30 nm). Apoptotic cells featured high YO-PRO-1 fluorescence and were quantified with FlowJo software.

2.4.2 Cell death of PDX cells and PBMCs

PDX cells and PBMCs were harvested after 48 h or 72 h stimulation, washed with PBS (RT) and finally resuspended in 250 µl PBS. Cells were immediately analyzed on a FACSCanto II and the percentage of viable or apoptotic cells, respectively, was determined by forward/side scatter (FSC/SSC) gating as described.[61] Exemplarily, FSC/SSC dot plots of control versus daunorubicin treated AML-372 PDX cells and PBMCs are shown in Figure 7. Specific apoptosis of gate B populations, as depicted in Figure 7, was calculated according to the following formula:

$$Specific\ \ apoptosis\,[\%] = \frac{Gate\ B\ Treated\ \ [\%] - Gate\ B\ DMSO\ \ [\%]}{100\,\% - Gate\ B\ DMSO\ \ [\%]}$$

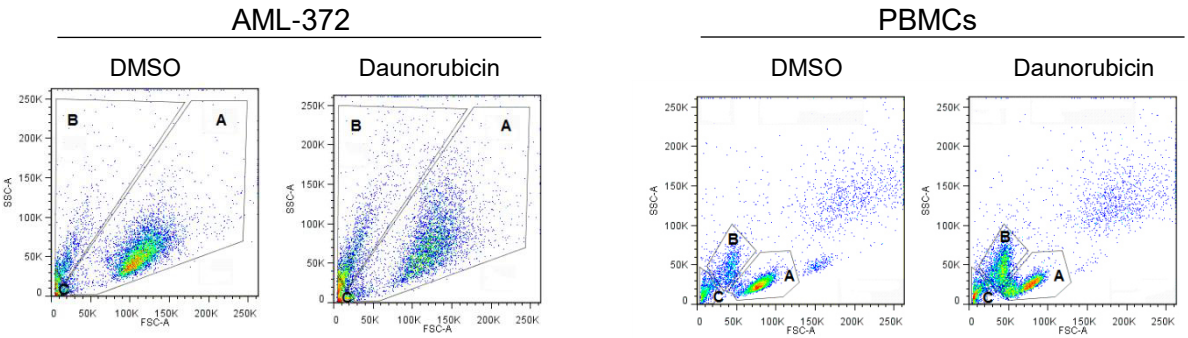

Figure 7 | Determination of viable and apoptotic cells in PDX and PBMC samples. Representative FSC/SSC dot plots of AML-372 and PBMC samples treated with daunorubicin versus DMSO control. Gate **A**: viable myeloblasts (AML-372) or lymphocytes (PBMCs), Gate **B**: apoptotic cells, Gate **C**: debris.

2.4.3 Cytosolic calcium

Cytosolic calcium levels were determined by loading the stimulated cell suspension with the calcium indicator Cal-520 AM.[62] Cells were incubated with 1 µM Cal-520 AM for 90 min at 37°C and 30 min at RT, then centrifuged (5 min, 400 g, RT), washed with Hanks and Hepes Buffer (HHBS, Table 11) to remove excess dye and resuspended in HHBS. The fluorescence intensity was analyzed on a FACSCanto II at Ex 488 nm and Em 530/30 nm. For quantification, debris was excluded and intracellular calcium levels were determined as the FITC-A median normalized to DMSO control.

HHBS (pH 7.2)			
$CaCl_2$	1.26 mM	$MgCl_2$ x 6 H_2O	0.49 mM
D-glucose	5.56 mM	$MgSO_4$ x 7 H_2O	0.41 mM
Hepes	20 mM	Na_2HPO_4	0.34 mM
KCl	5.33 mM	NaCl	137.9 mM
KH_2PO_4	0.44 mM	$NaHCO_3$	4.17 mM
H_2O			

Table 11 | Hanks and Hepes Buffer (HHBS)

2.4.4 Mitochondrial membrane potential

The mitochondrial membrane potential (ΔΨm) was measured by JC-1 staining. The dye aggregates in the electronegative interior of mitochondria emitting red fluorescence in healthy cells. Upon dissipation of ΔΨm, the dye remains monomeric in the cytosol and shows green fluorescence.[63] Stimulated cells were stained with 1 µg/ml JC-1 for 30 min at 37°C, washed with PBS to remove excess dye and resuspended in PBS. In parallel, compensation samples were prepared according to manufacturer's instructions using

the BD CompBeads Anti-mouse Ig, κ particles set and BD Alexa Fluor 488 and PE-conjugated antibodies (see section 2.1.3). Operating on a FACSCanto II, compensation of spectral overlap was performed prior to analysis of JC-1 stained cells (settings Alexa 488: Ex 488 nm, Em 530/30 nm; PE: Ex 488 nm, Em 585/42 nm). Debris was excluded and populations exposing green and red fluorescence were determined with FlowJo software plotting Alexa 488 against PE fluorescence intensity.

2.4.5 Reactive oxygen species

Reactive oxygen species (ROS) were detected using the redox-sensitive probe Carboxy-H_2DCFDA. Upon cleavage of the acetate groups by intracellular esterases and oxidation by the activity of ROS, the non-fluorescent precursor is converted to the highly fluorescent 2´-7´-dichlorofluorescein (DCF).[64] Stimulated cells were harvested, washed with PBS and loaded with Carboxy-H_2DCFDA (20 µM in PBS, incubation 45 min at 37°C). Cells were washed once again to remove excess dye and resuspended in PBS. The fluorescence intensity was immediately analyzed on a FACSCanto II at Ex 488 nm and Em 530/30 nm. For quantification, debris was excluded and intracellular ROS levels were determined as the FITC-A median relative to DMSO control.

2.5 Proliferation Assay

To analyze the proliferative capacity, 5.000 cells were seeded per well into 96-well plates and stimulated for 72 h with subtoxic concentrations of test compounds. Subsequently, CellTiter-Blue (CTB) reagent was added to each well at a volume ratio of 2:5 (v/v) and incubated for 4 h at 37°C. Viable cells reduced the CTB dye resazurin into resorufin, which is highly fluorescent. With an excitation at 550 nm, resorufin fluorescence was recorded at 595 nm using a Tecan SpectraFluor Plus microplate reader. As a reference, the cell number on day 0 was determined incubating three wells with CTB at the time of stimulation (Em Ctrl 0 h). Proliferation of cells was calculated relative to DMSO control according to the following formula:

$$Proliferation\ [\%] = \frac{Em\ \ Treated\ \ (72\,h) - Em\ \ Ctrl\ \ (0\,h)}{Em\ \ DMSO\ \ (72\,h) - Em\ \ Ctrl\ \ (0\,h)} \cdot 100$$

2.6 Colony Formation Assay

In order to assess the ability of single cells to form colonies after short-term stimulation, Jurkat or VCR-R CEM cells at a density of 0.4 x 10^6 cells/ml were treated for 4 h with test compounds. Cells were harvested, washed with PBS to remove stimulants and resuspended in growth medium. The cell density was determined with the cell viability analyzer ViCell XR and adjusted to 0.065 x 10^6 cells/ml. Aliquots of the cell suspension (V = 500 µl) were diluted with 6 ml of RPMI medium supplemented with 0.52% methylcellulose (MC) and 40% FCS to promote colony growth (final concentrations: 5.0 x 10^3 cells/ml in 0.4% MC medium). This suspension was seeded in triplicates (V = 2 ml per well in 6-well plates) and cells were allowed to grow into colonies for 5 d (VCR-R CEM cells) or 7 d (Jurkat cells). Colonies were subsequently incubated with the yellow tetrazolium dye MTT which is reduced to purple formazan in living cells.[65] Images of each well were recorded using a LU105M camera and LuCam software from Luminera. The number of colonies per well were determined with ImageJ software by cutting the area of interest, sharpening the colored pixels, adjusting threshold to subtract background grey levels and analyzing the number of particles. The count of colony forming units (CFU) was normalized to DMSO controls.

2.7 Immunoblotting

2.7.1 Cell lysis and cytosolic-mitochondrial fractionation

Analysis of cellular protein levels was performed by Western blot. Therefore, samples were harvested, washed once with ice-cold PBS and lyzed. For the preparation of whole cell lysates, cells were resuspended in phospho lysis buffer (Table 12), frozen at -20°C overnight and incubated for at least 30 min on ice. After centrifugation (10 min, 10.000 g, 4°C), one part of the supernatants was used for protein quantification and the remaining cell lysates were stored at -20°C if not immediately processed further.

Phospho lysis buffer (pH 7.5)			
NaCl	137 mM	$Na_4P_2O_7$ x 10 H_2O	2 mM
Tris base	20 mM	Glycerol	10 % (v/v)
Na_2EDTA	2 mM	Na_3VO_4	2 mM
Triton-X 100	1 % (v/v)	PMSF	1 mM
Na_2-β-Glycerophosphate x 5 H_20	20 mM	Complete 25x	4 % (v/v)
NaF	10 mM	H_2O	

Table 12 | Phospho lysis buffer for the preparation of whole cell lysates

For cytosolic-mitochondrial fractionation, cells were incubated with digitonin lysis buffer (Table 13) for 20 min on ice and centrifuged (10 min, 170 g, 4°C). The supernatant was collected (cytosolic fraction) and the cell pellet was permeabilized with Triton X-100 lysis buffer (0.1% Triton-X 100 in PBS) for 15 min on ice (mitochondrial fraction). Both fractions were once more centrifuged (10 min, 10.000 g, 4°C) to remove residual cell debris and further processes as whole cell lysates.

Digitonin lysis buffer (pH 7.2)			
Hepes (pH 7.2)	10 mM	Na_2EGTA	0.2 mM
Mannitol	210 mM	Succinate	5 mM
Sucrose	200 mM	BSA	0.15 % (w/v)
Digitonin	80 µg/ml	H_2O	

Table 13 | Digitonin lysis buffer for the separation of cytosolic from mitochondrial fractions

2.7.2 Protein quantification and sample preparation

In order to assure equal protein load, the bicinchoninic acid (BCA) assay was performed.[66] Therefore, 10 µl of cell lysates previously diluted 1:5 (v/v) in water or bovine serum albumin (BSA) standards (c = 0.125 - 2.0 mg/ml) were transferred to a 96-well plate in triplicates. Samples were incubated with 190 µl of BCA solution (Uptima, Interchim) for 30 min at 37°C in the dark. The reduction of Cu^{2+} to Cu^{+} leading to BCA chelate formation and a purple-colored product is proportional to the amount of protein. The absorbance was measured at 550 nm using a Tecan Sunrise reader and protein concentrations were determined by linear regression. Western blot samples were prepared mixing a lysate volume corresponding to 30 µg protein with 1/5 (v/v) of 5x SDS sample buffer (Table 14) and with 1x SDS sample buffer to a total volume of 40 µl. Prior to gel loading, samples were boiled for 5 min at 95°C.

5x SDS sample buffer	
Tris-HCl (pH 6.8)	3.125 M
Glycerol	50% (v/v)
SDS	5% (w/v)
DTT	2% (w/v)
Pyronin Y	0.025% (w/v)
H_2O	

1x SDS sample buffer	
5x SDS sample buffer	20% (v/v)
H_2O	

Table 14 | SDS buffers for Western blot sample preparation

2.7.3 Electrophoresis and blotting

For protein separation, discontinuous SDS-polyacrylamide gel electrophoresis (SDS-PAGE) was performed using Polyacrylamide (PAA) gels prepared as listed in Table 15. The PAA concentration was typically 12%, though adjusted to optimal separation conditions depending on the molecular weight of the protein of interest.

The chamber of a Mini Protean 3 system from Bio-Rad was supplied with electrophoresis buffer (Table 15) and gels were loaded with samples or 2 µl of Page Ruler Prestained protein ladder. Electrophoresis was performed for 21 min at 100 V and 45 min at 200 V for protein stacking and separation, respectively.

Stacking Gel	
Rotiphorese Gel 30	17% (v/v)
Tris-HCl (pH 6.8)	125 mM
SDS	0.1% (w/v)
TEMED	0.2% (v/v)
APS	0.1% (w/v)
H_2O	

Separation Gel 12%	
Rotiphorese Gel 30	40% (v/v)
Tris-HCl (pH 8.8)	375 mM
SDS	0.1% (w/v)
TEMED	0.1% (v/v)
APS	0.05% (w/v)
TCE	0.5% (v/v)
H_2O	

Electrophoresis buffer			
Tris	4.9 mM	SDS	0.1% (w/v)
Glycine	38 mM	H_2O	

Table 15 | Gels and buffer for SDS-PAGE

Prior to blotting, equal protein load was determined by stainfree detection of trichloroethanol (TCE) supplemented gels[67] using a ChemiDoc Touch Imaging System. In order to make proteins accessible for immunological detection, tank electroblotting onto

Amersham NC or PVCF membranes (GE Healthcare, 0.2 µM or 0.45 µM pore size) was performed for 1.5 h at 100 V and 4°C. The blot was run in cold 1x tank buffer listed in Table 16.

5x tank buffer	
Tris base	240 mM
Glycine	195 mM
H_2O	

1x tank buffer	
5x tank buffer	20% (v/v)
Methanol	20% (v/v)
H_2O	

Table 16 | Tank buffers for electroblotting

2.7.4 Protein detection

To prevent non-specific binding of antibodies, membranes were blocked for at least 1 h at RT with a 5% (w/v) solution of milk powder in TBS-T buffer (Table 17). Membranes were subsequently incubated with primary antibodies overnight at 4°C. After three washing steps with TBS-T, membranes were incubated with a suitable secondary antibody for 1 h at RT and washed again three times with TBS-T. Depending on the secondary antibody labeling, (A) enhanced chemiluminescence (ECL) or (B) infrared imaging was used to develop membranes.

(A) Proteins detected by HRP-catalyzed oxidation of luminol and chemiluminescence were visualized by incubating membranes for 1 min with ECL solution (Table 17). Membranes were either exposed to an X-ray film and developed with an AGFA Curix 60 system (applicable for PDI blots) or analyzed directly on a ChemiDoc Touch imaging system from Bio-Rad (applicable for all other blots).

(B) Proteins detected with IRDye coupled secondary antibodies were visualized using a Li-Cor Odyssey 2.1 infrared imaging system. Protein bands were recorded by scanning light emission at 800 nm (applicable for Actin blots).

TBS-T (pH 8.0)	
Tris base	24.8 mM
NaCl	190 mM
Tween 20	0.1% (v/v)
H_2O	

ECL solution	
Tris (pH 8.5)	100 mM
Luminol	2.5 mM
Coumaric acid	1 mM
H_2O_2	17 µM
H_2O	

Table 17 | Tris buffer for washing of membranes and ECL solution for protein detection

2.8 Co-Immunoprecipitation

Protein protein interactions were analyzed by co-immunoprecipitation (Co-IP). Therefore, Jurkat cells were stimulated for 24 h with test compounds, harvested, washed twice with ice cold PBS and incubated for 30 min on ice with Triton X-100 lysis buffer (Triton buffer, Table 18). Proteins were cleared from cell debris by centrifugation (10 min, 10.000 g, 4°C) and supernatants were subjected to BCA protein quantification as described in section 2.7.2. For magnetic labeling, 500 µg protein per sample was adjusted to 500 µl total volume with Triton buffer and gently mixed with 4 µg of precipitation antibody (Goat anti-BAP31 C-15) and 50 µl Protein G MicroBeads from Miltenyi Biotech for 45 min at 4°C. An equal amount of BAP31 C-15 was incubated in parallel with beads, but without lysate, and served as control of antibody heavy and light chains. BAP31 and interacting proteins were co-immunoprecipitated on Miltenyi µColumns. Therefore, columns were pre-rinsed once with Triton buffer, loaded with samples, washed four times with Triton buffer and finally once with low salt wash buffer (Table 18). Proteins were eluted with 95°C pre-heated 1x SDS sample buffer (Table 14) and analyzed by immunoblotting as described in sections 2.7.3 and 2.7.4. Antibodies used for detection were mouse anti-BAP31 B-10 (Santa Cruz) and mouse anti-CASP8 1C12 (Cell Signaling).

Triton buffer (pH 8.0)	
NaCl	150 mM
Tris HCl	50 mM
Triton X-100	1% (v/v)
Complete 25x	4 % (v/v)
H_2O	

Low salt wash buffer (pH 7.5)	
Tris HCl	20 mM
H_2O	

Table 18 | Triton X-100 lysis buffer and low salt wash buffer for Co-IP

2.9 UV-Crosslinking, Immunostaining and Confocal Microscopy

For target validation, the BAP31 protein was co-stained with the PS89 photo probe (JP-04) linked to a rhodamine reporter. Hela cells (0.02 x 10^6 cells/well) were seeded in ibidi 8-well µ-slides, allowed to adhere for 6 h and then incubated with 20 µM JP-04 for 20 min at 37°C. UV crosslinking of the photoreactive aryl azide to cellular target proteins was performed with a UV lamp at 366 nm for 30 min at RT. Cells were fixed with ice cold 4% paraformaldehyde (PFA) in RPMI cell culture medium supplemented with 10% FCS

for 15 min and then permeabilized for 3 x 5 min with 0.1% Triton X-100 in PBS at RT. For coupling of the rhodamine reporter dye, cells were incubated with the click reaction solution (Table 19) for 20 min at RT and subsequently washed three times with PBS to remove excessive dye. Immunostaining was performed with BAP31 HPA003906 from Sigma-Aldrich overnight at 4°C (1.6 µg/ml in PBS supplemented with 4% FCS), 4 x 10 min washing with PBS at RT and incubation with Anti-rabbit Alexa 488 A11008 from Thermo Fisher Invitrogen for 2 h at RT in the dark (2.5 µg/ml in PBS/4% FCS). As counterstain, Hoechst 33342 was added (c = 5 µg/ml) and cells were finally washed for 4 x 10 min with PBS before adding one drop of FluorSave mounting medium per well. Confocal microscopy was performed on a Leica SP8 LSM system and evaluation of co-stained areas was performed with the co-localization tool of Leica LAS X software.

Click reaction solution	
5-TAMRA-Azide	0.02 mM
$CuSO_4$	1 mM
Ascorbic acid	100 mM
PBS	

Table 19 | Click reaction solution

2.10 Activity-Based Protein Profiling and STRING Analysis

PS89 target identification was performed by Jan Vomacka in the laboratory of Prof. Stefan Sieber (TU Munich, Germany) using an activity-based protein profiling (ABPP) approach. Therefore, Jurkat cells were incubated with unmodified PS89 (c = 100 µM) or DMSO as control for 45 min at 37°C and in a second step with the PS89 photo probe (JP-04, c = 20 µM) or DMSO as control for 45 min at 37°C. Cells were lyzed in PBS with 1% (v/v) NP40 and 1% (w/v) sodium deoxycholate and sonication for 15 sec on ice. Sample preparation and mass spectrometry analysis of target proteins by gel-free ABPP and dimethyl labeling was performed as previously described.[68] Cutoff criteria for target identification were: (1) enrichment by photo probe $\log_2$ Probe/DMSO >1.6, $-\log_{10}$ p-value >2 and (2) PS89 competition $\log_2$ Probe/PS89 >0.

Protein network analysis was performed using STRING v10, a web resource of protein-protein interactions that is based on experimental data, computational prediction

methods and public text collections.[69] The functional connection of target proteins was further refined by Gene Ontology (GO) enrichment classification.[70]

2.11 Data Collection and Statistics

Assays were performed with three technical replicates per test and data from at least three independent experiments (biological replicates) are expressed as mean value ± SEM. Statistical analysis and calculation of EC_{50} values was performed with Prism 7 software from GraphPad. For Western blot and confocal microscopy experiments, representative images of at least three independent data sets are shown.

3 Results

3.1 Chemosensitization of Acute Leukemia Cells with PS89

3.1.1 Impact on Jurkat cell apoptosis, proliferation and colony formation

The concept of chemosensitization with the protein disulfide isomerase (PDI) inhibitor PS89 was initially evaluated in a dose-response apoptosis assay. While PS89 was applied at subtoxic concentrations (25 µM PS89, 7.8% apoptotic cells), the dose of etoposide (ETO) could be reduced at least by half to achieve equal cytotoxicity applying the combination treatment. This is in line with a shifted EC_{50} value by 2.1-fold (Figure 8a). The induction of apoptotic cell death was additionally verified by Western blotting and activation of the executioner caspase-3 (CASP3) as well as cleavage of the DNA repair enzyme poly ADP ribose polymerase (PARP) downstream of CASP3 (Figure 8b).

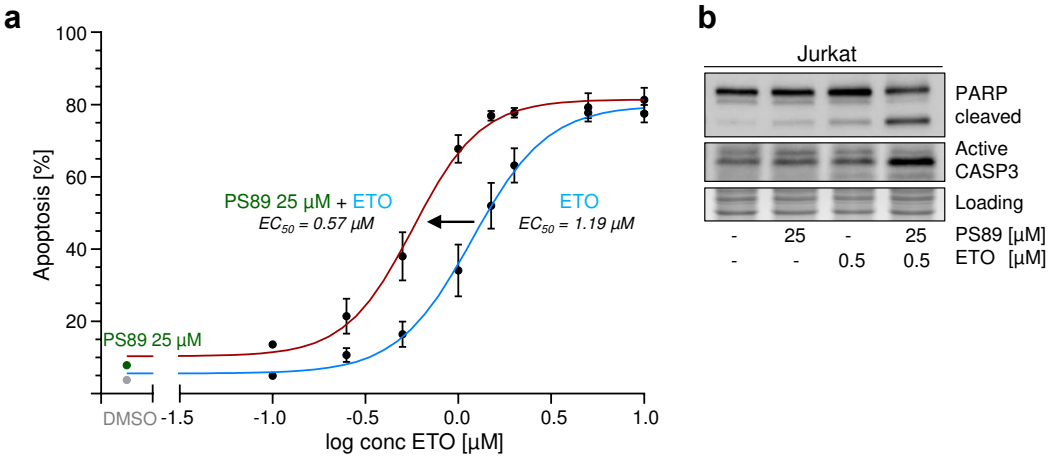

Figure 8 | Sensitizing effects of PS89 on Jurkat cell apoptosis. (**a**) Apoptosis of Jurkat cells treated with etoposide (ETO) in presence or absence of 25 µM PS89. Percentage of apoptotic cells was determined by propidium iodide staining and flow cytometry after 48 h. (**b**) Execution of apoptosis analyzed by immunoblotting. Jurkat cells were cultured for 48 h in drug supplemented medium and protein levels of active caspase-3 (CASP3) and poly ADP ribose polymerase (PARP) were determined.

Propidium iodide (PI) staining and flow cytometry revealed furthermore that PS89 had no effect on cell cycle while ETO treated Jurkat cells showed pronounced G2 cell cycle arrest (Figure 9). In combination treatment, G2 arrest still persisted accompanied by an increase of the subG1 apoptotic cell population featuring DNA fragmentation and therefore low PI fluorescence intensity.

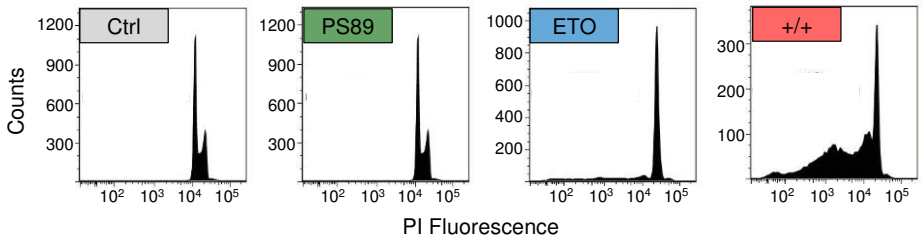

Figure 9 | Cell cycle analysis of PS89 and ETO treated Jurkat cells. Determination of cellular DNA content of Jurkat cells treated for 48 h with 25 µM PS89, 0.5 µM etoposide (ETO) or combination (+/+) by propidium iodide staining and flow cytometry.

Applying subtoxic concentrations of ETO in combination with PS89, the proliferation of Jurkat cells after 72 h treatment was inhibited more than additive (Figure 10a, inhibition of PS89 21.5% + ETO 27.1% < Combination 58.9%). Moreover, the long-term effects of the combination were studied exposing Jurkat cells to a 4 h pulse stimulation and monitoring the ability of single cells to grow into colonies for 7 days. As demonstrated in Figure 10b, PS89 and ETO both had mild effects on colony formation in single treatment (85% and 87% of control), tough the size and number of colony forming units (CFU) was highly decreased in combination (32% of control).

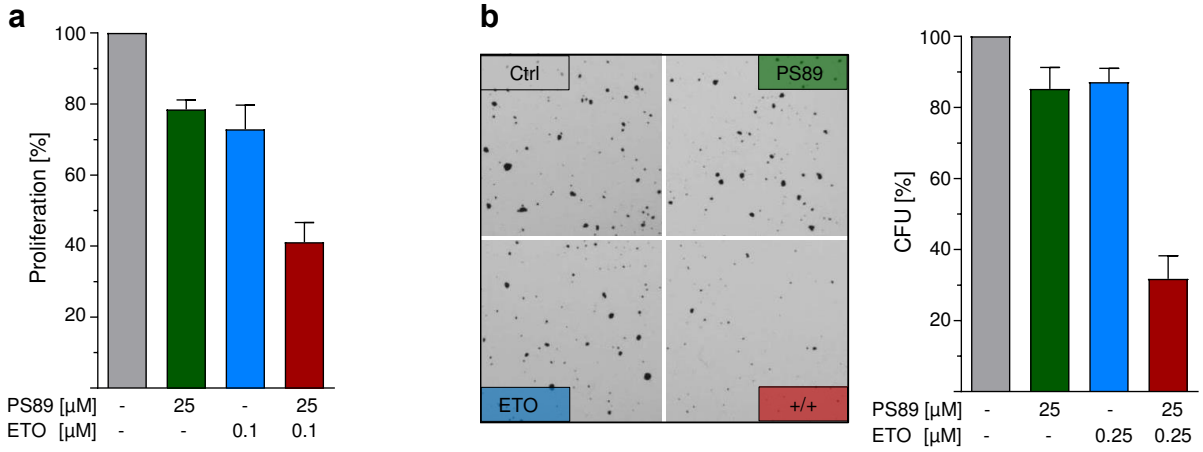

Figure 10 | Inhibition of proliferation and colony formation with PS89 and ETO. (**a**) Proliferation of Jurkat cells incubated with PS89 and etoposide (ETO). Cells were allowed to grow for 72 h, the number of viable cells was determined by CellTiter-Blue staining and normalized towards DMSO control. (**b**) Colony formation of Jurkat cells stimulated for 4 h with PS89 and ETO. Compounds were removed and cells reseeded at low density (5.000 cells/ml) in medium with increased viscosity. The number of colonies was quantified after 7 days of proliferation and normalized towards DMSO control.

3.1.2 Treatment of different acute leukemia cell lines and drug resistant cells

The ability of PS89 to induce synergistic apoptosis with cytostatics could be translated to acute leukemia cell lines of different lineage and corresponding treatments. This was demonstrated by PS89 combinations with daunorubicin (DNR) in HL-60 AML cells and vincristine (VCR) in CCRF-CEM ALL cells (Figure 11). Furthermore, vincristine resistant

(VCR-R) CEM cells responded towards 100 nM VCR in combination with PS89 (38.3% apoptotic cells), while cells were still resistant towards 10-fold higher VCR concentrations without co-stimulation (1000 nM VCR 6.8% apoptotic cells, Figure 11).

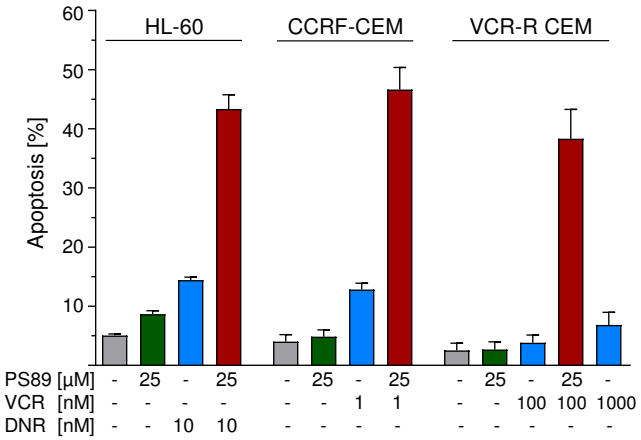

Figure 11 | Chemosensitization of HL-60, CCRF-CEM and vincristine resistant (VCR-R) CEM cells. Apoptosis of ALL and AML cell lines treated with PS89 and cytostatics (DNR: daunorubicin, VCR: vincristine). Percentage of apoptotic cells was determined by propidium iodide or YO-PRO-1 staining and flow cytometry after 48 h.

Further apoptosis studies with the vincristine resistant ALL cell line VCR-R CEM supported the results previously obtained in Jurkat cells. Combining PS89 with VCR, apoptosis induction was prevented by the pan-caspase inhibitor Q-VD-OPh (Figure 12a) which is in line with the activation of CASP3 and PARP cleavage observed by Western blotting (Figure 12b). Notably, the percentage of apoptotic cells was equally high and irrespective of PS89 or VCR pre-stimulation (Figure 13) which indicated that cell death induction by the combination treatment was rather dependent on parallel action of the compounds than a pre-sensitization of cells.

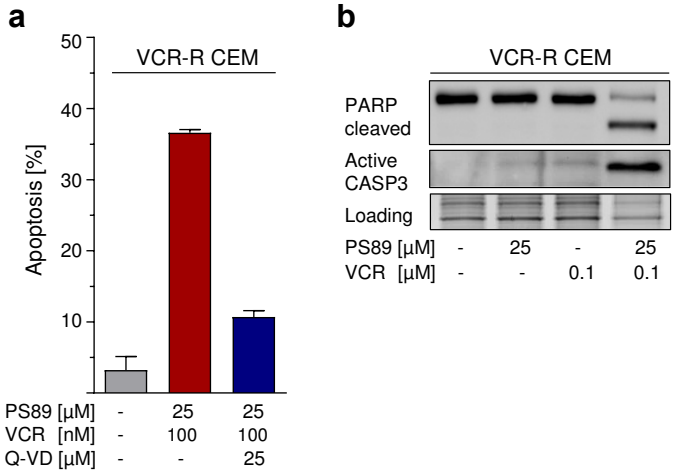

Figure 12 | Hallmarks of apoptosis in vincristine resistant (VCR-R) CEM cells. (**a**) Apoptosis of VCR-R CEM cells treated with PS89 and VCR in presence or absence of the pan-caspase inhibitor Q-VD-OPh. Percentage of apoptotic cells was determined by propidium iodide staining and flow cytometry after 48 h. (**b**) Execution of apoptosis analyzed by immunoblotting. VCR-R CEM cells were cultured for 48 h in drug supplemented medium and protein levels of active caspase-3 (CASP3) and poly ADP ribose polymerase (PARP) were determined.

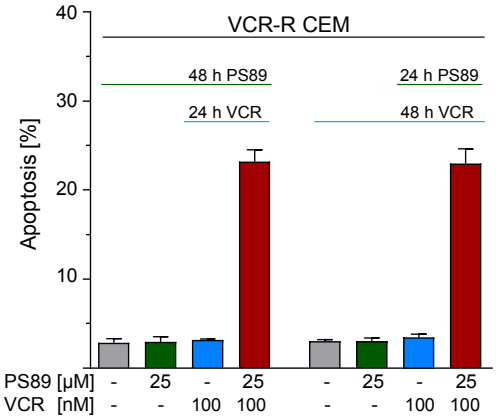

Figure 13 | Apoptosis induction independent of application schedule. Apoptosis of vincristine resistant (VCR-R) CEM cells after 24 h pre-treatment with PS89 or VCR followed by 24 h co-treatment. Percentage of apoptotic cells was determined by propidium iodide staining and flow cytometry.

The sensitizing effects of PS89 on colony formation after short-term treatment could be reproduced as well in VCR-R CEM cells. Though the cell line generally formed smaller colonies compared to Jurkat cells, the total number of colony forming units (CFU) was strongly decreased after short-term stimulation with the combination of PS89 and VCR (Figure 14).

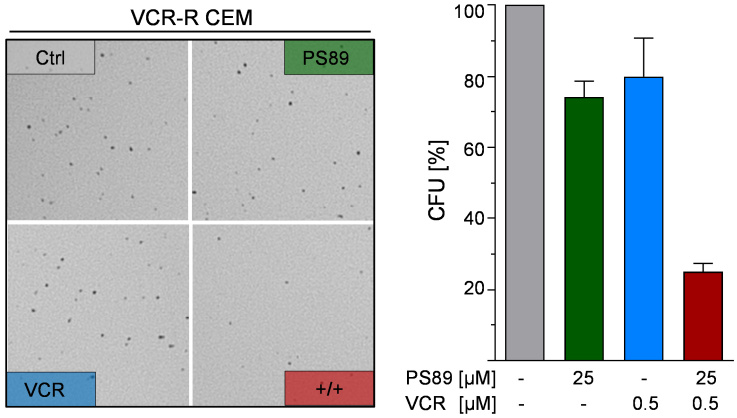

Figure 14 | Colony formation of vincristine resistant (VCR-R) CEM cells. After stimulation of VCR-R CEM cells for 4 h with PS89 and VCR, compounds were removed and cells reseeded at low density (5.000 cells/ml) in medium with increased viscosity. The number of colonies was quantified after 5 days of proliferation and normalized towards DMSO control.

3.1.3 Sensitization of acute leukemia patient derived xenograft cells

The broad applicability of PS89 as chemosensitizing co-treatment was confirmed as a promising approach in acute leukemia patient derived xenograft (PDX) cells. AML and ALL samples of diverse background (see section 2.1.1.2) were treated with PS89 and DNR (Figure 15a) or PS89 and VCR (Figure 15b). As a result, they generally showed clearly increased apoptosis rates in combination. Yet, the standard concentration of 25 µM PS89 was non-toxic on PDX cells, which is in accordance with previous results.

Notably, low response towards the combination treatments was observed in peripheral blood mononuclear cells (PBMCs) compared to PDX samples (Figure 15a+b).

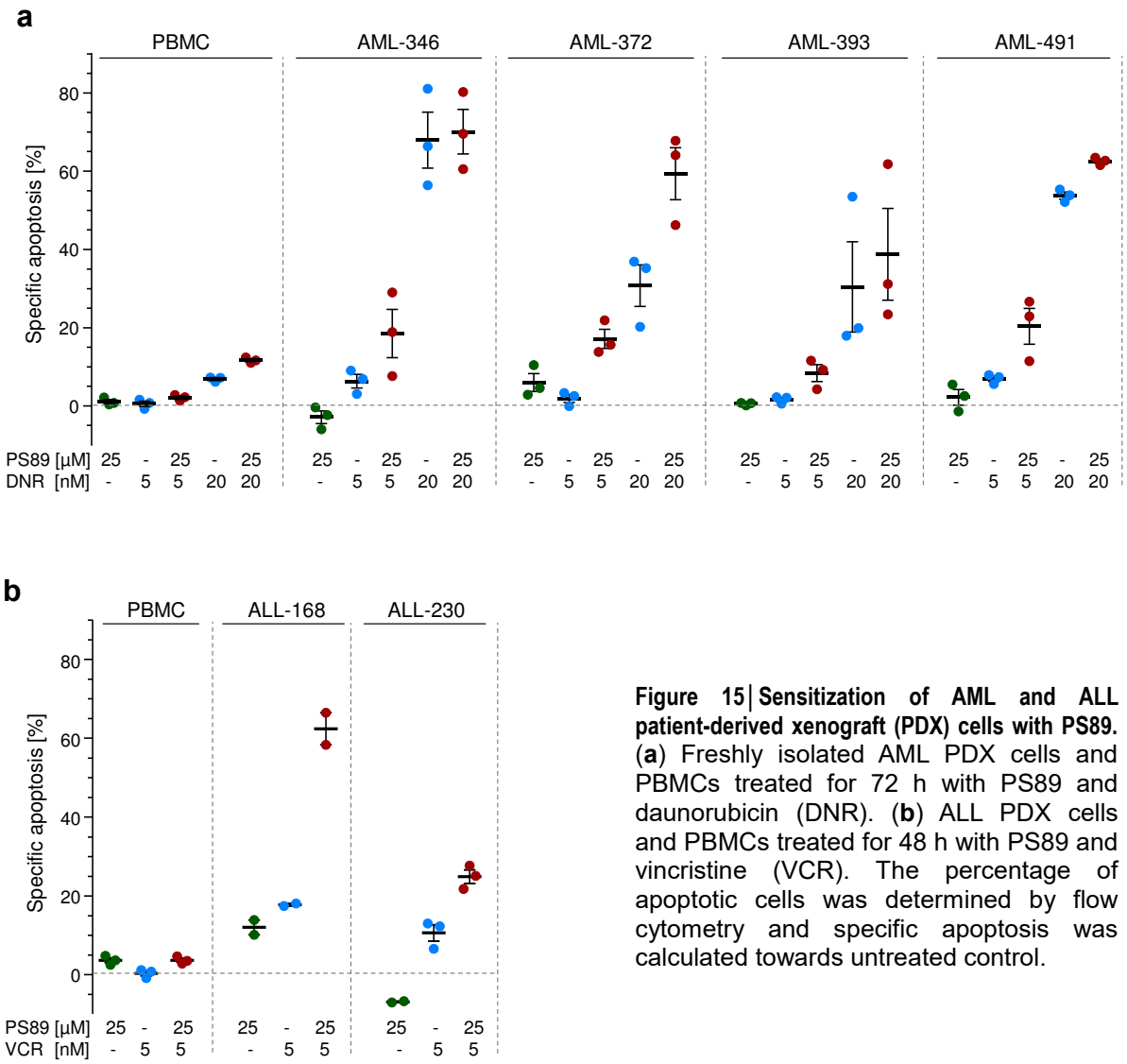

Figure 15 | Sensitization of AML and ALL patient-derived xenograft (PDX) cells with PS89. (**a**) Freshly isolated AML PDX cells and PBMCs treated for 72 h with PS89 and daunorubicin (DNR). (**b**) ALL PDX cells and PBMCs treated for 48 h with PS89 and vincristine (VCR). The percentage of apoptotic cells was determined by flow cytometry and specific apoptosis was calculated towards untreated control.

3.1.4 Exceptions prove the rule: antagonism of PS89 and cytarabine

As the standard 7+3 induction chemotherapy in AML is based on the antimetabolite cytarabine (Ara-C) together with an anthracycline, we tested if the chemosensitizing approach with PS89 could be translated to Ara-C combinations as well. Surprisingly, PS89 dose-dependently antagonized the effect of Ara-C in HL-60 AML cells (Figure 16). This result raised the question which mechanism accounted for the negative interference of PS89 with Ara-C and was subjected to further discussion in combination with the PS89 target screening presented in section 3.2.2.

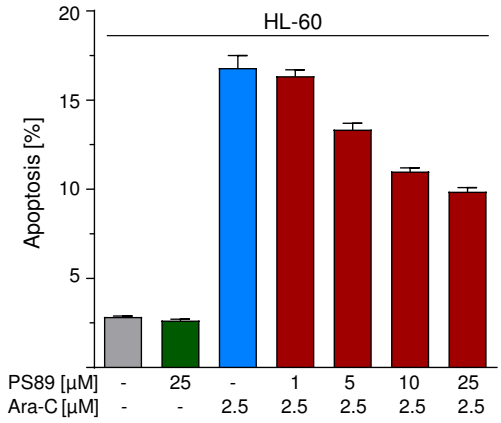

Figure 16 | Antagonizing effects of PS89 in combination with cytarabine (Ara-C). Apoptosis of HL-60 cells treated with PS89 and cytarabine (Ara-C) for 48 h. Percentage of apoptotic cells was determined by propidium iodide staining and flow cytometry.

3.2 PS89 Target Network Analysis

3.2.1 Single-target studies on protein disulfide isomerase

The initial characterization of PS89 revealed that the compound binds in close proximity to the catalytic center of protein disulfide isomerase (PDI) and inhibits its enzymatic activity.[49] Evaluating if this feature was responsible for the intensively pro-apoptotic cellular effects in combination with cytostatics, PDI genetic knockdown and overexpression experiments were performed. Similar to PS89, silencing of PDI did not affect basal apoptosis of Jurkat cells in non-treated cells (Figure 17a, DMSO control). However, no sensitizing effect of PDI silencing on etoposide (ETO) induced apoptosis or inhibition of proliferation was observed (Figure 17a+b). PDI knockdown efficiency on protein level was evaluated in parallel by Western blot (Figure 17c).

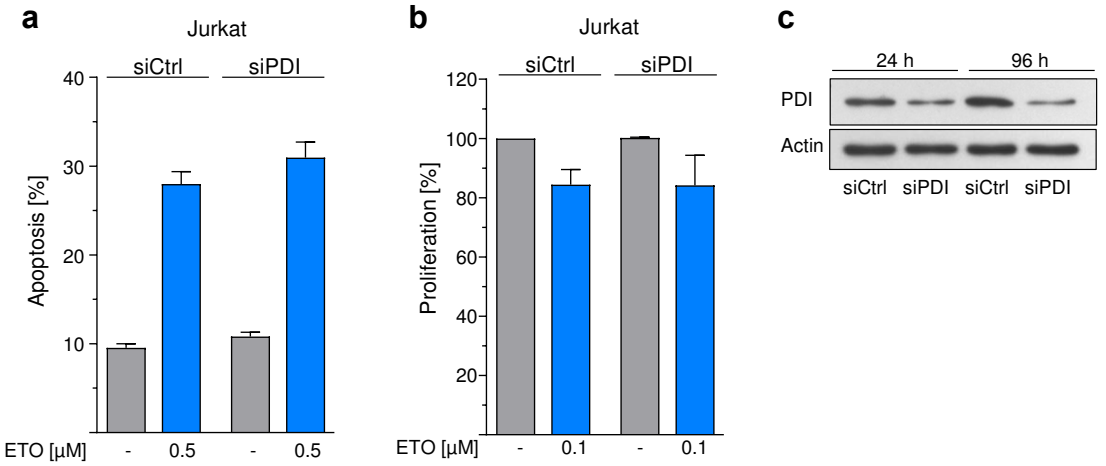

Figure 17 | Constant levels of Jurkat apoptosis and proliferation in protein disulfide isomerase (PDI) silenced cells. (**a**) Apoptosis of PDI silenced Jurkat cells (siPDI, 48 h) treated for further 48 h with etoposide (ETO). Percentage of apoptotic cells was determined by propidium iodide staining and flow cytometry. (**b**) Proliferation of PDI silenced Jurkat cells (siPDI, 24 h) incubated for further 72 h with ETO. The number of viable cells was determined by CellTiter-Blue staining and normalized towards DMSO control. (**c**) PDI protein levels analyzed in Jurkat cells by immunoblotting after 24 h and 96 h transfection with non-targeting siRNA (siCtrl) or siRNA against PDI (siPDI).

In order to cross-check if PS89 chemosensitizing effects were rescued by PDI overexpression, HEK 293 cells were chosen as convenient transfection hosts. After plasmid transfection, cells constantly expressed PDI at high protein levels (Figure 18a) and were subjected to PS89 and ETO stimulation. In combination treatments, PS89 showed an additional inhibition of proliferation both in control and overexpressing cells (Figure 18b). Thus, increased PDI levels did not alleviate functional signaling of PS89.

A screen of PDI expression in acute leukemia cell lines revealed in addition that Jurkat as well as CEM cells featured low endogenous PDI levels compared to HL-60 (Figure 18c). However, the chemosensitizing effects of PS89 were observed in all cell lines with a fixed 25 µM dose, as shown in section 3.1. In line with the overexpression study, this demonstrated once more that PDI protein levels did not correlate with sensitivity towards PS89 treatment.

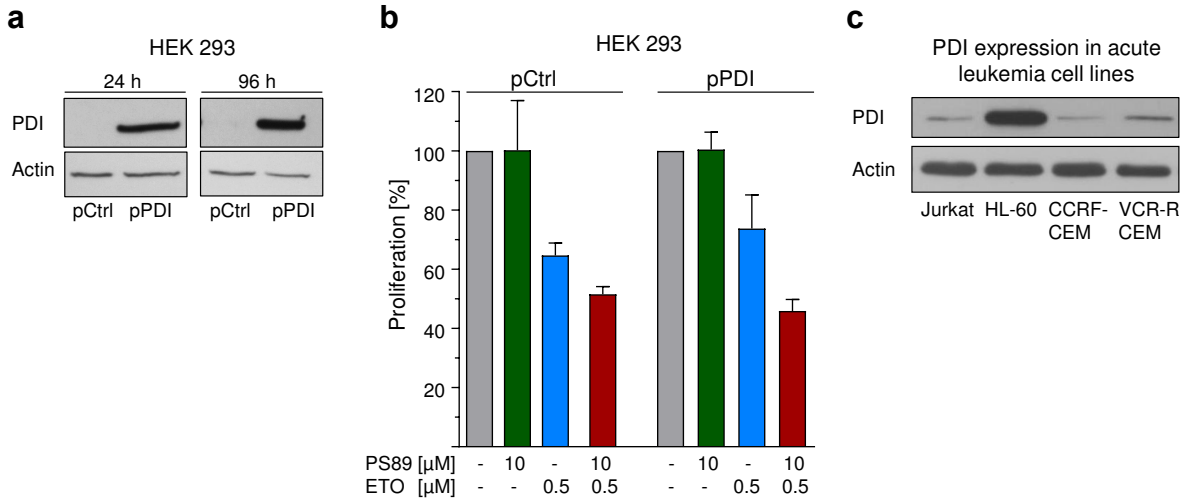

Figure 18 | Protein disulfide isomerase (PDI) expression and response to PS89 combination treatment. (**a**) PDI protein levels analyzed in HEK cells by immunoblotting after 24 h and 96 h transfection with empty vector pcDNA3.1 (pCtrl) or PDI vector (pPDI). (**b**) Proliferation of PDI overexpressing HEK cells (pPDI, 24 h) incubated for further 72 h with PS89 and etoposide (ETO). The number of viable cells was determined by CellTiter-Blue staining and normalized towards DMSO control. (**c**) PDI expression in acute leukemia cell lines determined by immunoblotting.

In summary, PDI silencing did neither sensitize cells towards ETO treatment, nor did overexpression of PDI rescue the functional effect of PS89. This indicated a more extensive pharmacodynamic profile of PS89.

3.2.2 Activity-based protein profiling of PS89 target proteins

In order to identify the proposed PS89 polytarget structure, activity-based protein profiling (ABPP) was applied in Jurkat cells as depicted in Figure 19. First, the PS89 photo probe modified by an alkyne handle (structure shown in Figure 19) was covalently linked to cellular targets in presence or absence of PS89. Co-incubation with the unmodified compound acting as a competitor was performed to exclude the identification of targets that were only enriched by the probe, but not by PS89. Subsequently, target proteins were enriched by biotin-avidin-pulldown, digested, labeled and analyzed by mass spectrometry (MS). Sample preparation and MS analysis was performed as described in section 2.10 by Jan Vomacka (group of Prof. Stefan Sieber, TU Munich, Germany).

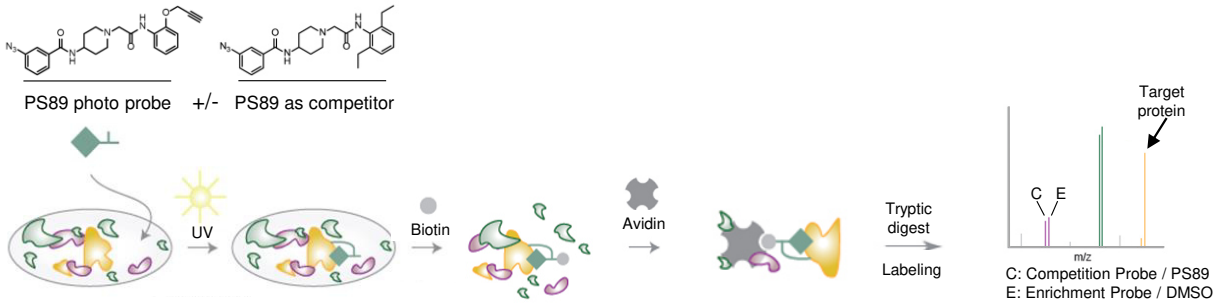

Figure 19 | Principle of target identification by activity-based protein profiling (ABPP). Jurkat cells were incubated with unmodified PS89 (c = 100 µM) or DMSO as control and in a second step with the PS89 photo probe (c = 20 µM). After cell lysis, biotin was conjugated to the alkyne group by cycloaddition and target proteins were identified by avidin pulldown, tryptic digestion and mass spectrometry. Scheme adapted from Vomacka *et al*.[68]

Raw data of the ABPP target identification accompanies this thesis as outlined in the appendix section 8.2. Illustrated in Figure 20a, $\log_2$-fold protein enrichments in photo probe samples compared to DMSO baseline levels were plotted against their statistical significance expressed as p-values. In the resulting volcano plot, proteins localized at the central symmetric part were unspecific binders, while the hits in the blue-colored area featured a >3-fold enrichment by the photo probe with p-values <0.01. This selection was further refined by the ability of PS89 to compete with the probe at the binding sites of the target proteins and is expressed by the size and coloring of dots in Figure 20b. In total, n = 42 target proteins were identified and ranked according to the degree of probe enrichment and PS89 competition (Table 20).

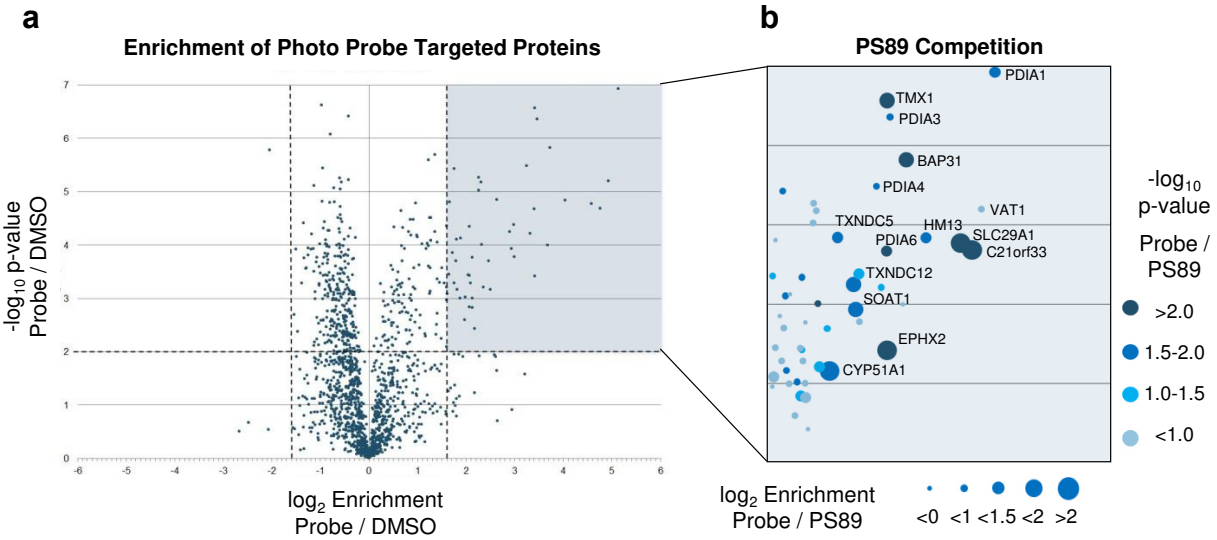

Figure 20 | Volcano plot of PS89 target proteins. (**a**) Proteins enriched by the PS89 photo probe compared to basal protein levels (DMSO control). Targets enriched >3-fold ($\log_2$ Enrichment Probe / DMSO >1.6) and with $-\log_{10}$ p-value >2 are highlighted. (**b**) Competition of PS89 at photo probe binding sites. Proteins enriched by the photo probe ('Probe'), but depleted after PS89 pre-treatment ('PS89') are accentuated with increasing dot size ($\log_2$ Enrichment Probe / PS89) and color intensity ($-\log_{10}$ p-value Probe / PS89).

			Probe / DMSO				Probe / PS89				Overall Score
Gene names	Protein names	Mol. weight [kDa]	log2 enrichment		-log10 p-value		log2 enrichment		-log10 p-value		
			enrichment	Rank	enrichment	Rank	enrichment	Rank	enrichment	Rank	
C21orf33	ES1 protein homolog, mitochondrial	25,64	4,767	3	4,682	14	4,642	1	4,318	1	3,5
TMX1	Thioredoxin-related transmembrane protein 1	31,791	3,417	9	6,568	2	1,738	6	3,141	3	4,8
BCAP31	B-cell receptor-associated protein 31	27,991	3,725	6	5,819	4	1,543	7	2,345	6	6,0
SLC29A1	Equilibrative nucleoside transporter 1	50,219	4,584	4	4,770	13	2,130	3	2,049	7	6,2
P4HB	Protein disulfide-isomerase	57,116	5,131	1	6,927	1	1,289	10	1,956	10	7,0
EPHX2	Bifunctional epoxide hydrolase 2	62,615	3,419	8	3,416	30	3,693	2	3,315	2	7,7
PDIA6	Protein disulfide-isomerase A6	47,837	3,409	10	4,669	15	1,096	15	2,731	4	10,5
HSD17B12	Very-long-chain 3-oxoacyl-CoA reductase	34,324	2,893	16	4,242	19	1,516	8	1,986	9	11,5
SOAT1	Sterol O-acyltransferase 1	64,734	2,932	15	3,930	23	1,952	5	1,868	12	12,0
HM13	Minor histocompatibility antigen H13	36,813	4,037	5	4,837	12	1,012	17	1,637	17	14,2
CYP51A1	Lanosterol 14-alpha demethylase	56,805	2,502	18	3,159	35	2,018	4	1,668	15	15,2
PDIA4	Protein disulfide-isomerase A4	72,932	3,247	12	5,485	5	0,946	23	1,669	14	15,2
PDIA3	Protein disulfide-isomerase A3	56,782	3,464	7	6,360	3	0,838	26	1,660	16	15,7
TXNDC5	Thioredoxin domain-containing protein 5	40,369	2,628	17	4,840	11	1,217	14	1,553	20	16,0
TMEM214	Transmembrane protein 214	77,15	2,315	21	4,007	22	0,916	24	2,683	5	16,8
TXNDC12	Thioredoxin domain-containing protein 12	19,206	2,982	14	4,372	16	1,217	13	1,095	25	17,7
CYB5B	Cytochrome b5 type B	14,846	2,357	20	3,202	33	1,308	9	1,113	24	19,8
HMOX2	Heme oxygenase 2	36,032	3,322	11	4,212	20	0,968	21	1,083	26	20,8
ATL3	Atlastin-3	60,541	1,757	38	5,427	6	0,603	33	1,991	8	21,0
ATP2A2	Sarcoplasmic/endoplasmic reticulum calcium ATPase 2	109,73	2,064	29	4,338	18	0,900	25	1,630	18	22,2
SPCS2	Signal peptidase complex subunit 2	17,027	2,063	30	2,835	40	1,277	11	1,469	21	22,3
VAT1	Synaptic vesicle membrane protein VAT-1 homolog	41,92	4,925	2	5,195	8	0,789	28	0,674	36	23,0
HCCS	Cytochrome c-type heme lyase	30,601	2,258	24	5,015	10	0,959	22	0,888	31	23,3
HADHA	Trifunctional enzyme subunit alpha, mitochondrial	82,999	1,803	36	4,103	21	0,760	29	1,755	13	23,5
SQLE	Squalene monooxygenase	53,067	2,066	28	3,425	29	0,976	20	1,447	22	23,5
TMPO	Lamina-associated polypeptide 2, isoforms beta/gamma	50,67	1,819	35	3,163	34	0,992	18	1,611	19	23,8
DHCR7	7-dehydrocholesterol reductase	54,489	1,601	42	4,355	17	0,983	19	1,136	23	23,8
PARK7	Protein deglycase DJ-1	19,891	2,125	26	2,823	41	1,262	12	0,982	28	24,5
ENDOD1	Endonuclease domain-containing 1 protein	55,016	1,988	32	3,019	37	0,726	30	1,908	11	25,2
CLPTM1L	Cleft lip and palate transmembrane protein 1-like protein	58,355	2,465	19	3,692	25	0,713	31	1,026	27	26,7
VDAC2	Voltage-dependent anion-selective channel protein 2	31,566	2,261	23	5,264	7	0,415	37	0,892	30	27,3
PRKCSH	Glucosidase 2 subunit beta	60,192	1,615	41	3,083	36	1,069	16	0,885	32	28,8
TXNRD1	Thioredoxin reductase 1, cytoplasmic	60,078	2,092	27	3,280	31	0,592	34	0,901	29	30,7
VDAC3	Voltage-dependent anion-selective channel protein 3	30,658	2,303	22	5,173	9	0,288	40	0,557	37	30,8
ALDH3A2	Fatty aldehyde dehydrogenase	44,648	2,988	13	3,772	24	0,425	36	0,164	41	31,8
SACM1L	Phosphatidylinositide phosphatase SAC1	66,966	1,653	40	3,446	27	0,603	32	0,852	34	33,2
LRRC59	Leucine-rich repeat-containing protein 59	34,93	2,049	31	3,437	28	0,531	35	0,727	35	33,2
COMT	Catechol O-methyltransferase	24,449	1,967	33	2,588	42	0,803	27	0,455	38	34,2
FKBP8	Peptidyl-prolyl cis-trans isomerase FKBP8	44,561	1,754	39	3,279	32	0,330	38	0,871	33	35,5
CANX	Calnexin	67,567	1,789	37	3,691	26	0,278	41	0,308	40	37,5
OCIAD1	OCIA domain-containing protein 1	27,626	1,871	34	2,993	39	0,327	39	0,357	39	38,2
NT5DC1	5-nucleotidase domain-containing protein 1	51,844	2,129	25	2,998	38	0,120	42	0,086	42	38,5

Table 20 | List of PS89 target proteins. Proteins identified by ABPP were determined as PS89 target proteins by the following criteria: (1) Probe / DMSO: >3-fold enrichment (log_2 Probe / DMSO >1.6) and -log_{10} p-value >2. (2) Probe / PS89 log_2 enrichment >0. Ranks were assigned according to the degree of enrichment and reproducibility. The overall score was calculated as the average of all ranks with double weighting the Probe/PS89 competition values.

3.2.3 Target network and Gene Ontology analysis

Evaluating the polypharmacological profile of PS89, protein-protein interaction analysis was performed using the STRING database.[69] As shown in Figure 21a, 23 out of 42 PS89 target proteins were involved in a network with significantly more interactions than expected for a random set of proteins drawn from the genome. As this enrichment indicated that the proteins are biologically connected, the network was further analyzed by Gene Ontology (GO) functional classification for common cellular components (GO CC) and biological processes (GO BP, Figure 21b).[70] Regarding GO CC, a highly significant number of PS89 target proteins (n=22, FDR 5.9e-12) was localized in the endoplasmic reticulum (orange circles). Functionally, proteins involved in 'Cellular Homeostasis' and in particular 'Cell Redox Homeostasis' were highly enriched in the data set of PS89 targets in Jurkat cells (FDR 9.1e-07 and 6.7e-09). Exhibiting high overall scores (see Table 20), these terms included PDIA1 (gene name *P4HB*), a number of further PDI isoforms that have been linked with chemoresistance,[45, 71] and the B-cell receptor-associated protein 31 (BAP31, gene name *BCAP31*).

a

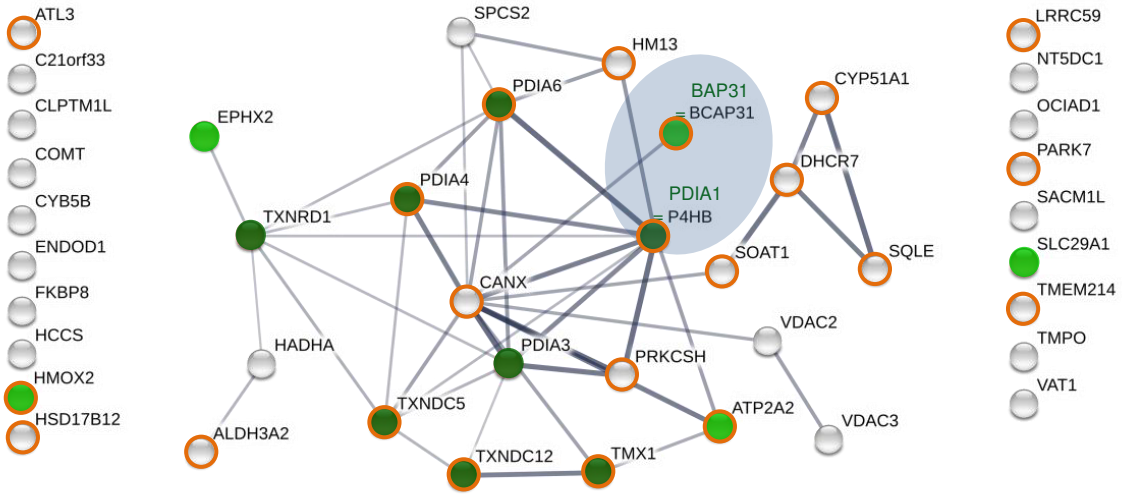

b

Pathway ID	*Pathway Description*	*Count in Gene Set*	*FDR*
Cellular Component (GO)			
GO:0005783	Endoplasmatic Reticulum	22	5.9e-12
Biological Process (GO)			
GO:0045454	Cell Redox Homeostasis	8	6.7e-09
GO:0019725	Cellular Homeostasis	13	9.1e-07

Figure 21 | STRING network of PS89 target proteins. (**a**) Protein-protein interaction analysis of PS89 target proteins (n=42) by the web resource STRING v10. Line thickness indicates the strength of data support. (**b**) Functional enrichment analysis of the STRING network by Gene Ontology (GO) classification. Most prominent terms of GO Cellular Component (orange circles) and GO Biological Process (green dots) are highlighted.

3.3 Signal Transduction via the BAP31-Caspase-8 Axis

Summarizing sections 3.1 and 3.2, apoptosis of acute leukemia cells was not induced *per se* targeting the ER redox environment with PS89, but was rather dependent on the stimuli of cytostatics. Inquiring how those induce cell death, the majority of cytostatics has in common that the mitochondrial pathway plays the predominant role for the execution of apoptosis.[72-74] Therefore, we hypothesized dynamics between the ER and mitochondria in PS89 combination treatments and particularly expected a crucial function of the B-cell receptor-associated protein 31 (BAP31). This protein is a major pro-apoptotic communicator at the interface of ER and mitochondria[26, 75] as well as one of the most prominent PS89 targets (Figure 20 and Table 20).

3.3.1 Co-staining of the PS89 photo probe and BAP31

For BAP31 target validation, a co-staining was performed using a BAP31-specific antibody and the PS89 photo probe linked to a rhodamine reporter (5-TAMRA-Azide) by click chemistry. Besides the supposed ER specificity of both, overlapping fluorescence was computed and revealed distinct co-localized ER network structures of PS89 photo probe-rhodamine (red) and BAP31-Alexa 488 (green, Figure 22a). This suggested a consolidated binding to the same protein target. Analyzed in parallel, no background staining of either the Alexa 488 secondary antibody or the dye 5-TAMRA-Azide was detected (Figure 22b).

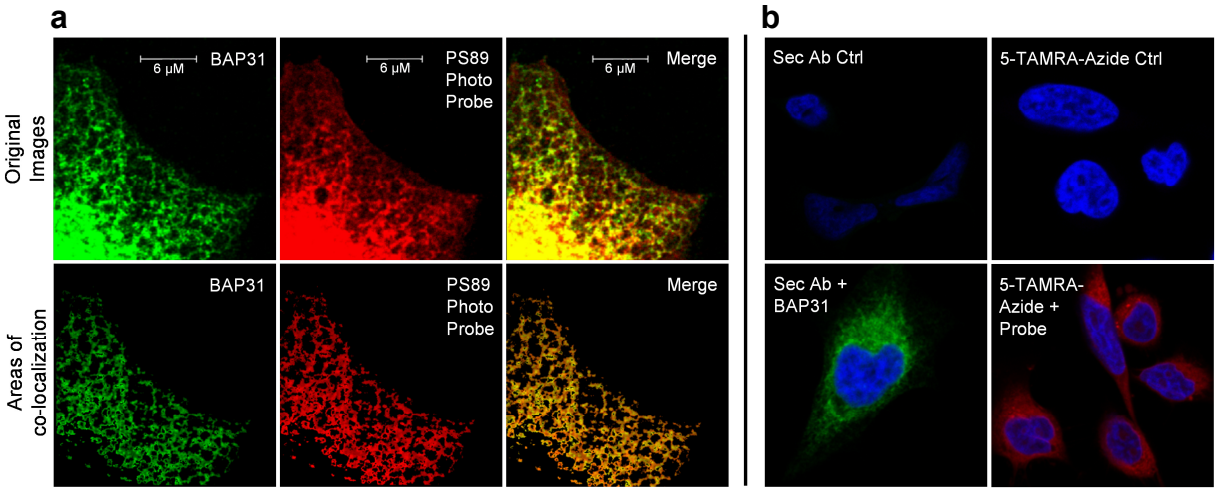

Figure 22 | Co-localization of BAP31 and the PS89 photo probe. (**a**) Immunofluorescence staining of B-cell receptor-associated protein 31 (BAP31, green) and the PS89 photo probe linked to a rhodamine reporter (5-TAMRA-Azide, red) in Hela cells. Representative original confocal microscopy images (upper row) and areas of co-localization analyzed with Leica LAS X software (lower row) are shown. (**b**) Left column: control of secondary antibody background with respect to BAP31 primary + secondary antibody staining (Sec Ab + BAP31). Right column: control of 5-TAMRA-Azide background with respect to PS89 photo probe samples after UV crosslinking and coupling to the rhodamine reporter (5-TAMRA-Azide + Probe). Nuclei were stained with Hoechst 33342.

3.3.2 Cleavage of BAP31 and caspase-8 in PS89 and etoposide treated cells

Following the hypothesis of a BAP31 dependent pathway linking ER redox disturbance and signaling of cytostatics, the cleavage of BAP31 into the pro-apoptotic p20BAP31 fragment was analyzed. Considering that caspase-8 (CASP8) executes BAP31 cleavage, the expression and processing of CASP8 was evaluated concurrently. In PS89 and ETO combination treated cells, an increased CASP8 activity represented by p43/41 cleavage products was detected compared to ETO single treatment (Figure 23a). Moreover, cleavage of BAP31 was only present in PS89 combination treated cells and, as an early trigger, already visible after 24 h stimulation (Figure 23b).

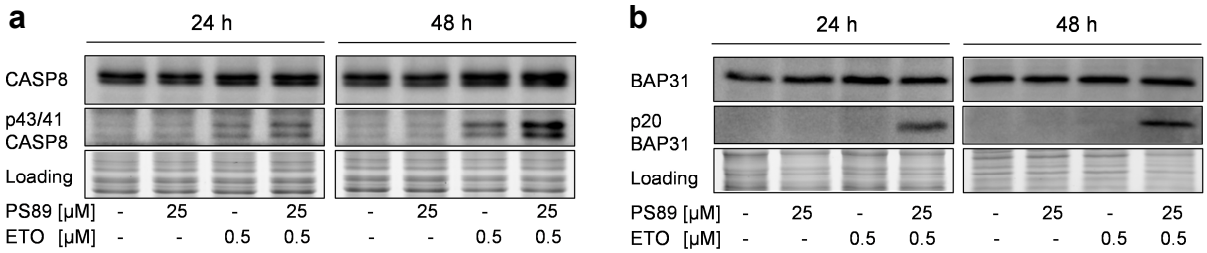

Figure 23 | Cleavage of endogenous CASP8 and BAP31. Jurkat cells treated with PS89 and etoposide (ETO) were subjected to Western blot analysis. (**a**) Protein level of the caspase-8 (CASP8) zymogen and the cleavage products p43/41 CASP8 determined after 24 h and 48 h. (**b**) Protein level of B-cell receptor-associated protein 31 (BAP31) and the cleavage product p20BAP31 determined after 24 h and 48 h.

3.3.3 Co-immunoprecipitation of the BAP31-caspase-8 complex

It has been shown previously that BAP31 within a protein complex serves as a platform for CASP8 activation upon apoptotic stimuli and death effector domain (DED) interactions.[29] Hence, the influence of PS89 on the BAP31-CASP8 association was examined. In co-immunoprecipitated samples (BAP31 pulldown), pro-CASP8 was associated with BAP31 independently of treatment. Though cleaved p43/41 CASP8 was only detected in the presence of both stimulants, PS89 and ETO (Figure 24). The BAP31 antibody incubated without lysate served as control of heavy and light chains which were detected on the protein gel (Loading), but not on the blot (Lane 5, Ab Ctrl).

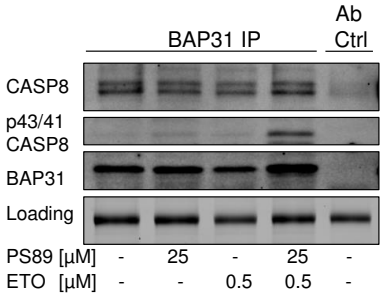

Figure 24 | Co-immunoprecipitation of BAP31, pro- and cleaved CASP8. B-cell receptor-associated protein 31 (BAP31) was precipitated from Jurkat cell lysates after 24 h stimulation with PS89 and etoposide (ETO). Blots were probed for BAP31 and caspase-8 (CASP8). BAP31 antibody served as control of heavy and light chains and an equal amount of precipitation antibody was confirmed on stainfree gels (loading).

3.3.4 Suppression of apoptosis by caspase-8 inhibition

In order to provide further evidence that apoptosis induced by PS89 and ETO combination treatments is critically dependent on CASP8 activity, cells were stimulated in presence of the irreversible CASP8 inhibitor Z-IETD-FMK, which dose-dependently reduced the number of apoptotic cells (Figure 25a). The specificity of Z-IETD-FMK was confirmed by immunoblot analysis of CASP8 showing reduced auto-catalytic activity and p43/41 cleavage, respectively. In accordance, the ratio of apoptotic cells in PS89 combination versus ETO single treatment was lower in CASP8 deficient Jurkat cells (Figure 25b, 1.7-fold in CASP8 -/- Jurkat vs. 2.8-fold in wildtype Jurkat cells). The stable CASP8 knockout was confirmed by Western blot (Figure 25b).

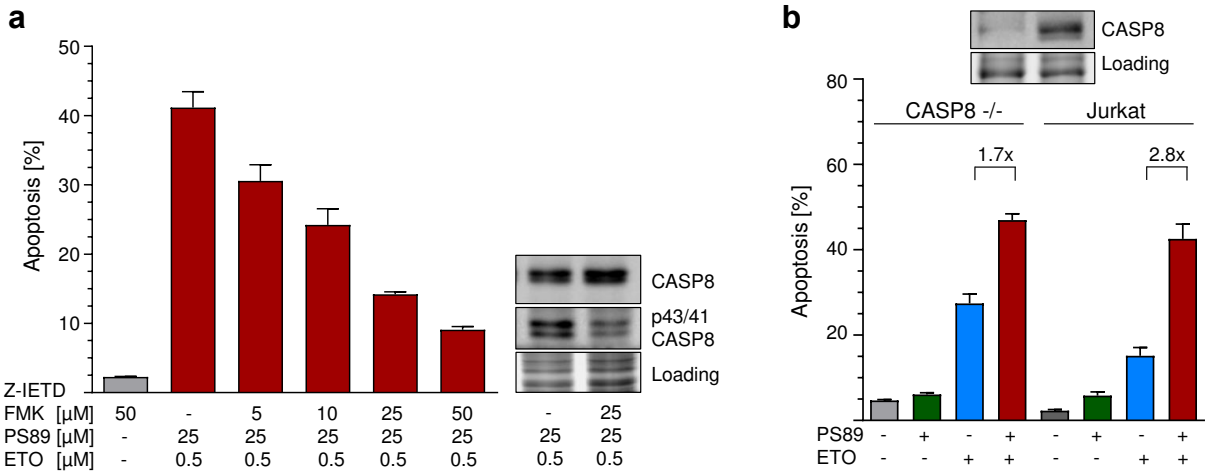

Figure 25 | Decreasing apoptosis by CASP8 inhibition or knockout. (**a**) Apoptosis of Jurkat cells treated with PS89 and etoposide (ETO) in presence of the specific caspase-8 (CASP8) inhibitor Z-IETD-FMK after 48 h. Percentage of apoptotic cells was determined by propidium iodide staining and flow cytometry. Protein expression of CASP8 and the cleavage products p43/41 CASP8 was determined by Western blot. (**b**) Apoptosis of CASP8 deficient (CASP8 -/-) or wildtype Jurkat cells treated with PS89 25 µM and ETO (250 nM and 500 nM, respectively) for 48 h. Percentage of apoptotic cells was determined by propidium iodide staining and flow cytometry. Knockout of CASP8 was verified by Western Blot.

3.3.5 Prevention of PS89 chemosensitization by BAP31 silencing

As the activation of the BAP31-CASP8-axis was now clearly demonstrated in PS89 combination treatments, the consequence of BAP31 silencing, supposed to disable binding of PS89 to its direct target, was studied. In control transfected cells (siCtrl), PS89 was able to significantly increase ETO triggered apoptosis as expected. However, BAP31 knockdown (siBAP31) prevented additional cytotoxicity of the combination compared to ETO single treatment (Figure 26). Efficient siRNA knockdown of BAP31 was determined in parallel by immunoblotting.

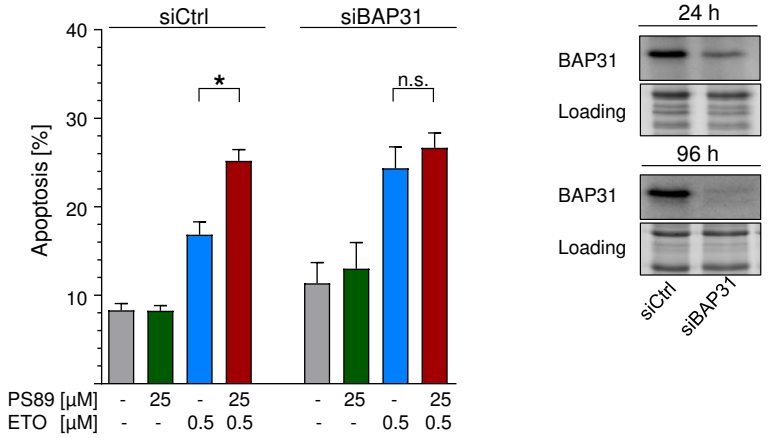

Figure 26 | Non-significant effect of PS89 in BAP31 silenced cells. Apoptosis of Hela cells transfected with non-targeting siRNA (siCtrl) or BAP31 specific siRNA (siBAP31). 6 h post-transfection, cells were treated with PS89 and etoposide (ETO) for 48 h. Percentage of apoptotic cells was determined by propidium iodide staining and flow cytometry. Statistics: One way ANOVA, Bonferroni, $p<0.01$. Silencing of BAP31 was verified by Western blot.

3.4 Pro-Apoptotic Crosstalk at the ER-Mitochondrial Interface

3.4.1 Elevation of cytosolic calcium levels

A consequence of BAP31 cleavage is calcium release from the ER mediating ER-mitochondrial crosstalk.[29, 31] A shifted Cal-520 fluorescence intensity and thus higher cytosolic calcium levels were observed in PS89 combination treated cells after 48 h compared to ETO single treatment (Figure 27a). Further, a time-dependent analysis of intracellular calcium was performed normalizing the Cal-520 mean fluorescence intensity to DMSO control. Interestingly, amplification of calcium release was observed from 24 h to 48 h in PS89 combination, but not ETO single treated cells (Figure 27b).

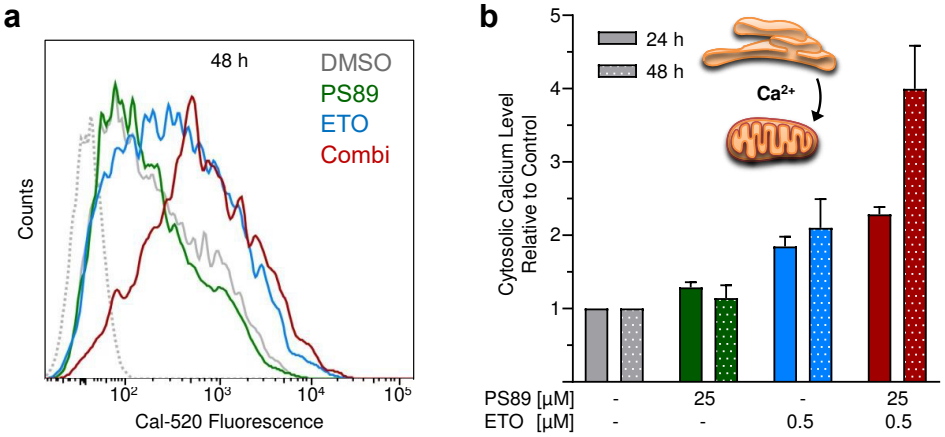

Figure 27 | Time-dependent increase of intracellular calcium levels. (**a**) Fluorescence intensity of Cal-520 determined by FACS analysis of Jurkat cells after 48 h treatment (dotted grey line: unstained control, grey: DMSO, green: PS89 25 µM, blue: etoposide (ETO) 0.5 µM, red: combination). (**b**) Mean values of Cal-520 fluorescence intensity normalized to DMSO control after 24 h and 48 h treatment.

3.4.2 Dissipation of mitochondrial membrane potential and intrinsic apoptosis

Mitochondria are able to buffer high levels of cytosolic calcium, though an overload and prolonged opening of the permeability transition pore (MPTP) coincide with disruption of the mitochondrial membrane potential (ΔΨm).[76] The ratio of cells with intact and dissipated ΔΨm is therefore indicative for mitochondrial damage. Using the dye JC-1 which exhibits ΔΨm-dependent aggregation, mitochondrial depolarization was demonstrated by a decrease in the red/green fluorescence ratio in PS89 and ETO treated Jurkat cells after 48 h (Figure 28a). In addition, a quantification of the cell population with dissipated membrane potential confirms that mitochondrial damage is highly increased by co-incubation of ETO with PS89 (Figure 28b, 24 h: ETO 9% vs. Combination 19%; 48 h: ETO 21% vs. Combination 55%).

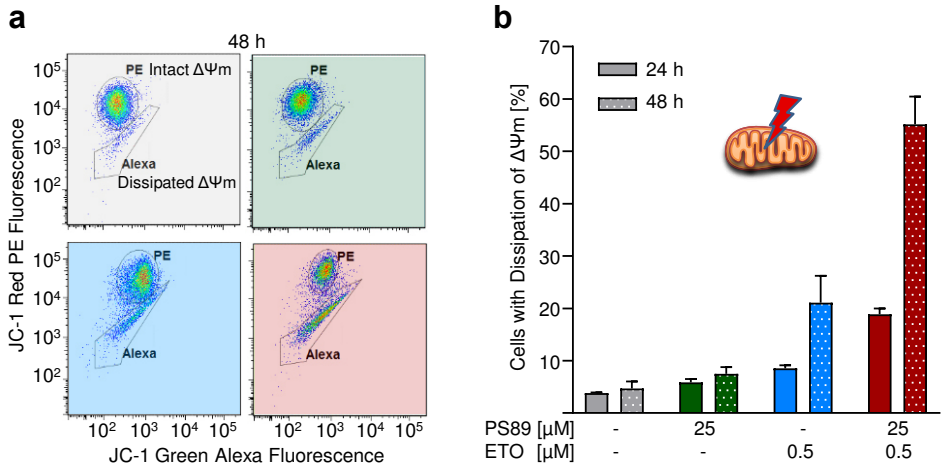

Figure 28 | Disruption of the mitochondrial membrane potential (ΔΨm). (**a**) JC-1 staining and FACS analysis of Jurkat cells after 48 h treatment (grey: DMSO, green: PS89 25 µM, blue: etoposide (ETO) 0.5 µM, red: combination). Two populations with intact or dissipated ΔΨm are distinguished dependent on the PE (red) / Alexa (green) fluorescence ratio. (**b**) Quantification of Jurkat cells with dissipated ΔΨm after 24 h and 48 h treatment.

Mitochondrial apoptosis proceeds upon the assembly of the pro-apoptotic proteins Bax and Bak into oligomeric pore complexes which trigger mitochondrial outer membrane permeabilization (MOMP). As a tightly regulated process, MOMP is further under control of several Bcl-2 family proteins including anti-apoptotic Bcl-2 and Bcl-xL. As shown in Figure 29a, Jurkat cells overexpressing Bcl-2 or Bcl-xL were significantly less sensitive towards PS89 combination treatments than the empty vector cell line Jurkat/*neo*. This demonstrated that cell death was effectively executed only upon functional mitochondrial apoptosis signaling. The overexpression of anti-apoptotic proteins in Jurkat/*Bcl-2* and Jurkat/*Bcl-xL* cells was confirmed by Western blot (Figure 29b).

As a result of MOMP, pro-apoptotic factors such as cytochrome c (Cyt c) are released from the intermembrane space of mitochondria into the cytosol. Therefore, a separation of mitochondria from cytosolic fractions was performed prior to immunoblot analysis. For the purity of fractions, the voltage-dependent anion channel (VDAC) was indicative as it is located at the outer mitochondrial membrane and was not detected in the cytosolic part (Figure 29c). In contrast, Cyt c was found in the cytosol of PS89 and ETO combination treated cells which supported the significance of apoptosis execution via the intrinsic pathway (Figure 29c).

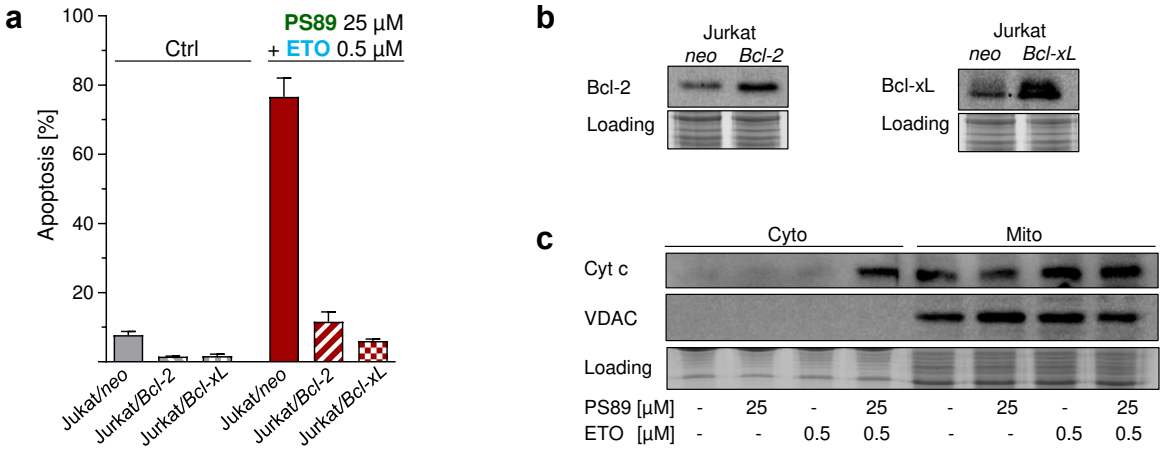

Figure 29 | Mitochondrial apoptosis. (**a**) Suppression of apoptosis induction in Jurkat cells overexpressing Bcl-2 (Jurkat/*Bcl-2*) or Bcl-xL (Jurkat/*Bcl-xL*) compared to the empty vector cell line (Jurkat/*neo*). Cells were treated with PS89 and etoposide (ETO) for 48 h. Percentage of apoptotic cells was determined by propidium iodide staining and flow cytometry. (**b**) Verification of Bcl-2 and Bcl-xL overexpression by Western blot. (**c**) Cytochrome c (Cyt c) protein levels in cytosolic (Cyto) and mitochondrial (Mito) fractions analyzed by Western blot after treatment of Jurkat cells with PS89 and ETO for 48 h. The voltage-dependent anion channel (VDAC) was analyzed in parallel to verify Cyto-Mito fractionation.

3.4.3 Generation of reactive oxygen species

Mitochondrial damage is accompanied by an accumulation of reactive oxygen species (ROS).[77, 78] Using the redox-sensitive dye Carboxy-H_2DCFDA, ROS induction by ETO was verified and ROS levels were further amplified in combination treatment with PS89 (Figure 30a). This was quantified normalizing the shift of DCF fluorescence intensity towards DMSO control (Figure 30b, mean intensity ETO: 816 vs. PS89 + ETO: 1356). ROS signaling from mitochondria to the ER provokes further disturbance of ER redox homeostasis and finally closes the feedback loop.

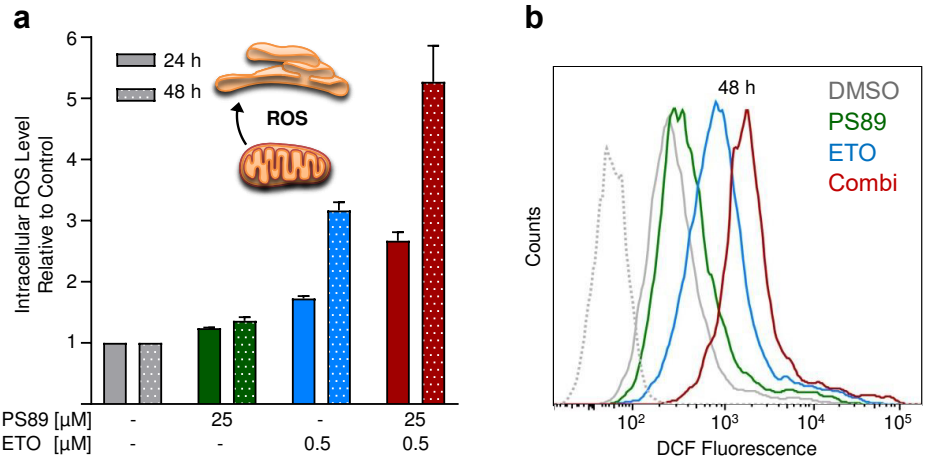

Figure 30 | PS89 mediated amplification of ROS production. (**a**) Jurkat cells treated for 24 h or 48 h with PS89 and etoposide (ETO) were loaded with the redox sensitive dye Carboxy-H_2DCFDA and analyzed by flow cytometry. Intracellular reactive oxygen species (ROS) levels are expressed as mean values of DCF fluorescence intensity normalized to DMSO control. (**b**) Representative overlay of DCF fluorescence curves determined by flow cytometry after 48 h treatment (dotted grey line: unstained control, grey: DMSO, green: PS89 25 µM, blue: ETO 0.5 µM, red: combination).

3.5 Summary

In summary, PS89 highly increases the effectiveness of cytostatics through a crosstalk and mutual amplification of pro-apoptotic stress triggers promoting mitochondrial apoptosis (Figure 31). This is achieved by directly targeting a network of ER homeostasis proteins which is depicted by the main targets BAP31 and PDI in the graphical summary. BAP31 critically contributes to the communication from ER to mitochondria resulting from cleavage into p20BAP31 by active caspase-8 and subsequent calcium release, both explicitly favored in presence of the chemosensitizer PS89. Thus, the present study discloses the potential of dually targeting the ER-mitochondrial apoptosis network as a novel and strongly synergistic drug combination strategy.

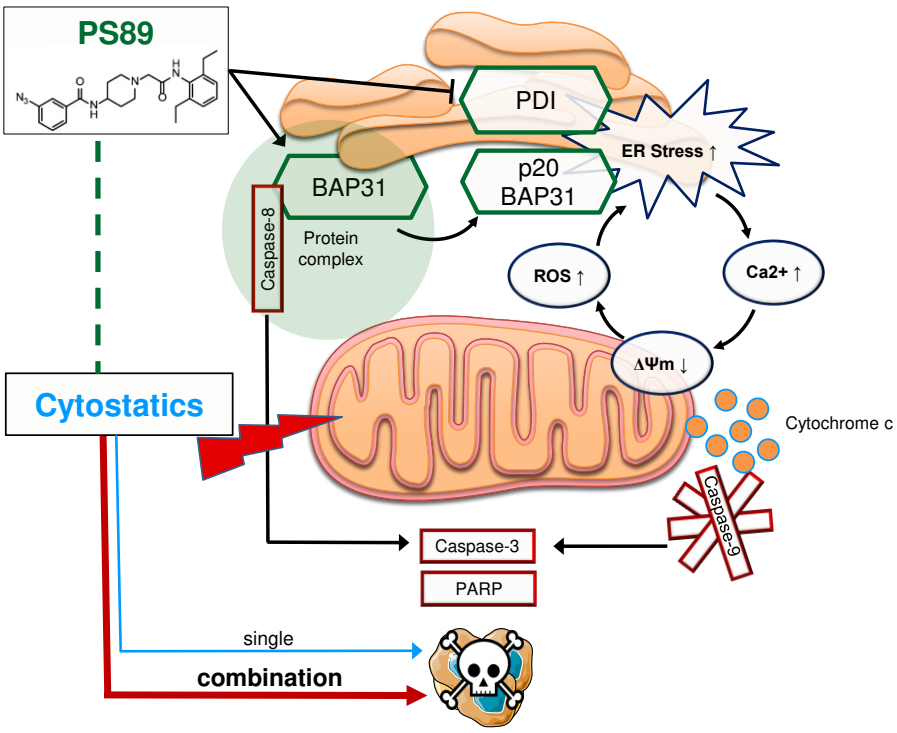

Figure 31 | Communication at the ER-mitochondrial interface of cell death in PS89 combination treatments. The polypharmacological profile of the small molecule compound PS89 targeting a network of ER homeostasis proteins is represented by its main targets PDI and BAP31. Upon apoptotic stimuli of cytostatics and exclusively in presence of PS89, BAP31 is cleaved by caspase-8 to pro-apoptotic p20BAP31. Subsequent calcium release from the ER and increased ER stress promote loss of mitochondrial membrane potential (ΔΨm) and mitochondrial apoptosis. In turn, elevated production of reactive oxygen species (ROS) feeds back to the ER and is able to provoke further ER stress and calcium release. The mutual amplification of ER-mitochondrial stress triggers finally leads to synergistic activation of executioner caspases and apoptosis in the combinatory treatment approach with cytostatics and the chemosensitizer PS89.

4 Discussion

4.1 PS89: a Drug Candidate for Combination Therapies

4.1.1 Chemosensitization of acute leukemia cells

This work reveals that activating the apoptotic machinery at the ER-mitochondrial interface by PS89 and cytostatics is a highly favorable strategy to sensitize acute leukemia cells. Strikingly, the term chemosensitization applies here as PS89 demonstrated the ability to increase the effectiveness of chemotherapeutics although the compound itself was employed at subtoxic concentrations in all assays.

Motivated by the initial observation that PS89 sensitized Jurkat cells towards etoposide treatment, the concept was successfully transferred to further acute leukemia models. Here, the co-stimulation with PS89 resulted in a highly synergistic apoptosis response in ALL and AML cell lines, drug resistant and patient derived xenograft (PDX) cells. In particular, PS89 was able to sensitize relapsed AML PDX cells with poor prognostic features.[57] As the doses of chemotherapeutics could be reduced at least by half in combination with PS89 while maintaining efficacy, this approach may especially be interesting for the treatment of acute leukemia patients unable to receive intensive chemotherapy. Indeed, there remains a significant unmet need for novel therapeutic strategies in this subgroup and as one promising approach, the combination of low-intensity treatments with novel agents has been proposed.[19]

The positive interference of PS89 with cytostatics was at the same time not limited to etoposide, but also achieved in combination with daunorubicin and vincristine. Of note, drugs targeting ER homeostasis constitute a novel compound class which is supposed to be successful independent of major ALL and AML mutations and may serve as a powerful option to overcome resistances against established drugs. At lower concentrations of cytostatics, the combination with PS89 additionally resulted in strongly inhibited proliferation and colony formation of leukemia cells. Altogether, this broad applicability and favorable chemosensitizing properties qualify PS89 as a promising drug candidate.

4.1.2 Directions in PS89 drug development

In order to exploit the full potential of PS89, two major issues were envisaged for further drug development: 1) the mechanistic background of the synergistic interaction which was particularly addressed in the present work and 2) the pharmacokinetic and pharmacodynamic characterization of PS89 *in vivo* which will be briefly discussed in the following section.

A precondition for *in vivo* studies is the demonstration of PS89 safety and the evaluation of appropriate dosing. At the current stage, this point is supported by an initial toxicity test of our lab that showed good tolerability of PS89 after daily i. p. injection of 10 - 30 mg/kg doses into SCID mice.[79] Then, pharmacokinetic studies are required as the bioavailability and metabolism of PS89 remain open issues so far. At least from a structural point of view, PS89 features suitable druglike properties and satisfies the Lipinski rule of five indicating oral bioavailability. Regarding pharmacologic interactions, the present study already recognized a therapeutically relevant antagonism of PS89 with cytarabine (Ara-C). This is likely based on the binding of PS89 to the equilibrative nucleoside transporter 1 (ENT1, gene name *SLC29A1*) which was identified in the proteomics target screening. This presumably blocks the transport capacity of ENT1 which is responsible for the cellular uptake of Ara-C. Finally, the efficacy as well as dose-response relationship of PS89 in combination with cytostatics needs to be evaluated *in vivo*. Here, it is envisaged that established leukemia models of patient-derived cells growing in mice will be of special prognostic value.[56, 57]

Approaching to the mechanistic point of the agenda, several conclusions could be drawn already from the functional *in vitro* data. The activity of PS89 in several cell culture models indicated a broadly applicable rather than cell-type specific signaling. This was critically dependent on an apoptotic trigger by cytostatics, though independent of their direct targets. And as finally shown by pre- versus co-stimulation experiments, apoptosis induction of PS89 combinations was most effective and therefore basically relied on the concurrent interaction of both compounds. Aiming to elucidate this crosstalk, the present work on PS89 targets will be discussed with reference to the current understanding of chemotherapy response.

4.2 Determinants of Response to Chemotherapy

It is well-established that the majority of classic cytostatics initiate apoptosis via the mitochondrial pathway.[72-74] However, it has been poorly understood which mechanisms account for the differential success of chemotherapy between individuals and why some cells are more sensitive than others. In an approach to answer this question, the response to chemotherapy was recently correlated with the distinct proximity of cells' mitochondria to the apoptotic threshold, a property called mitochondrial priming.[80, 81] This 'readiness for apoptosis' was defined by the balance of pro- and anti-apoptotic buffers within a cell and governed by the Bcl-2 family. As it has been shown that acute leukemias are among the most highly primed cancers, they are generally more chemosensitive than others.[80] Moreover, the therapeutic index in AML was in fact determined by the priming of myeloblasts relative to normal hematopoietic stem cells.[82] Translated to the present findings that ALL and AML PDX cells were more vulnerable towards PS89 combination treatments than PBMCs, it is conceivable that their pretreatment priming accounts for the discrete sensitivity. In terms of the mechanistic PS89 study, it is however even more important to note that mitochondria are not only the main executers of apoptosis, but also gatekeepers which determine the sensitivity towards cytotoxic chemotherapy.

As outlined in section 4.1, we could increase the sensitivity of even chemoresistant leukemic cells with PS89 and cytostatics, which was accompanied by activation of the executioner caspase-3 and cleavage of the DNA repair enzyme PARP. Notably, not only these downstream hallmarks of apoptosis, but also the dissipation of the mitochondrial membrane potential as well as cytochrome c release from mitochondria was strongly supported by the co-treatment with PS89. This was of interest as the proteomics target screen revealed that the most prominent PS89 target proteins were located at the ER. In line, PS89 has been shown to inhibit the ER-resident protein disulfide isomerase (PDI) previously.[49] Thus, we envisaged that PS89 affected the mitochondrial apoptosis threshold or priming, respectively, through an ER triggered input to the intrinsic pathway. Henceforward, this hypothesis was subjected to further investigation and the most apparent way guided us to the prominent PS89 target PDI at first.

4.3 PDI Inhibition and the PS89 Target Network

It is common understanding that PDI inhibitors act by accumulating misfolded proteins which leads to ER stress, activation of the unfolded protein response (UPR) and cell death.[42, 47, 48] As the connection from the UPR to the mitochondrial apoptotic pathway is well-established,[24] this link seemed conclusive to explain the sensitizing effects of the PDI inhibitor PS89. However, no induction of ER stress or UPR was observed in our previous study applying PS89 at subtoxic concentrations, but only together with etoposide.[49] This indicated that activation of the ER stress response is not primary induced by PS89, but rather results from the disability of the ER to resolve a stress condition triggered by PS89 in cooperation with cytostatics.

Hence, the causative responsibility of the PS89 main target PDI for the chemosensitizing effects was evaluated. Surprisingly, PDI silencing had no effect on Jurkat cell viability or the sensitivity of cells towards etoposide treatment. The consequences of PDI knockdown are however controversially discussed in literature concerning the direct effect of PDI silencing,[47, 83] as well as the ability to sensitize cancer cells.[71, 84] The feasibility of a single PDI knockdown was additionally questioned by another report because many ER stress chaperones feature PDI activity as well. The authors therefore proposed to overexpress PDI instead and evaluate if this abrogated the functional effect of PDI inhibitors.[85] This strategy was not successful to rescue PS89 activity either, but correlated with the observation that the effectiveness of PS89 was entirely independent of PDI expression in leukemia cell lines. So, we concluded that the strong sensitizing properties were rather a result of polypharmacology than single-targeting of PDI.

This was supported by the PS89 activity-based protein profiling (ABPP) approach in conjunction with STRING network analysis. It revealed a total of 7 PDI family members targeted by PS89 including PDIA3, PDIA4 and PDIA6 which all potentially mediate chemoresistance and were recognized as promising drug targets previously.[45, 71] Moreover, a recent report highlighted that the function of PDIA6 is not restricted to protein folding, but also controls UPR signaling by direct interaction with the ER stress sensor IRE1α.[86] As a consequence, a higher responsiveness to ER stress and decreased proliferation was observed in PDIA6 depleted cells. This direct involvement in the

control of the UPR uncovered a novel perspective on the function of PDIs and encourages their further investigation as physiologic regulators as well as drug targets.

Taking into account that the 7 PDI isoforms were further meshed in a PS89 target network of overall 23 proteins, it seems likely that this broad-spectrum targeting of ER homeostasis finally imparts PS89 the ability to mediate the robust sensitizing effects that have been observed. In a broader context, this opinion supports the argumentation for network pharmacology to combat complex diseases such as cancer.[50, 87] In this conception, multi-target strategies rather than the 'one drug, one target' paradigm are proposed to be superior to rewire cancer-specific networks.[88, 89] Adopting this network view to elucidate how combination therapy works, it remains interesting how drugs interact beyond the border of subcellular compartments. This leads back to the still pending question, namely how PS89 and cytostatics finally cooperate to activate the UPR and stimulate mitochondrial apoptosis.

4.4 Bidirectional Communication at the ER-Mitochondrial Interface

Summarizing sections 4.2 and 4.3, PS89 targets a network of proteins in the ER, while mitochondria critically determine the response towards cytotoxic chemotherapy. The integrity of mitochondria and the intrinsic pathway of apoptosis are regulated by a sophisticated array of checks and balances. These are in turn significantly influenced by the capability of the ER to either buffer cellular stress conditions or switch to pro-death signaling upon irreparable ER stress. This close relation of ER and mitochondria has been thoroughly reviewed resulting in the notion that cell fate is essentially dependent on the crosstalk of apoptotic signaling at the ER-mitochondrial interface.[24-27]

Applying cytostatics together with the ER targeting compound PS89, we demonstrate here that the concept of ER-mitochondrial 'amplification by communication' can be exploited for combination therapy. This statement is based on data disclosing a strong induction of calcium and ROS as well as pro-apoptotic signaling via the ER resident B-cell receptor-associated protein 31 (BAP31). Depicting how they are interconnected, this set of data will be discussed with reference to literature.

Stimulating cells with PS89 combinations, the primary events affecting mitochondria are most likely triggered by cytostatics in a p53-dependent manner or by direct binding to mitochondria complex I, a novel mechanism shown for DNA-targeting agents recently.[78] This promotes the accumulation of mitochondrial ROS, which is in accordance with the present data showing elevated ROS levels in etoposide treated cells. Alternatively, cytostatics bridge the ER-mitochondrial interface via the mitochondrial fission 1 protein (Fis1) which has been demonstrated to form a complex with BAP31 and facilitate the caspase-8 (CASP8) mediated cleavage into p20BAP31.[29] Analyzing this route in the present work, PS89 in combination with etoposide highly enhanced the activation of CASP8 which coincided with BAP31 cleavage. Of note, the cleavage of endogenous BAP31 was not only shown with cytostatics previously, but also with the ER stress inducer Brefeldin A.[32] We therefore anticipate that ER redox disturbance by mitochondrial ROS and PDI inhibition by PS89 highly support the processing of BAP31.

Temporally, BAP31 cleavage and consequent calcium release from the ER have been identified as early events in apoptosis signaling from mitochondria to ER and back.[29] Indeed, the processing of BAP31 was observed in co-treated cells already after 24 h. Subsequently, an amplification of calcium release was shown between 24 h and 48 h in PS89 combination, but not etoposide single treated cells. This supports that PS89 is the main actor to establish ER-driven feedback. Mitochondria-directed calcium flux finally promotes mitochondrial outer membrane permeabilization (MOMP) and cytochrome c release,[24, 27] which was demonstrated to be increased in PS89 co-stimulated cells as well.

In summary, PS89 is able to augment apoptotic triggers of cytostatics by lowering the threshold to tune pro-apoptotic feedback from the ER. With reference to the concept of S. Grimm who specified the ER-mitochondrial 'social network of cell death',[25] it is conceivable that this feedback achieves the significant amplification effect by reaching numerous mitochondria for cell death induction, even if the original cytostatics stimulus targeted only a few. PS89 could therefore stably intensify the response towards cytostatics treatment in a variety of acute leukemia cell lines and PDX cells. This altogether discloses the potential of targeting the ER-mitochondrial apoptosis network as a novel and strongly synergistic drug combination strategy.

4.5 PS89 as the First Small-Molecule Compound Targeting BAP31

It was now clearly demonstrated that the highly positive interference of PS89 with the signaling of cytostatics happens at the ER-mitochondrial interface. An implication of BAP31 in the crosstalk of PS89 with cytostatics was identified in addition. However, one aspect that made us especially curious about BAP31 was not addressed so far. It is the fact that BAP31 was not only mediator, but also a direct target of PS89. The binding of PS89 to BAP31 was initially recognized by the proteomics target screen and according to the ranking score, BAP31 was among the three most highly enriched proteins. This was validated by a staining of the PS89 photo probe with a BAP31-specific antibody showing consolidated binding to the same target. In order to understand how the binding of PS89 influences BAP31, a closer examination of the BAP31 protein complex is required. As already mentioned, Fis1 was shown to form a tripartite complex with BAP31 and caspase-8 (CASP8).[29] This complex seems to be further under control of the cell death-inducing p53-target protein 1 (CDIP1) as well as the anti-apoptotic proteins Bcl-2 and Bcl-xL.[32] However, the dynamics which regulate the balance of pro- and anti-apoptotic proteins within the complex have not been clarified yet.

PS89 is to our knowledge the first BAP31 binding small-molecule compound described and was shown to facilitate BAP31 cleavage upon cytostatics stimuli. Thus, we propose that PS89 may serve as a valuable tool to study the complex dynamics and to manipulate BAP31 interactions that favor the pro-apoptotic output. While an option to realize this project will be discussed in section 4.6, the particular interaction of BAP31 with CASP8 was already addressed in the present study.

BAP31 is a substrate of CASP8 but at the same time, the BAP31 protein complex has been identified to serve as a platform for CASP8 activation.[29] This is based on a variant death effector domain (vDED) that was recognized in BAP31 and responsible for the interaction with CASP8.[29, 90] Here we show for the first time the intermediate p43/41 cleavage product of CASP8 associated with BAP31, which still holds a DED-domain for DED-DED interaction. This supports the suggestion of Iwasawa *et al*. [29] that further processing into the finally active p18 fragment in fact happens at the BAP31 complex. Thus, the activation of CASP8 independent of an extrinsic stimulus likely accounts for the

critical role of CASP8 in the apoptosis signaling of PS89 combination treatments. This was demonstrated by significantly decreased apoptosis rates in presence of the CASP8 inhibitor Z-IETD-FMK.

Finally evaluating the significance of BAP31, it is important to consider that we detected p43/41 CASP8 association as well as BAP31 cleavage exclusively in PS89 co-treated cells and silencing of BAP31 did furthermore rescue the chemosensitizing effect. Therefore, we conclude that BAP31 binding is a crucial feature for the bioactivity of PS89. The impact of BAP31 as a druggable tumor target certainly needs further validation and in line, a systematic analysis of BAP31 expression in hematological malignancies is missing to date. Though, overexpression of BAP31 seems to correlate with chemoresistance as shown in fludarabine-resistant mantle cell lymphoma[91] as well as proteasome inhibitor-adapted myeloma cells.[92] This altogether motivates a deeper analysis of BAP31 in hematologic cancers and particularly its role in the regulation of apoptotic signaling.

4.6 Future Perspectives

4.6.1 The influence of PS89 on BAP31 complex dynamics

In order to predict how PS89 interacted either with the membrane-bound or the cytosolic domain of BAP31, the discovery of the PS89 binding site will be a relevant field of future research. This could assist further drug optimization studies to develop PS89 derivatives with improved BAP31 binding properties. However, the structural biology approach is currently limited by the fact that a crystal structure has only been resolved for the C-terminal cytosolic part of BAP31 yet.[93]

Thus, a more feasible proceeding seems the examination of protein-protein interactions. The Biological General Repository for Interaction Datasets (BioGRID)[94] currently lists 79 interactors that have been discovered for BAP31. As those interactions are potentially altered through the binding of PS89, a future study aims to elucidate the composition of BAP31 binding proteins using immunoprecipitation and mass spectrometry as previously described.[95] This method has the potential to uncover how PS89 influences the BAP31 complex, if it acts in favor of pro-apoptotic interactions or for instance by displacing anti-apoptotic proteins such as Bcl-2 and Bcl-xL.

4.6.2 The potential of dually targeting the ER and mitochondria

Besides the identification of BAP31 as a novel target of PS89, the present study particularly shed light on the capability to provoke pro-apoptotic ER-mitochondrial crosstalk by combinatory pharmaceutical intervention. In this area, we propose versatile chances for future drug development. For example, BH3 mimetics that specifically modify mitochondrial integrity have been identified as a powerful novel compound class to trigger intrinsic apoptosis and encouraging results were recently shown in an AML phase II study with ABT-199.[96] Yet, the combination of ABT-199 with PS89 is currently evaluated in our lab aiming to expand the applicability of PS89 combinations beyond classic cytostatics. Alternative to PDI inhibitors, it is also conceivable that proteasome or HSP90 inhibitors are valuable combination partners to tune a pro-apoptotic ER stress response.[23]

4.6.3 Analysis of ER-mitochondrial communication by time-lapse microscopy

The kinetics of ER and mitochondrial stress triggers will finally be part of the future agenda. This project is motivated by the successful implementation of a method to monitor apoptotic processes in time-lapse.[97] As depicted in Figure 32a, the technique is based on single-cell patterning which allows to observe particular cells over the time period of stimulation. As cells are co-incubated with fluorescent markers, specific events such as ROS, calcium, caspase-8 and mitochondrial membrane potential can be tracked in parallel. The data of the time-lapse video can then be fitted to determine the onset of the markers and the number of cells that respond to different stimuli (Figure 32a). In the precise case of PS89 combination treatments, it will be of special interest which apoptotic triggers are primary or secondary in the crosstalk of ER and mitochondria. Moreover, it will be exciting how PS89 alters the kinetics of the fluorescent markers in comparison to the single treatment with cytostatics.

While the method was established with adherent cells, it is currently aimed to optimize the patterning for single-cell studies of leukemia cells (performed by Alexandra Murschhauser, group of Prof. Joachim Rädler, LMU Munich, Germany). One approach is the immobilization of Jurkat cells by antibody patterning. Yet, single-seeded Jurkat cells could be analyzed after 24 h incubation with stimulants, the redox-sensitive dye CellROX

and propidium iodide (Figure 32b). These initial studies collectively reveal the potential of this method which is not less than the design of rational drug combinations through an improved understanding of cellular communication.

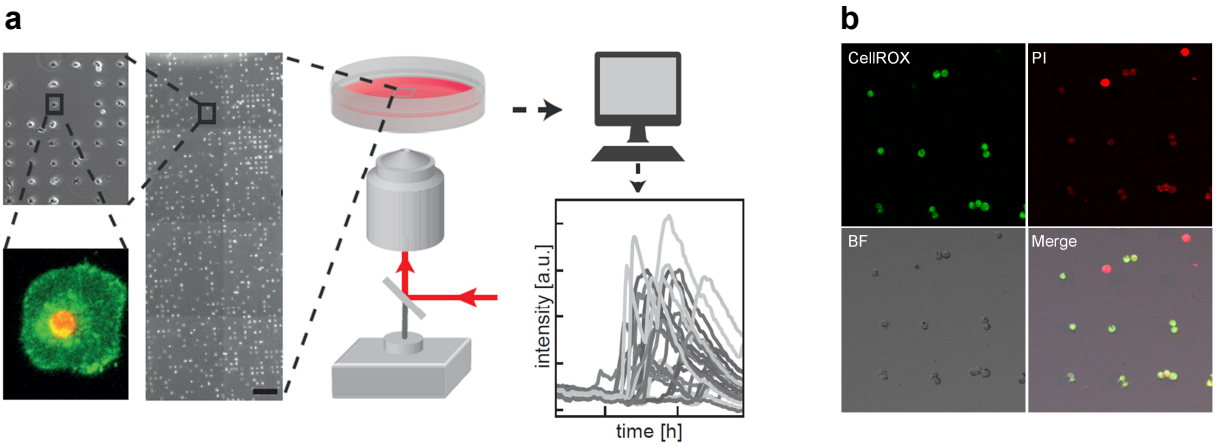

Figure 32 | Time-lapse microscopy of single-cell fluorescent markers. (**a**) Protein-coated microarrays are generated following plasma-induced patterning of µ-slides. Adherent cells distribute on the patterned sites after seeding. They are then exposed to apoptotic stimuli and monitored for activation of fluorescent markers using a fluorescence microscope. An automated image processing enables high-throughput analysis of the kinetics of single-cell fluorescence. Scheme adapted from Röttgermann *et al.*[97] (**b**) Preliminary data for Jurkat single-cell analysis. Microarrays were coated with a CD55 IgM antibody prior to seeding of Jurkat cells (8.000 cells/well). Cells were incubated with 25 µM PS89, 250 nM etoposide, 100 nM CellROX and 0.01 mg/ml propidium iodide. Images were taken after 24 h treatment.

5 Side Project: Vioprolide A

5.1 Introduction

Vioprolides are a family of natural compounds which were isolated from the myxobacterium *Cystobacter violaceus* and first published in 1996.[98] The cyclic structure of the compounds is composed of eight amino acids plus one glyceric acid and is shown for Vioprolide A (VioA) and Vioprolide D (VioD) in Figure 33. For all studies, Vioprolide stocks were provided by Prof. Rolf Müller (Saarland University, Saarbrücken, Germany).

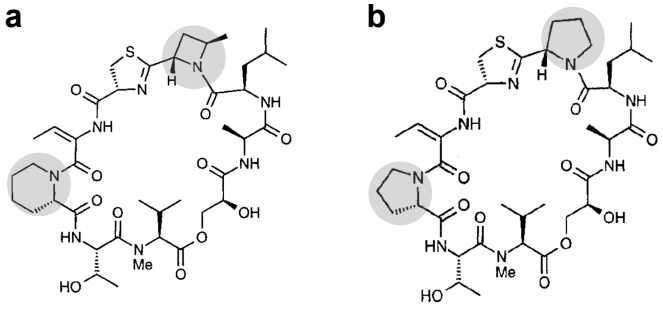

Figure 33 | Chemical structure of Vioprolides. (**a**) Vioprolide A and (**b**) Vioprolide D. The structural differences are highlighted.

The initial publication indicated a cytotoxic activity of Vioprolides, though a deeper biological evaluation has been missing since then. Within the DFG research group FOR 1406, the Vioprolide project was resumed and aimed to characterize the functional effects on cancer cells as well as the mechanisms behind. Therefore, the transcriptomic regulation in Vioprolide treated cells was assessed using the sequencing approach MACE (Massive Analysis of cDNA Ends).

5.2 Anticancer effects of Vioprolide A

The treatment of Jurkat cells with low nanomolar concentrations of VioA showed a dose-dependent inhibition of proliferation which was analyzed after 72 h (Figure 34a). As Jurkat cells visibly exhibited apoptotic phenotypes at concentrations >5 nM, induction of apoptosis was subsequently quantified applying higher concentrations which effectively escalated the percentage of apoptotic cells (Figure 34b, 50 nM VioA: 75% apoptotic cells). Notably, peripheral blood mononuclear cells (PBMCs) of healthy donors were largely unaffected by VioA treatment, even at high concentrations up to 250 nM VioA (Figure 34c).

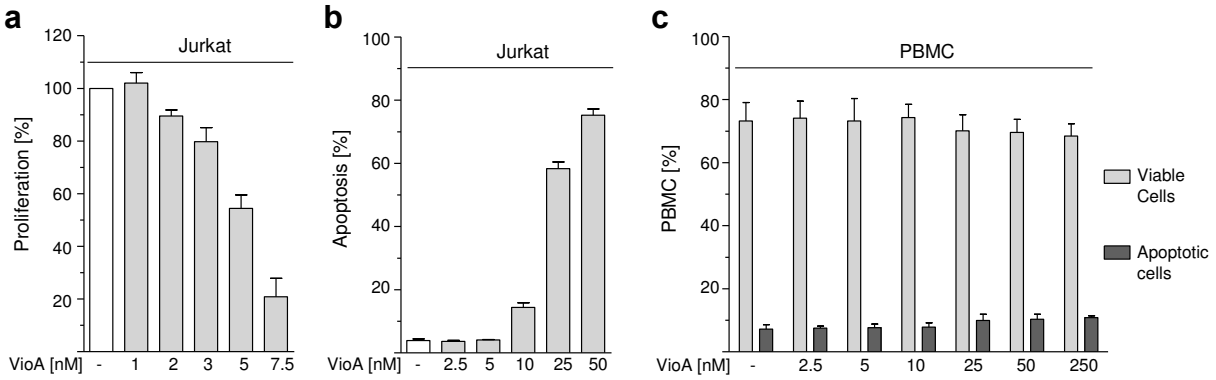

Figure 34 | Antileukemic effects of Vioprolide A. (**a**) Proliferation of Jurkat cells incubated with Vioprolide A (VioA) for 72 h. The number of viable cells was determined by CellTiter-Blue staining and normalized towards DMSO control. (**b**) Apoptosis of Jurkat cells treated with VioA for 24 h. Percentage of apoptotic cells was determined by propidium iodide staining and flow cytometry. (**c**) Peripheral blood mononuclear cells (PBMCs) treated with VioA for 24 h. The percentage of apoptotic cells was determined by flow cytometry.

Aiming to translate VioA mediated anticancer effects to other tumor models, the adherent bladder carcinoma cell line T24 was chosen. Similar to Jurkat cells, VioA inhibited to proliferative capacity of T24 cells (Figure 35a). Though quite contrary to Jurkats, apoptosis was significantly lower in T24 cells at higher VioA concentrations (Figure 35b, 50 nM VioA: 5% apoptotic cells). Finally studying the ability of T24 single cells to grow into colonies, a pre-stimulation of the culture with subtoxic doses of VioA showed a long-term effect and inhibited colony formation (Figure 35c).

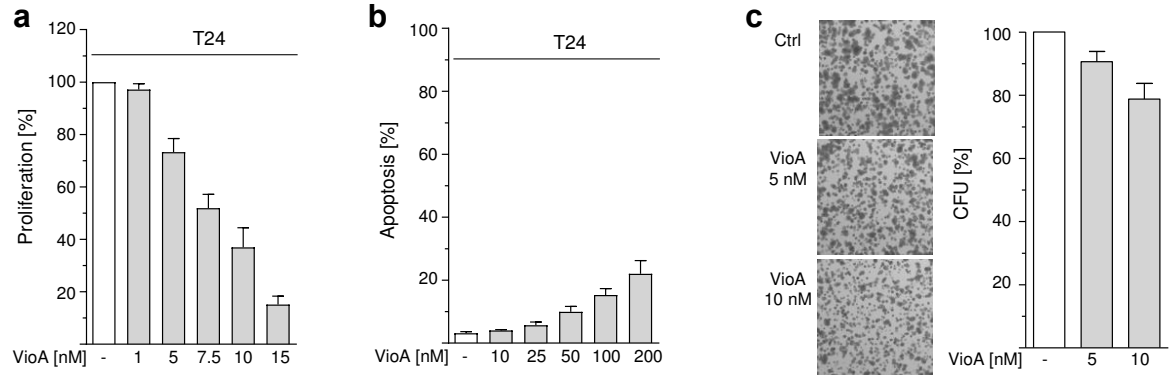

Figure 35 | Anticancer effects of Vioprolide A in T24 bladder carcinoma cells. (**a**) Proliferation of T24 cells (DSMZ, cultured in McCoy's medium, 10% FCS, Pen/Strep) after 72 h stimulation with Vioprolide A (VioA). The number of viable cells was determined by CellTiter-Blue staining and normalized towards DMSO control. (**b**) Apoptosis of Jurkat cells treated with VioA for 24 h. Percentage of apoptotic cells was determined by propidium iodide staining and flow cytometry. (**c**) Clonogenic assay of T24 cells pre-stimulated for 24 h with VioA. Cells were detached, compounds removed by washing and cells reseeded at low density (1250 cells/ml). Colonies were stained after 7 days of proliferation with crystal violet (0.5% w/v in 20% methanol/H_2O) and images were taken after several washing steps and removal of excessive dye. For quantification, crystal violet was solubilized (0.1 M sodium citrate in 50% ethanol/H_2O) and absorbance was measured at 550 nm (Tecan Sunrise). The percentage of colony forming units (CFU) was expressed as absorbance values normalized to DMSO control.

As metastasis of primary tumor cells to distant organs remains a major challenge in the management of solid cancers, the ability of VioA to inhibit migration of T24 was finally evaluated using xCELLigence impedance measurement (Roche Diagnostics). The method allows real-time monitoring of cells migrating through a 8 µM porous membrane towards a chemoattractant as representatively shown in Figure 36a. The cell index is proportinal to the number of migrating cells and was inhibited with increasing concentrations of VioA applied at subtoxic doses. The antimigratory effects of VioA were confirmed by the quantitative analysis showing a decreased slope of the curves during the time interval of continous migration (Figure 36b).

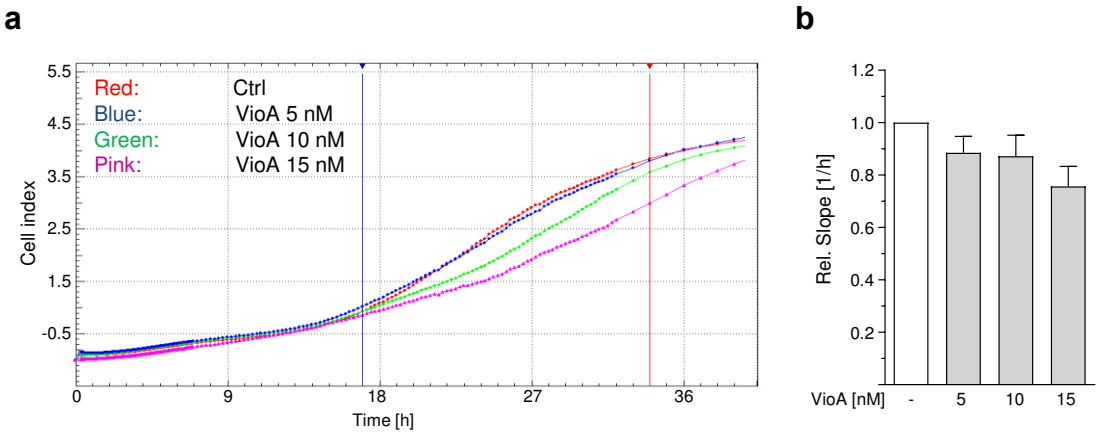

Figure 36 | Antimigratory effects of Vioprolide A. (**a**) Representative curves of an xCELLigence real-time migration experiment. Equilibrated 16-well CIM plates were loaded with FCS-supplemented medium at the bottom part and 40.000 cells/well in McCoy medium without FCS in presence or absence of Vioprolide A (VioA) at the upper part. Chemotaxis was monitored at 37°C by impedance measurement. (**b**) Quantification of the linear slope during constant migration with RTCA software (Roche Diagnostics). Slope values were normalized to DMSO control.

5.3 Comparative analysis of Vioprolide A and Vioprolide D

The publication introducing Vioprolides in 1996 indicated a distinct specificity of the family members against fungi, yeast and mammalian cells.[98] Here, a comparative dose-response study of Vioprolides A and D on Jurkat cell apoptosis revealed an EC_{50} of 22.0 nM for VioA, while VioD was nearly two log cycles less active (Figure 37, EC_{50} = 1.67 µM). This result indicated that the slight structural differences in N-heterocycles as outlined in Figure 33 have a significant impact on the bioactivity of Vioprolides.

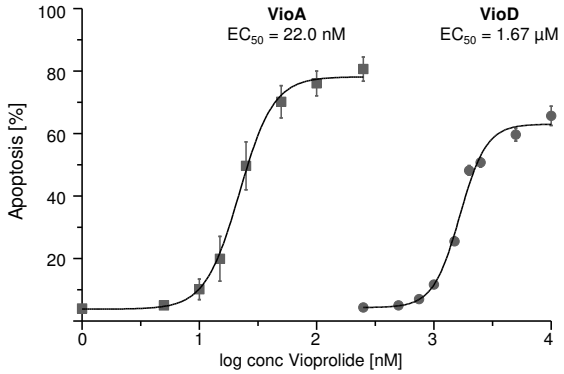

Figure 37 | Dose-dependent apoptosis induction of Vioprolide derivatives. Apoptosis of Jurkat cells treated with Vioprolide A (VioA) or Vioprolide D (VioD) for 24 h. Percentage of apoptotic cells was determined by propidium iodide staining and flow cytometry. EC_{50} values were calculated with GraphPad Prism.

5.4 Massive analysis of cDNA ends (MACE) transcriptome analysis

5.4.1 Method description

Approaching to elucidate biological pathways affected by the cyclic peptide, a transcriptome analysis of cells stimulated with Vioprolide A was performed. In cooperation with Dr. Iris Bischoff (Goethe University, Frankfurt, Germany), the screening method MACE (Massive Analysis of cDNA Ends) from GenXPro (Frankfurt, Germany) was applied. This features an improved detection of rare and short transcripts without the need of length-based normalization compared to full-length RNA-Seq. The experimental procedure is outlined in Figure 38a. First, the method required the isolation of RNA from stimulated cells and controls. This was followed by the preparation of the cDNA library which was performed with the MACE Kit from GenXPro. It started with barcode tagging of each sample (n=6) and reverse transcription, then fragmentation and enrichment of cDNA ends and eventually ligation of adaptors necessary for next-generation sequencing (NGS). In the final step, the library was conditioned for sequencing using the MiSeq Kit v3 (Illumina, San Diego, CA, USA) allowing deep sequencing with 25 million reads overall or approximately 4 million reads per sample. One read means that 150 bp of each amplified cDNA fragment was sequenced and finally assigned to one of the samples by their individual barcodes. During library preparation, in process control of oligo size ensured that fragmentation by sonication provided appropriate pieces of cDNA as shown in Figure 38b (average size specified: 200 bp). Furthermore, the successful ligation of adapter sequences was confirmed by a shift of average fragment size from 214 bp to 275 bp.

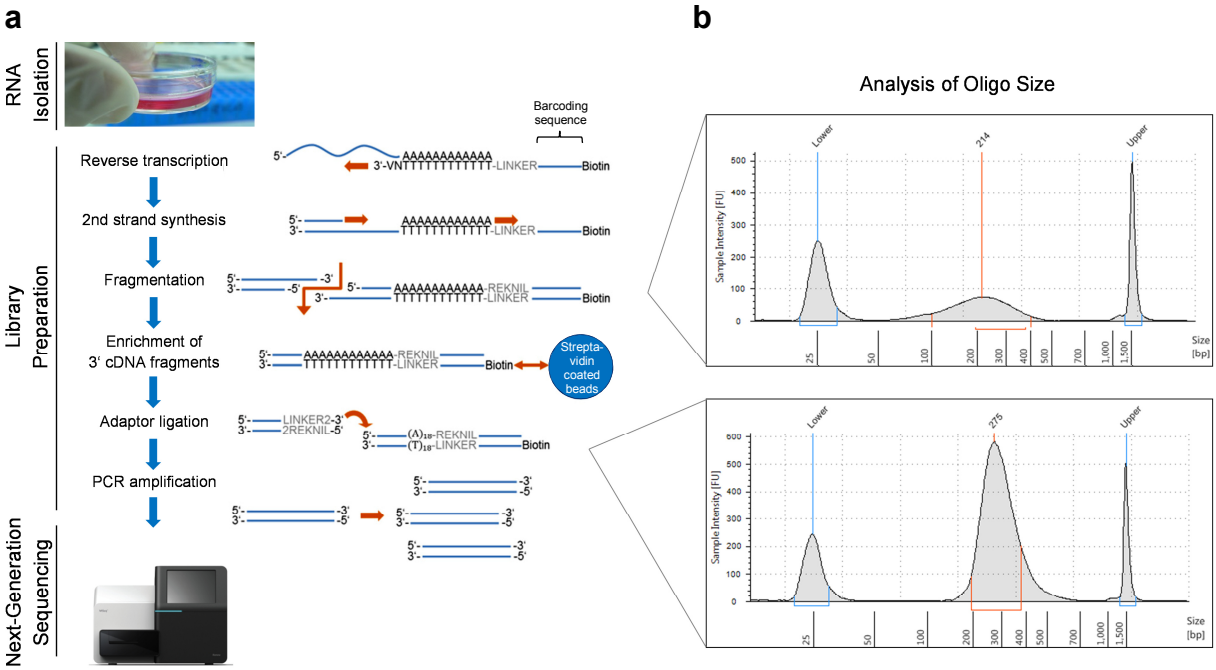

Figure 38 | Massive analysis of cDNA ends (MACE). (**a**) Schematic overview of MACE transcriptome analysis adapted from Afonso-Grunz *et al.*[99] RNA was isolated with the RNeasy Mini Kit (Qiagen, Hilden, Germany) and RNA amount determined using a NanoDrop Spectrophotometer ND-1000 (Peqlab, Erlangen, Germany). 4 µg of RNA was put in to prepare the cDNA library with the MACE Kit according to manufacturer's instructions (GenXPro, Frankfurt, Germany). Fragmentation was performed with a Bioruptor Plus sonication device from Diagnode (Liege, Belgium), cDNA was purified with SPRI magnetic beads (Agencourt AMPure XP, Beckman Coulter, Brea, CA, USA) and enriched with streptavidin affinity beads (provided by GenXPro). After adaptor ligation, cDNA was released from affinity beads, amplified on a GeneAmp PCR System 9700 (Thermo Fisher, Waltham, MA, USA) and purified again (SPRI beads). NGS was performed on a MiSeq system using the MiSeq v3 Kit (Illumina, San Diego, CA, USA) (**b**) In-process control of oligo size during library preparation. The size of cDNA fragments was determined on a 2200 TapeStation using High Sensitivity D1000 ScreenTape (Agilent, Santa Clara, CA, USA). Peaks designated 'Lower' and 'Upper' are ScreenTape reference DNAs and the central peak marks the size of cDNA fragments.

5.4.2 Data processing

A total of six samples were analyzed by MACE identifying 31890 different reads overall.

- Jurkat HD (high-dose): 24 h VioA treatment (c = 50 nM) vs. Jurkat DMSO control
- Jurkat LD (low-dose): 24 h VioA treatment (c = 7.5 nM) vs. Jurkat DMSO control
- T24: 24 h VioA treatment (c = 15 nM) vs. T24 DMSO control

Note: VioA stocks used for MACE analysis featured lower cytotoxic activity than stocks used in section 5.2 which demanded an adjustment of doses (Jurkat 24 h: <10% apoptotic cells with VioA 50 nM)

As the cellular basal level of transcripts varies even without treatment, the results of Jurkat HD and LD including n=2 independent data sets of Jurkat contols were subjected to further analysis. Therefore, the gene list was extracted using Microsoft Excel and the selection criteria outlined in Table 21. All raw data of Jurkat and T24 cells accompany this thesis as described in section 8.2.

Category	Selection criteria
Unique mapping	Exclusion if sequence is not uniquely assigned to one specific gene (e. g. sequence match with two of more transcripts)
High expression	>10 normalized reads in control or treated cells
Transcript regulation	A) Control vs. VioA treated: For normalized reads >10: fold-change >2 (log_2fold change >1) For normalized reads >20: fold-change >1.5 (log_2fold change >0.6) B) Control vs. Control: Exclusion if log_2fold change in (Ctrl vs. Ctrl) x2 > (Ctrl vs. VioA) C) Equal tendency of transcript regulation (up or down) in VioA high-dose (Jurkat HD) and low-dose (Jurkat LD) treatment

Table 21 | Selection criteria for MACE data analysis. The criteria were applied to extract significantly regulated genes from the transcriptome of Jurkat cells treated for 24 h with Vioprolide A (Jurkat HD).

Applying the criteria of Table 21, n=616 regulated genes were finally extracted from the transcriptome of VioA treated Jurkat cells (Jurkat HD) in comparison to DMSO control.

5.4.3 Gene Ontology and KEGG pathway analysis

Evaluating if the identified genes were commonly involved in the regulation of specific biological processes or pathways, the data set was first subjected to Gene Ontology (GO) analysis[70] using the RAMONA interface (Remotely Accessible Multilevel ONtology Analysis).[100] As shown in Figure 39, the biological process most likely affected by VioA was cholesterol biosynthesis with n=10 regulated against n=44 background genes which belong to the category 'cholesterol biosynthetic process'.

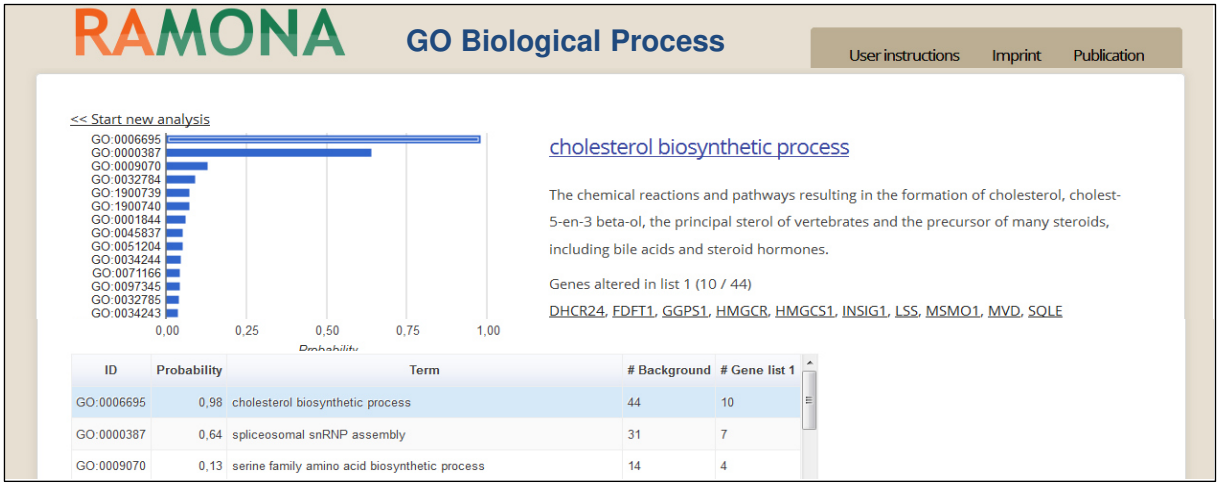

Figure 39 | RAMONA analysis of Gene Ontology (GO) biological processes regulated by Vioprolide A. The Jurkat HD data set (n=616 genes) was analyzed with the single-model tool of the RAMONA interface against homo sapiens genomic background. Results for Gene Ontology (biological process) are shown.

The GO analysis indicated a modulation of transcripts involved in cholesterol biosynthesis, though did not distinguish between up- or down-regulation. Therefore, the expression of the cholesterol-related genes was examined in the original gene list of control versus VioA treated Jurkat cells. As a result and with exception of Geranylgeranyl pyrophosphate synthase (GGPS1), n=9 out of 10 genes were down-regulated (Table 22). These included HMG-CoA reductase (HMGCR, Ctrl 225.44 vs. VioA 105.61 normalized reads) which is the rate-limiting enzyme in cholesterol biosynthesis. Of note, SREBF2 which encodes the sterol regulatory element-binding protein 2 (SREBP-2), was also identified to be down-regulated by VioA. This is of special interest as SREPB-2 is a key transcription factor controlling cholesterol homeostasis. SREBP-2 responsive genes include HMGCS1 (HMG-CoA synthase), HMGCR (HMG-CoA reductase) and squalene synthase (FDFT1),[101] all of which were likewise found at lower transcript levels upon VioA treatment (Table 22).

Gene	Protein Name	Ctrl JurkatHD	VioA JurkatHD	log_2FoldChange JurkatHDctrl_vs_VioA
DHCR24	Delta(24)-sterol reductase	20,84	9,40	**1,15**
FDFT1	Squalene synthase	190,39	101,27	**0,91**
GGPS1	Geranylgeranyl pyrophosphate synthase	69,15	135,27	**-0,97**
HMGCR	3-hydroxy-3-methylglutaryl-coenzyme A reductase	225,44	105,61	**1,09**
HMGCS1	Hydroxymethylglutaryl-CoA synthase	72,94	24,60	**1,57**
INSIG1	Insulin-induced gene 1 protein	310,69	177,95	**0,80**
LSS	Lanosterol synthase	18,94	9,40	**1,01**
MSMO1	Methylsterol monooxygenase 1	375,10	149,74	**1,32**
MVD	Diphosphomevalonate decarboxylase	12,31	3,62	**1,77**
SQLE	Squalene monooxygenase	388,36	250,29	**0,63**
SREBF2	Sterol regulatory element-binding protein 2	16,10	5,79	**1,48**

Table 22 | List of genes involved in the regulation of cholesterol biosynthesis. The list shows original MACE data for DMSO control (Ctrl) and Vioprolide A (VioA) treated Jurkat cells (Jurkat HD). The upper part lists all genes which were regulated by VioA and involved in 'cholesterol biosynthetic process' according to the Gene Ontology classification. The bottom line shows data for the transcription factor SREBF2.

Besides the Gene Ontology classification, RAMONA offers a pathway analysis tool which has its source in the KEGG (Kyoto Encyclopedia of Genes and Genomes) database. Feeding the RAMONA interface once again with the n=616 VioA regulated genes, the pathways with the highest probability of regulation included the terms 'RNA transport' (17/164, gene list/background) which is ubiquitously discovered, 'Protein processing in ER' (14/167) and 'Steroid biosynthesis' (5/20).

Considering the KEGG steroid biosynthetic pathway together with previous results finally enabled to visualize the different levels of VioA mediated transcript alteration (Figure 40). In addition to the five down-regulated genes on the level of 'Steroid biosynthesis' according to KEGG, the genes HMGCS1, HMGCR and MVD (Diphosphomevalonate decarboxylase) are outlined which are involved in the superordinate pathway 'Terpenoid backbone biosynthesis'.

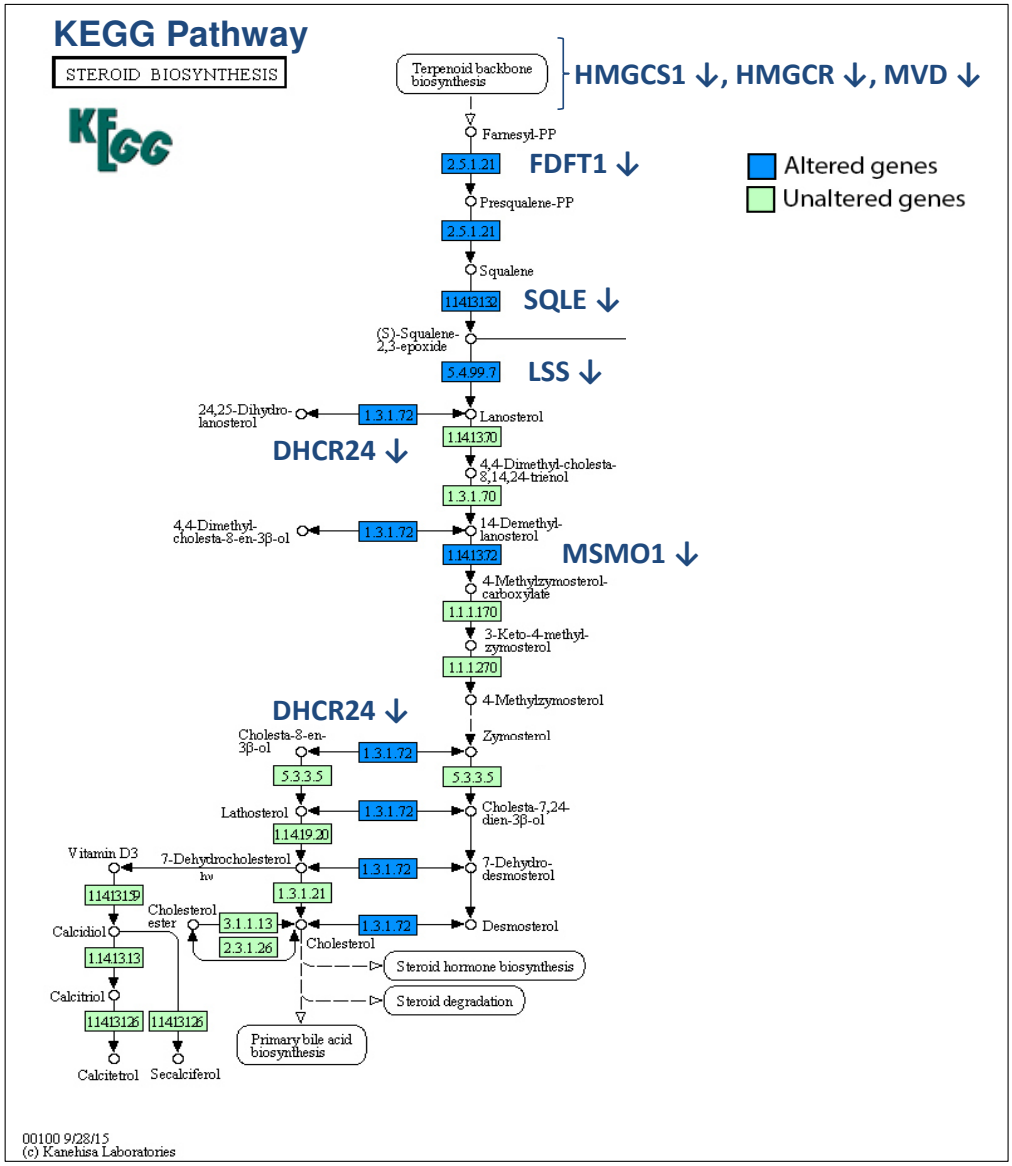

Figure 40 | RAMONA analysis of the KEGG pathway 'Steroid biosynthesis'. The Jurkat HD data set (n=616 genes) was analyzed with the single-model tool of the RAMONA interface against homo sapiens genomic background. Results for altered gene expression in the KEGG pathway 'Steroid biosynthesis' are shown in blue. In addition, altered genes encoding proteins of the KEGG 'Terpenoid backbone biosynthesis' pathway are listed.

5.5 Future prospects

As indicated by MACE, a multilevel down-regulation of genes involved in the cholesterol biosynthetic pathway by VioA treatment suggests a decrease of total cellular cholesterol. This in turn could have a therapeutic implication: as cholesterol levels and HMGCR were shown to be increased in acute leukemia samples exposed to standard chemotherapy, a co-treatment of cytostatics with cholesterol synthesis inhibitors was proposed.[102, 103] Furthermore, cholesterol depletion of free and especially membrane-bound cholesterol was recently shown to inhibit proliferation and oncogenic Ras signaling of hepatocellular carcinoma cells.[104] However, if cholesterol levels are indeed reduced upon VioA treatment and to which extend this feature finally accounts for the anti-proliferative and pro-apoptotic action of VioA requires further validation.

Moreover, omics screens generally offer a wide scope of possibilities for data extraction and interpretation which may lead to different conclusions. Further bioinformatics analyses of the MACE data could therefore reveal additional pathways that are affected by VioA treatment and contribute to its mode of action. Subsequently, all screening data require a biological validation meaning the verification of VioA mediated gene regulation first on mRNA level by qPCR and second on protein level by Western blot. Finally, the functional consequences of individual gene or network alterations need to be characterized. For the present approach, this will implicate the determination of cholesterol in different cellular compartments and its effect on oncogenic signaling pathways.

In order to further improve our understanding of VioA dynamics, the next step in the Vioprolide project is the identification of direct VioA targets by activity-based protein profiling (ABPP). The results of the proteomic screen could then be correlated with the MACE data. Therefore, the RAMONA interface may serve as a valuable tool since it is not limited to single-stage analysis, but features a cooperative model for the interpretation of data on two different levels (for example mRNA and protein).[100] Finally, the combination of direct targets and transcriptomics has the potential to highly enhance the understanding of the compound's polypharmacological profile and to put forward a crucial strategy for drug discovery in the omics era. Besides, the identification of direct

target proteins by ABPP and subsequent binding studies could help to comprehend the distinct differences in the activities of Vioprolide derivatives that have been outlined here in the comparative study of VioA and VioD.

Beyond the pharmacological characterization of VioA triggered signaling, future studies will be able to refer to the strong anticancer effects of VioA that were demonstrated here. These include anti-proliferative, pro-apoptotic and anti-migratory features which altogether stress the versatile potential of VioA against hematologic malignancies as well as solid cancers. In conclusion, the present study encourages further *in vitro* and *in vivo* testing of these highly active natural compounds.

6 Contribution: P8-D6

6.1 Introduction

Topoisomerases are vital for many cellular processes such as DNA replication and transcription as they account for the movement and relaxation of torsional strains in the genetic material. Inhibitors of topoisomerases including etoposide and anthracyclines are front-line cytostatics in the therapy of hematologic and solid cancers. Though, side effects such as secondary malignancies and emerging resistances raise a significant need for novel topo-targeting molecules.[17] Recently, the chemical optimization of naturally occurring benzo[*c*]phenanthridinde alkaloids by Christopher Meier (group of Prof. Bernd Clement, Christian Albrechts University, Kiel) yielded the highly active compound P8-D6 which equipotently inhibits human topoisomerase I and II activities. In order to further characterize the molecular and functional action of this promising compound, a set of experiments was performed in our lab with Jurkat ALL cells. Here, P8-D6 showed strong growth-inhibitory and pro-apoptotic effects at low nanomolar concentrations (50 nM P8-D6: 61.4% apoptotic cells after 24 h). Moreover, cells arrested in the G2 phase of the cell cycle and the phosphorylation of histone H2AX indicated double-strand breaks as the main apoptotic trigger of P8-D6. Additionally, P8-D6 in combination with the chemosensitizing compound PS89 (characterized in sections 1-4) demonstrated clearly enhanced growth inhibition and apoptosis induction. These results together with the synthetic protocol of P8-D6, its druggability properties and an *in vivo* toxicity study have been recently published in ChemMedChem.[105]

6.2 Original Article: A Dual Topoisomerase Inhibitor of Intense Pro-Apoptotic and Antileukemic Nature for Cancer Treatment

The full article highlighting P8-D6 is presented on the following pages and listed under the Pubmed ID 28099785. Supplementary information including detailed method descriptions accompanies the article on the ChemMedChem homepage.

ChemPubSoc Europe

DOI: 10.1002/cmdc.201700026

CHEMMEDCHEM Communications

A Dual Topoisomerase Inhibitor of Intense Pro-Apoptotic and Antileukemic Nature for Cancer Treatment

Christopher Meier,[a] Tamara N. Steinhauer,[a] Fabian Koczian,[b] Birte Plitzko,[a] Katharina Jarolim,[c] Ulrich Girreser,[a] Simone Braig,[b] Doris Marko,[c] Angelika M. Vollmar,[b] and Bernd Clement*[a]

Classic cytotoxic drugs remain indispensable instruments in antitumor therapy due to their effectiveness and a more prevalent insensitivity toward tumor resistance mechanisms. Herein we describe the favorable properties of 6-(*N*,*N*-dimethyl-2-aminoethoxy)-11-(3,4,5-trimethoxyphenyl)pyrido[3,4-*c*][1,9]phenanthroline (P8-D6), a powerful inducer of apoptosis caused by an equipotent inhibition of human topoisomerase I and II activities. A broad-spectrum effect against human tumor cell lines at nanomolar concentrations, as well as strong antileukemic effects, were shown to be superior to those of marketed topoisomerase-targeting drugs and dual topoisomerase inhibitors in clinical trials. The facile four-step synthesis, advantageous drugability properties, and initial in vivo data encourage the application of P8-D6 in appropriate animal tumor models and further drug development.

Members of the human topoisomerase (topo) enzyme family play crucial roles in many cellular actions involving the movement and relaxation of torsional strains in the genetic material. Their detailed intra-nuclear functions have been studied extensively and are well described in the literature.[1–5] As these operations are required for vital processes such as DNA replication, transcription, chromatin assembly, and DNA methylation, topoisomerases I and II have emerged as fundamental targets for the chemotherapeutic treatment of malignant tumors.[6–10] Approved topo-targeting drugs such as camptothecin derivatives, acting as topo I poisons, and primarily epipodophyllotoxins and anthracyclines that interfere with topo II are highly effective front-line cytostatic agents for the treatment of systemic cancers and solid tumors.[5,8] The efficacy and experience in clinical use on the one hand, but also dose- and/or therapy-limiting side effects and emerging resistance mechanisms against these agents on the other, demonstrate a significant medical need for novel topo-targeting molecules.[1,5,6,11–13] Much effort has gone into the design of dual topo I/II inhibitors that exhibit high cytotoxicity and high affinity for both enzyme classes. In this regard, the complete inhibition of topoisomerase activity in tumor cells was shown to be extremely effective in vitro and in vivo in a broad range of tumor types.[1,14–20] Consequently, dual topo I/II inhibitors were evaluated in phase I/II clinical trials: pyrazoloacridine (PZA, **1**), benzopyridoindole intoplicine (**2**), phenazine derivatives XR11576 (**3**) and XR5944 (**4**), batracylin (**5**), and the indenoquinolinone TAS-103 (**6**) (Figure 1), as well as the etoposide derivative tafluposide and the homocamptothecin elomotecan.[1,14,21–28] Although preclinical studies were very promising for these derivatives, their effectiveness could not be transferred to the clinic yet.

Naturally occurring benzo[*c*]phenanthridine alkaloids offer a broad variety of pharmacological activities.[29–33] Among them, the quaternary ammonium salts fagaronine and nitidine (**7**) were found to possess moderate dual topo I/II poisoning activity.[34–36] In the mid-1990s our research groups evaluated a facile and straightforward synthetic route to 11-substituted 6-aminobenzo[*c*]phenanthridines.[37] The antitumor activity of derivatives **8** was observed to be high in vitro and in vivo, but unfortunately their dissatisfactory physicochemical properties (solubility: low-micromolar range, log$D_{7.4} \approx 5$) limited further development of this compound class (Figure 2).[38,39]

To overcome these disadvantages, we synthesized aza-analogs of benzo[*c*]phenanthridines (compounds **9**–**14**) by using various *o*-methylhetarene carbonitriles, and the core system was systematically adapted and optimized for both physicochemical properties and cytotoxicity (Figure 2).[39–42] Applying the concept of an aminoalkyl side chain linked to a planar core system to achieve DNA intercalation as well as anti-topoisomerase activity,[18] the pyrido[3,4-*c*][1,9]phenanthroline P8-D6 (**19**) was found to be by far the most potent derivative of our compound library. Compound **19** was accessible via a simple four-step synthetic protocol commencing with commercially available starting materials to form the 6-amino-11,12-dihydro derivative **17** in a two-fold ring closure including one-pot synthesis (Scheme 1).[39]

Dehydrogenation with Pd/C followed by diazotation with $NaNO_2$ in acidic aqueous medium yielded **18**.[40,43] The final step gave the O-alkylated derivative P8-D6 (**19**) via Mitsunobu reaction in an overall yield of 12% (Scheme 1).[44]

[a] Dr. C. Meier, Dr. T. N. Steinhauer, Dr. B. Plitzko, Dr. U. Girreser, Prof. Dr. B. Clement
Department of Pharmaceutical and Medicinal Chemistry, Pharmaceutical Institute of the Christian Albrechts University in Kiel, Gutenbergstraße 76, 24118 Kiel (Germany)
E-mail: bclement@pharmazie.uni-kiel.de

[b] F. Koczian, Dr. S. Braig, Prof. Dr. A. M. Vollmar
Department of Pharmacy, Center for Drug Research, Pharmaceutical Biology, University of Munich, Butenandtstraße 5–13, 81377 Munich (Germany)

[c] K. Jarolim, Prof. Dr. D. Marko
Department of Food Chemistry and Toxicology, University of Vienna, Währinger Straße 38, 1090 Vienna (Austria)

Supporting information for this article can be found under: http://dx.doi.org/10.1002/cmdc.201700026.

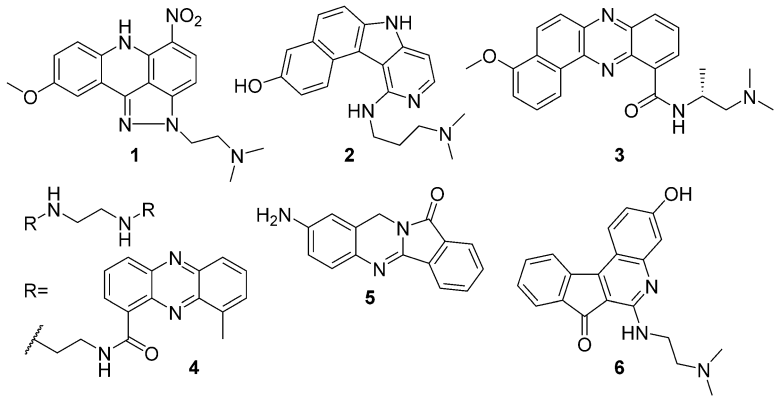

Figure 1. Dual topoisomerase I/II inhibitors in clinical development.[1,14,21–27]

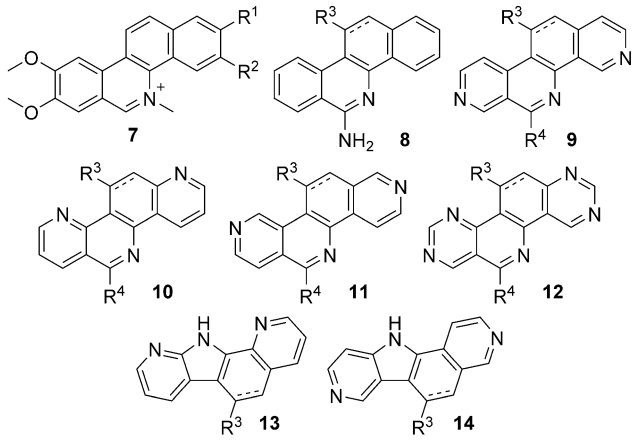

Figure 2. Natural-product-inspired development of aza-analogs of benzo[*c*]-phenanthridines.[37–42] R^1 = OH, R^2 = OCH_3: fagaronine; R^1–R^2 = OCH_2O: nitidine; R^3 = variously substituted aryl or alkyl groups; R^4 = H, OH, NH_2, or various hydrophilic sidechains.

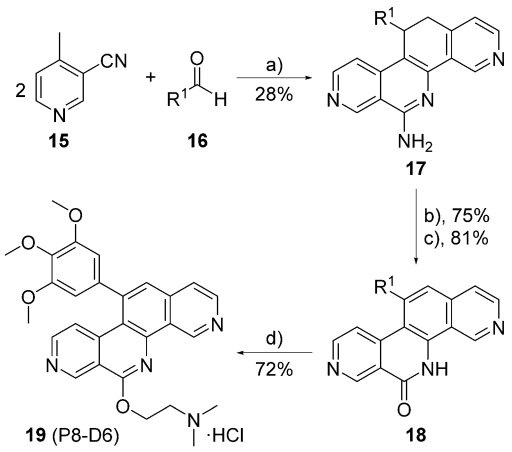

Scheme 1. Four-step synthesis of P8-D6 (**19**) starting from commercially available building blocks:[39,40,43,44] a) KO*t*Bu, DMPU, 3 h, RT; b) Pd/C, DMPU, 10 min, reflux; c) $NaNO_2$, H_3PO_2, H_2SO_4, AcOH, 1 h, 0 °C; d) dimethylaminoethanol, TPP, DIAD, THF, 72 h, RT, $HCl_{(g)}$, CH_2Cl_2. R^1 = 3,4,5-trimethoxyphenyl.

Cytotoxicity was evaluated by the treatment of 60 human tumor cell lines from nine different tumor types with P8-D6 (NCI-60 DTP human tumor cell line screening, NCI, Bethesda, MD, USA). Compound **19** showed outstanding overall activity (expressed as average 50% growth inhibition (GI_{50}) across all 60 cell lines) of 49 nM, in the range of the natural alkaloid camptothecin. Its growth-inhibitory effect was 4- to 10-fold higher than other dual topo I/II inhibitors recently elaborated in clinical trials (Table 1). Besides the good response observed for all tumor types, the sensitivity of leukemia cells and non-small cell lung cancer (NSCLC) cells toward P8-D6 was noted.[45]

P8-D6 is able to inhibit the catalytic activities of both type I and II topoisomerases at low micromolar concentrations in vitro (Figure 3 A,B). In this connection there is no significant discrimination between topo IIα, which reaches maximum protein levels in the G_2/M phase in human cells, and topo IIβ, which is

Table 1. Comparison of the cytotoxicity of topoisomerase targeting agents.

Compound	$\frac{\sum GI_{50}[a]}{60}$	GI_{50} [μM][b]		
		Leukemia	NSCLC	Colon cancer
Topoisomerase I inhibitors				
CPT[c]	0.04	0.02	0.02	0.08
Irinotecan	0.84	0.20	0.07	1.70
Topotecan	0.04	0.01	0.02	0.09
Topoisomerase II inhibitors				
Etoposide	1.32	0.21	0.79	2.51
Teniposide	0.40	0.05	0.27	0.71
Doxorubicin	0.14	0.07	0.07	0.26
Dual topoisomerase I/II inhibitors				
P8-D6	0.05	0.02	0.03	0.06
PZA[d]	0.20	0.17	0.17	0.12
Intoplicine	0.53	0.47	0.23	0.50

[a] Mean 50% growth inhibition over all 60 cell lines; data taken from the DTP-NCI databank, NCI-60 screening data set from September 2014.[45] [b] Average GI_{50} values for all comparable cell lines of corresponding tumor type. [c] Camptothecin. [d] Pyrazoloacridine.

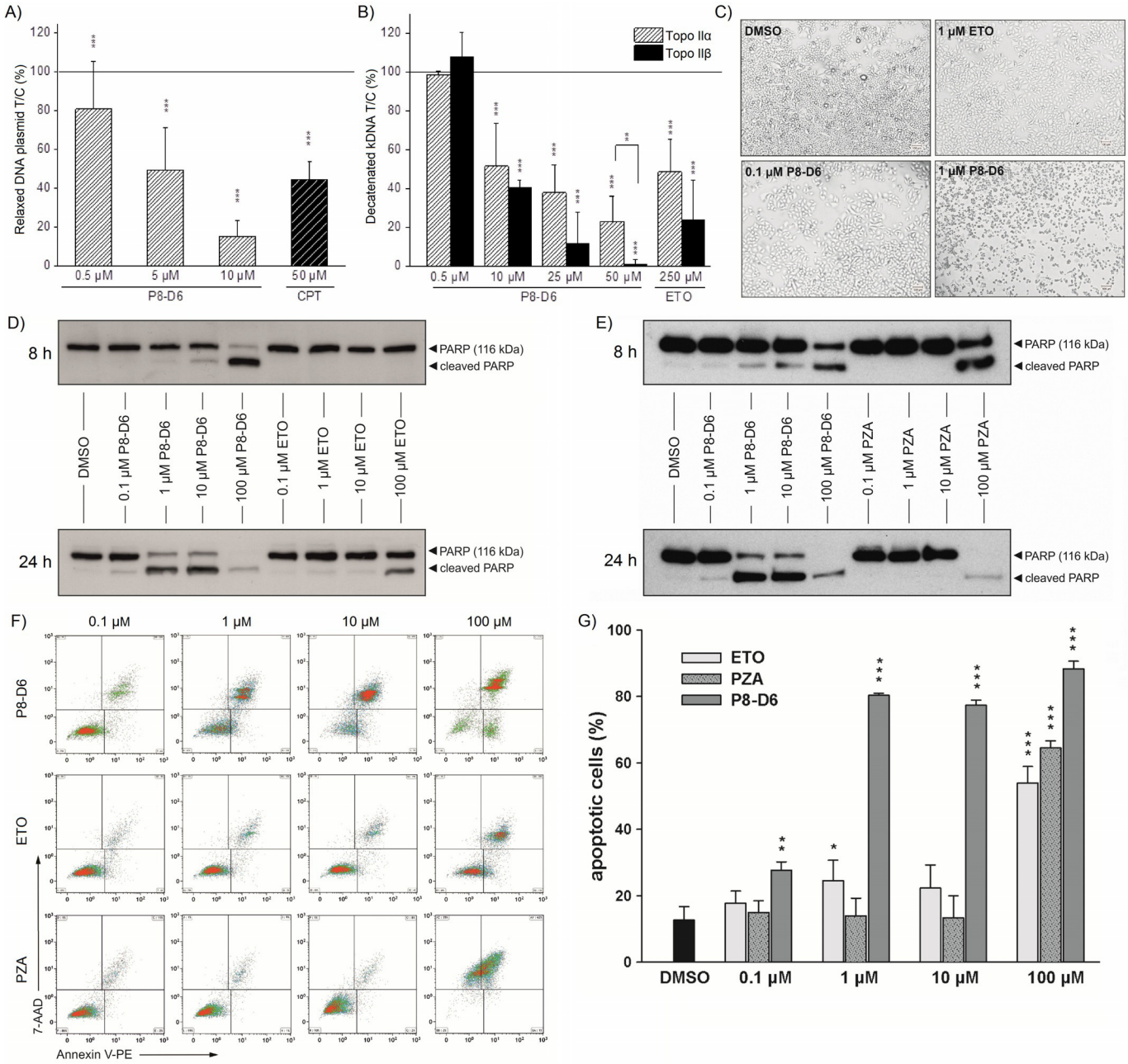

Figure 3. P8-D6 is a highly pro-apoptotic dual topoisomerase inhibitor. A) Inhibition of topoisomerase I activity (relaxation assay). B) Inhibition of topoisomerase IIα and IIβ (decatenation assay). C) HeLa cells after incubation (24 h) with P8-D6 or etoposide. D),E) PARP apoptosis assay in HeLa cells (ETO/PZA reference). F) Flow cytometric analysis of pro-apoptotic effects on HeLa cells (after 24 h). G) Quantitative determination of apoptotic cells by flow cytometry (after 24 h). Significant differences relative to DMSO control: $***p \leq 0.001$, $**p \leq 0.01$, $*p \leq 0.05$.

expressed independently of proliferative status and cell cycle.[1] A topo-independent DNA attraction, as has been previously reported for structurally related substances, is likewise postulated.[18,46]

Using flow cytometric analysis of Annexin V-PE and 7-AAD stained HeLa cells as well as the detection of caspase-mediated PARP cleavage, it could be demonstrated that P8-D6 is a strong and rapid inductor of apoptosis (Figure 3 C–G).[47,48] Low-micromolar concentrations of P8-D6 showed pro-apoptotic effects after incubation for 8 h, whereas no PARP cleavage was observed for etoposide (ETO) or the dual topo inhibitor PZA before reaching a concentration of 100 µM (Figure 3 D,E). After 24 h incubation, 100- to 1000-fold lower amounts of P8-D6 were sufficient to induce apoptosis in cells, relative to cultivation in the presence of ETO or PZA (Figure 3 D,E). PZA treatment also led to partial necrosis of the HeLa cells at these concentrations (Figure 3 F).

P8-D6 was furthermore tested for antileukemic effects on Jurkat ALL cells. Making up 30% of all childhood cancers, leukemia is the most common cancer in children, with acute lymphoid leukemia (ALL) being most prevalent.[49] The Jurkat ALL cell line was shown to be sensitive toward P8-D6 treatment, in

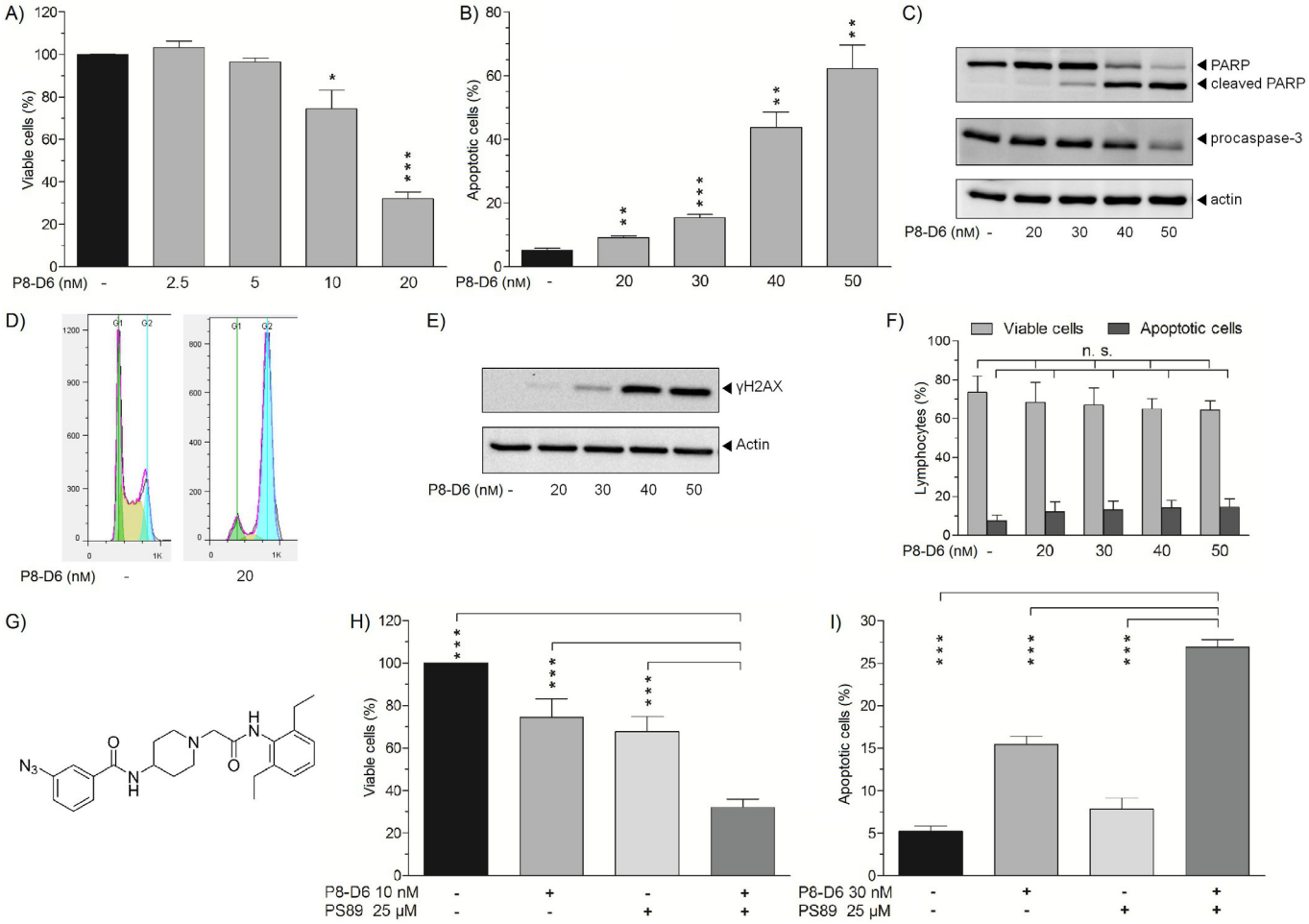

Figure 4. The strong antileukemic effects of P8-D6 and activity toward healthy human lymphocytes. A) Dose-dependent inhibition of Jurkat ALL cell proliferation by treatment with P8-D6 (Cell TiterBlue® assay, 72 h). B) Dose-dependent induction of apoptosis in Jurkat ALL cells by P8-D6 (Nicoletti assay, 24 h). C) Decrease of procaspase-3 levels and PARP cleavage in Jurkat ALL cells as hallmarks of apoptosis (P8-D6 treatment, 24 h); actin = loading control. D) Cell-cycle arrest in the G_2 phase by P8-D6 treatment (propidium iodide staining, 24 h). E) Phosphorylation of histone H2A.X as sensitive proof of DNA double-strand breaks in Jurkat ALL cells (P8-D6 treatment, 24 h). F) No pro-apoptotic effects of P8-D6 on healthy human lymphocytes (FACS analysis, 24 h). G) Structure of the chemosensitizing protein disulfide isomerase inhibitor PS89. H) Growth inhibition of Jurkat ALL cells by P8-D6 in combination with PS89 (Cell TiterBlue® assay, 72 h). I) Induction of apoptosis in Jurkat ALL cells by P8-D6 in combination with PS89 (Nicoletti assay, 24 h).

accordance with the NCI-60 results. Using proliferation assays, flow cytometric (FACS) analysis as per protocols reported by Nicoletti et al.,[50,51] and western blotting, strong growth-inhibitory and pro-apoptotic effects at low nanomolar concentrations could be confirmed (Figure 4A–C).

Propidium iodide staining and FACS analysis was also used to evaluate the effects of P8-D6 on the cell cycle. As shown in Figure 4D, the presence of the substance led to an arrest in the G_2 phase, as expected for a topo inhibitor.[52] Additionally, dose-dependent phosphorylation of histone H2A.X (γH2A.X) in Jurkat ALL cells clearly indicates DNA double-strand breaks as the main apoptotic trigger of P8-D6 (Figure 4E).[53]

To examine its selectivity for tumor cells, the cytotoxic effect of P8-D6 was also investigated on healthy human lymphocytes isolated from whole blood. The results indicate no response of lymphocytes toward P8-D6 concentrations that are already intensively cytotoxic and pro-apoptotic to the leukemia cell line (Figure 4F).

Recently, the selective protein disulfide isomerase inhibitor PS89 was found to sensitize cancer cells toward etoposide treatment (structure shown in Figure 4G).[54] In this regard, we analyzed the effects of P8-D6 in combination with the chemosensitizing compound PS89, clearly indicating enhanced growth inhibition and triggering of apoptosis by sub- or less toxic P8-D6 concentrations toward Jurkat ALL cells in the presence of PS89 (Figure 4H,I).

In addition to its pharmacological advantages, P8-D6 exhibits a physicochemical profile that encourages its development as promising drug candidate in antineoplastic chemotherapy. A solubility of ~1 mM in phosphate buffer (pH 7.4) as well as accordance with Lipinski's rule of five parameters for the prediction of oral bioavailability, including a log$D_{7.4}$ value of 3.7, would allow even per oral administration (parameters determined using HPLC analytics).[55]

To evaluate the initial in vivo tolerability of P8-D6, female athymic nude mice ($n = 9$ vs. nine mice receiving PBS control)

were treated intravenously (i.v.) with various unique doses of P8-D6 in PBS. This maximum tolerated dose (MTD) study revealed a good tolerability of 1 mg kg^{-1} body weight (bw) of P8-D6 with regard to further in vivo efficacy studies (Figure 5). In higher concentrations the compound showed dose-dependent toxicity (parameters: body weight, clinical signs), while loss of body weight and apathy of study animals in the 5 mg kg^{-1} group were reversible over the period of the study (Figure 5).

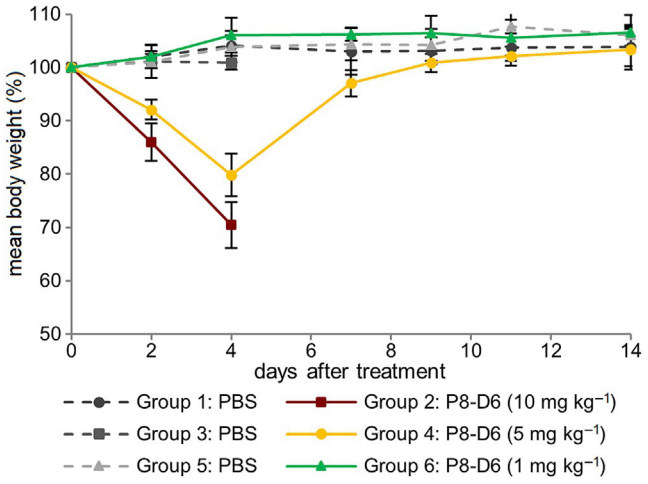

Figure 5. Intravenous application of single dose P8-D6 vs. phosphate-buffered saline (PBS) control in athymic nude mice.

Contrary to macroscopic alterations that had been reported for mice administered etoposide at low and high doses i.v. in similar studies,[56] no significant changes in organs were observed for study animals that received i.v. injections of P8-D6 up to 5 mg kg^{-1} bw (necropsy findings).

Because tumor cells require an enormous amount of cell components involved in DNA-related growth and replication, members of the human topoisomerase family are pivotal targets in antitumor therapy. In summary, our drug candidate P8-D6 exhibits a number of advantages. The strong and equipotent inhibition of topo I, IIα, and IIβ by a dual topoisomerase inhibitor with an unprecedented excellent cytotoxicity, rapid and effective tumor-cell-specific pro-apoptotic and antileukemic activity, as well as facile synthetic access in combination with favorable physicochemical properties, underscore the importance of further in vivo evaluations of P8-D6 in adequate animal tumor models. Given the improved hydrophilicity of P8-D6, it is not necessary to provide solubilizing agents for i.v./i.m. or intraperitoneal (i.p.) injections or infusions, as this was previously demonstrated in an in vivo tolerability study, which also provided some initial i.v. dosage information.

The studies described herein clearly highlight P8-D6 as being much better than the clinically evaluated dual topo inhibitor PZA regarding apoptosis-inducing effects. Therefore, this can be considered a substantial enrichment in the development of novel agents that target both topoisomerase I and II, raising hope for clinical efficacy, in contrast to previously developed drug candidates of this class. Besides the administration of P8-D6 alone or in combination with other cytostatic agents or chemosensitizing compounds, P8-D6 could be an excellent component in antibody–drug conjugates (ADCs) or other related modern techniques, most likely applicable against a broad variety of tumor types.[57]

Acknowledgements

We thank the US National Cancer Institute (NCI, Developmental Therapeutics Program (DTP), Division of Cancer Treatment and Diagnosis, dtp.cancer.gov) for its excellent screening service. Special thanks to M. Koburg for great performance during her Bachelor thesis supporting the leukemia part of the P8-D6 study. Many thanks to M. Ulrich for assisting with the lymphocyte isolation, as well as M. Säring and F.-B. Lichtenberger for excellent assistance during apoptosis studies.

Keywords: antitumor agents · apoptosis · heterocycles · ring closure · topoisomerase inhibitors

[1] R. van Gijn, R. R. H. Lendfers, J. H. M. Schellens, A. Bult, J. H. Beijnen, *J. Oncol. Pharm. Pract.* **2000**, *6*, 92–108 and references therein.
[2] J. J. Champoux, *Annu. Rev. Biochem.* **2001**, *70*, 369–413 and references therein.
[3] Y. Pommier, *Nat. Rev. Cancer* **2006**, *6*, 789–802 and references therein.
[4] J. L. Nitiss, *Nat. Rev. Cancer* **2009**, *9*, 338–350 and references therein.
[5] J. E. Deweese, N. Osheroff, *Nucleic Acids Res.* **2009**, *37*, 738–748 and references therein.
[6] Y. Pommier, *ACS Chem. Biol.* **2013**, *8*, 82–95 and references therein.
[7] J. L. Nitiss, *Nat. Rev. Cancer* **2009**, *9*, 327–337 and references therein.
[8] Y. Pommier, *Chem. Rev.* **2009**, *109*, 2894–2902 and references therein.
[9] J. M. Fortune, N. Osheroff, *Prog. Nucleic Acid Res. Mol. Biol.* **2000**, *64*, 221–253 and references therein.
[10] L.-Y. Lu, H. Kuang, G. Korakavi, X. Yu, *J. Biol. Chem.* **2015**, *290*, 851–860 and references therein.
[11] C. A. Felix, C. P. Kolaris, N. Osheroff, *DNA Repair* **2006**, *5*, 1093–1108.
[12] L. J. Lewis, P. Mistry, P. A. Charlton, H. Thomas, H. M. Coley, *Anti-Cancer Drugs* **2007**, *18*, 139–148 and references therein.
[13] C. M. Whitacre, E. Zborowska, N. H. Gordon, W. Mackay, N. A. Berger, *Cancer Res.* **1997**, *57*, 1425–1428.
[14] S. Salerno, F. Da Settimo, S. Taliani, F. Simorini, C. La Motta, G. Fornaciari, A. M. Marini, *Curr. Med. Chem.* **2010**, *17*, 4270–4290.
[15] H.-B. Kwon, C. Park, K.-H. Jeon, E. Lee, S.-E. Park, K.-Y. Jun, T. M. Kadayat, P. Thapa, R. Karki, Y. Na, M. S. Park, S. B. Rho, E.-S. Lee, Y. Kwon, *J. Med. Chem.* **2015**, *58*, 1100–1122.
[16] B.-L. Yao, Y.-W. Mai, S.-B. Chen, H.-T. Xie, P.-F. Yao, T.-M. Ou, J.-H. Tan, H.-G. Wang, D. Li, S.-L. Huang, L.-Q. Gu, Z.-S. Huang, *Eur. J. Med. Chem.* **2015**, *92*, 540–553.
[17] J. Janočková, J. Plšíková, J. Koval', R. Jendželovský, J. Mikeš, J. Kašpárková, V. Brabec, S. Hamuľaková, P. Fedoročko, M. Kožurková, *Bioorg. Chem.* **2015**, *59*, 168–176.
[18] L. Dalla Via, G. Marzaro, A. Ferrarese, O. Gia, A. Chilin, *Eur. J. Med. Chem.* **2014**, *77*, 103–109 and references therein.
[19] S.-T. Zhuo, C.-Y. Li, M.-H. Hu, S.-B. Chen, P.-F. Yao, S.-L. Huang, T.-M. Ou, J.-H. Tan, L.-K. An, D. Li, L.-Q. Gua, Z.-S. Huang, *Org. Biomol. Chem.* **2013**, *11*, 3989–4005.
[20] S.-O. Kim, K. Sakchaisri, N. R. Thimmegowda, N. K. Soung, J.-H. Jang, Y. S. Kim, K. S. Lee, Y. T. Kwon, Y. Asami, R. L. Erikson, B. Y. Kim, *PLoS One* **2013**, *8*, e53908.
[21] S. L. Berg, S. M. Blaney, J. Sullivan, M. Bernstein, R. Dubowy, M. B. Harris, *Am. J. Pediatr. Hematol./Oncol.* **2000**, *22*, 506–509.
[22] A. A. Adjei, J. M. Reid, C. Erlichman, J. A. Sloan, H. C. Pitot, S. R. Alberts, R. M. Goldberg, L. J. Hanson, S. Ruben, S. A. Boerner, P. Atherton, M. M. Ames, S. H. Kaufmann, *Invest. New Drugs* **2002**, *20*, 297–304.

[23] J. L. Grem, N. Harold, B. Keith, A. P. Chen, V. Kao, C. H. Takimoto, J. M. Hamilton, J. Pang, M. Pace, G. B. Jasser, M. G. Quinn, B. P. Monahan, *Clin. Cancer Res.* **2002**, *8*, 2149 – 2156.
[24] M. J. A. de Jonge, S. Kaye, J. Verweij, C. Brock, S. Reade, M. Scurr, L. van Doorn, C. Verheij, W. Loos, C. Brindley, P. Mistry, M. Cooper, T. Judson, *Br. J. Cancer* **2004**, *91*, 1459 – 1465.
[25] W. Verborg, H. Thomas, D. Bissett, J. Waterfall, J. Steiner, M. Cooper, E. M. Rankin, *Br. J. Cancer* **2007**, *97*, 844 – 850.
[26] S. Kummar, M. E. Gutierrez, L. W. Anderson, R. W. Klecker, A. Chen, A. J. Murgo, J. H. Doroshow, J. M. Collins, *Cancer Chemother. Pharmacol.* **2013**, *72*, 917 – 923.
[27] R. B. Ewesuedo, L. Iyer, S. Das, A. Koenig, S. Mani, N. J. Vogelzang, R. L. Schilsky, W. Brenckman, M. J. Ratain, *J. Clin. Oncol.* **2001**, *19*, 2084 – 2090.
[28] I. F. Trocóniz, J. M. Cendrós, E. Soto, J. Pruñonosa, A. Perez-Mayoral, C. Peraire, P. Principe, P. Delavault, F. Cvitkovic, T. Lesimple, R. Obach, *Cancer Chemother. Pharmacol.* **2012**, *70*, 239 – 250.
[29] S. Simeon, J. L. Rios, A. Villar, *Pharmazie* **1989**, *44*, 593 – 597 and references therein.
[30] Z. Dvorák, V. Kubáň, B. Klejdus, J. Hlaváč, J. Vičar, J. Ulrichová, V. Šimánek, *Heterocycles* **2006**, *68*, 2403 – 2422.
[31] F. Fleury, A. Sukhanova, A. Ianoul, J. Devy, I. Kudelina, O. Duval, A. J. P. Alix, J. C. Jardillier, I. Nabiev, *J. Biol. Chem.* **2000**, *275*, 3501 – 3509.
[32] Y.-C. Chang, P.-W. Hsieh, F.-R. Chang, R.-R. Wu, C.-C. Liaw, K.-H. Lee, Y.-C. Wu, *Planta Med.* **2003**, *69*, 148 – 152.
[33] A. Šedo, K. Vlašicová, P. Barták, R. Vespalec, J. Vičar, V. Šimánek, J. Ulrichová, *Phytother. Res.* **2002**, *16*, 84 – 87.
[34] L. K. Wang, R. K. Johnson, S. M. Hecht, *Chem. Res. Toxicol.* **1993**, *6*, 813 – 818.
[35] A. K. Larsen, L. Grondard, J. Couprie, B. Desoize, L. Comoe, J.-C. Jardillier, J.-F. Riou, *Biochem. Pharmacol.* **1993**, *46*, 1403 – 1412.
[36] J. M. Pezzuto, S. K. Antosiak, W. M. Messmer, M. B. Slaytor, G. R. Honig, *Chem.-Biol. Interact.* **1983**, *43*, 323 – 339.
[37] a) B. Clement, M. Weide, U. Wolschendorf, I. Kock, *Angew. Chem. Int. Ed.* **2005**, *44*, 635 – 638; *Angew. Chem.* **2005**, *117*, 641 – 645 and references therein; b) B. Clement, U. Girreser, T. N. Steinhauer, C. Meier, D. Marko, G. Aichinger, I. Kaltefleiter, L. Stenzel, D. Heber, M. Weide, U. Wolschendorf, I. Zebothsen, D. zur Nieden, *ChemMedChem* **2016**, *11*, 2155 – 2170.
[38] I. Kock, D. Heber, M. Weide, U. Wolschendorf, B. Clement, *J. Med. Chem.* **2005**, *48*, 2772 – 2777 and references therein.
[39] C. Meier, J. Kotthaus, L. Stenzel, U. Girreser, D. Heber, B. Clement, *Tetrahedron* **2012**, *68*, 9105 – 9112 and references therein.
[40] C. Meier, P. Sömmer, U. Girreser, B. Clement, *Synthesis* **2013**, *45*, 893 – 895 and references therein.
[41] T. N. Steinhauer, U. Girreser, C. Meier, M. Cushman, B. Clement, *Chem. Eur. J.* **2016**, *22*, 8301 – 8308.
[42] T. N. Steinhauer, D. S. Längle, C. Meier, U. Girreser, L. Stenzel, D. Heber, B. Clement, *Chem. Eur. J.* **2015**, *21*, 6668 – 6672.
[43] R. Beugelmans, J. Chastanet, H. Ginsburg, L. Quintero-Cortes, G. Roussi, *J. Org. Chem.* **1985**, *50*, 4933 – 4938.
[44] E. Kiselev, S. DeGuire, A. Morrell, K. Agama, T. S. Dexheimer, Y. Pommier, M. Cushman, *J. Med. Chem.* **2011**, *54*, 6106 – 6116.
[45] National Cancer Institute, *NCI-60 Growth Inhibition Data*, September 2014 Release, GI_{50} Data: https://dtp.cancer.gov/dtpstandard/dwindex/index.jsp (accessed February 7, 2017).
[46] M. Nagarajan, A. Morrell, B. C. Fort, M. R. Meckley, S. Antony, G. Kohlhagen, Y. Pommier, M. Cushman, *J. Med. Chem.* **2004**, *47*, 5651 – 5661 and references therein.
[47] C. Dive, C. D. Gregory, D. J. Phipps, D. L. Evans, A. E. Milner, A. H. Wyllie, *Biochem. Biophys. Acta Mol. Cell Res.* **1992**, *1133*, 275 – 285 and references therein.
[48] C. Soldani, A. I. Scovassi, *Apoptosis* **2002**, *7*, 321 – 328 and references therein.
[49] E. Ward, C. DeSantis, A. Robbins, B. Kohler, A. Jemal, *Ca-Cancer J. Clin.* **2014**, *64*, 83 – 103.
[50] I. Nicoletti, G. Migliorati, M. C. Pagliacci, F. Grignani, C. Riccardi, *J. Immunol. Methods* **1991**, *139*, 271 – 279.
[51] C. Riccardi, I. Nicoletti, *Nat. Protoc.* **2006**, *1*, 1458 – 1461.
[52] B. Clifford, M. Beljin, G. R. Stark, W. R. Taylor, *Cancer Res.* **2003**, *63*, 4074 – 4081.
[53] T. T. Paull, E. P. Rogakou, V. Yamazaki, C. U. Kirchgessner, M. Gellert, W. M. Bonner, *Curr. Biol.* **2000**, *10*, 886 – 895.
[54] J. Eirich, S. Braig, L. Schyschka, P. Servatius, J. Hoffmann, S. Hecht, S. Fulda, S. Zahler, I. Antes, U. Kazmaier, S. A. Sieber, A. M. Vollmar, *Angew. Chem. Int. Ed.* **2014**, *53*, 12960 – 12965; *Angew. Chem.* **2014**, *126*, 13174 – 13179.
[55] C. A. Lipinski, F. Lombardo, B. W. Dominy, P. J. Feeney, *Adv. Drug Delivery Rev.* **1997**, *23*, 3 – 25.
[56] C. L. Bregman, R. A. Buroker, R. S. Hirth, A. R. Crosswell, S. K. Durham, *Toxicol. Pathol.* **1994**, *22*, 528 – 535.
[57] C. Peters, S. Brown, *Biosci. Rep.* **2015**, *35*, e00225.

Manuscript received: January 12, 2017
Accepted Article published: January 18, 2017
Final Article published: February 8, 2017

7 References

1. US National Cancer Institute. What You Need To Know About Leukemia. 2013; **13-3775**(https://www.cancer.gov/).

2. Leukemia and lymphoma society. Facts spring 2014. 2014; (https://www.lls.org/).

3. Ward E, DeSantis C, Robbins A, Kohler B, Jemal A. Childhood and adolescent cancer statistics, 2014. *CA: a cancer journal for clinicians* 2014; **64**(2)**:** 83-103.

4. Howlader N, Noone A, Krapcho M, Miller D, Bishop K, Altekruse S*, et al.* SEER cancer statistics review, 1975–2013. *Bethesda, MD: National Cancer Institute* Updated September 12, 2016; (https://seer.cancer.gov/csr/1975_2013/).

5. Pui C-H, Robison LL, Look AT. Acute lymphoblastic leukaemia. *The Lancet* 2008; **371**(9617)**:** 1030-1043.

6. Weng AP, Ferrando AA, Lee W, Morris JP, Silverman LB, Sanchez-Irizarry C*, et al.* Activating mutations of NOTCH1 in human T cell acute lymphoblastic leukemia. *Science* 2004; **306**(5694)**:** 269-271.

7. Hong D, Gupta R, Ancliff P, Atzberger A, Brown J, Soneji S*, et al.* Initiating and cancer-propagating cells in TEL-AML1-associated childhood leukemia. *Science* 2008; **319**(5861)**:** 336-339.

8. Döhner H, Weisdorf DJ, Bloomfield CD. Acute myeloid leukemia. *New England Journal of Medicine* 2015; **373**(12)**:** 1136-1152.

9. Zwaan CM, Kolb EA, Reinhardt D, Abrahamsson J, Adachi S, Aplenc R*, et al.* Collaborative efforts driving progress in pediatric acute myeloid leukemia. *Journal of Clinical Oncology* 2015; **33**(27)**:** 2949-2962.

10. Frei E, Holland JF, Schneiderman MA, Pinkel D, SELKIRK G, FREIREICH EJ*, et al.* A comparative study of two regimens of combination chemotherapy in acute leukemia. *Blood* 1958; **13**(12)**:** 1126-1148.

11. Pui C-H, Evans WE. Treatment of acute lymphoblastic leukemia. *New England Journal of Medicine* 2006; **354**(2)**:** 166-178.

12. Hoelzer D, Bassan R, Dombret H, Fielding A, Ribera J, Buske C. Acute lymphoblastic leukaemia in adult patients: ESMO Clinical Practice Guidelines for diagnosis, treatment and follow-up. *Annals of Oncology* 2016; **27**(suppl 5)**:** v69-v82.

13. Clinical trial number NCT00651261. Daunorubicin, Cytarabine, and Midostaurin in Treating Patients With Newly Diagnosed Acute Myeloid Luekemia. Access March 22, 2017; (https://www.clinicaltrials.gov/).

14. Stone RM, Mandrekar S, Sanford BL, Geyer S, Bloomfield CD, Dohner K*, et al.* The multi-kinase inhibitor midostaurin (M) prolongs survival compared with placebo (P) in combination

with daunorubicin (D)/cytarabine (C) induction (ind), high-dose c consolidation (consol), and as maintenance (maint) Therapy in Newly Diagnosed Acute Myeloid Leukemia (AML) Patients (pts) Age 18-60 with FLT3 Mutations (muts): an international prospective randomized (rand) P-controlled double-blind trial (CALGB 10603/RATIFY [Alliance]). *Blood* 2015; **126**(23)**:** 6-6.

15. Döhner H, Estey E, Grimwade D, Amadori S, Appelbaum FR, Büchner T*, et al.* Diagnosis and management of AML in adults: 2017 ELN recommendations from an international expert panel. *Blood* 2016**:** blood-2016-2008-733196.

16. Kavallaris M. Microtubules and resistance to tubulin-binding agents. *Nature Reviews Cancer* 2010; **10**(3)**:** 194-204.

17. Nitiss JL. Targeting DNA topoisomerase II in cancer chemotherapy. *Nature Reviews Cancer* 2009; **9**(5)**:** 338-350.

18. Kadia T, Ravandi F, Cortes J, Kantarjian H. New drugs in acute myeloid leukemia. *Annals of Oncology* 2016; **27**(5)**:** 770-778.

19. Erba HP. Finding the optimal combination therapy for the treatment of newly diagnosed AML in older patients unfit for intensive therapy. *Leukemia research* 2015; **39**(2)**:** 183-191.

20. Luo B, Lee AS. The critical roles of endoplasmic reticulum chaperones and unfolded protein response in tumorigenesis and anticancer therapies. *Oncogene* 2013; **32**(7)**:** 805-818.

21. Tameire F, Verginadis II, Koumenis C. Cell intrinsic and extrinsic activators of the unfolded protein response in cancer: Mechanisms and targets for therapy. *Seminars in Cancer Biology* 2015; **33:** 3-15.

22. Hetz C, Chevet E, Harding HP. Targeting the unfolded protein response in disease. *Nature reviews Drug discovery* 2013; **12**(9)**:** 703-719.

23. Wang M, Kaufman RJ. The impact of the endoplasmic reticulum protein-folding environment on cancer development. *Nat Rev Cancer* 2014; **14**(9)**:** 581-597.

24. Shore GC, Papa FR, Oakes SA. Signaling cell death from the endoplasmic reticulum stress response. *Current opinion in cell biology* 2011; **23**(2)**:** 143-149.

25. Grimm S. The ER–mitochondria interface: The social network of cell death. *Biochimica et Biophysica Acta (BBA) - Molecular Cell Research* 2012; **1823**(2)**:** 327-334.

26. Eletto D, Chevet E, Argon Y, Appenzeller-Herzog C. Redox controls UPR to control redox. *Journal of cell science* 2014; **127**(17)**:** 3649-3658.

27. Bhat TA, Chaudhary AK, Kumar S, O'Malley J, Inigo JR, Kumar R*, et al.* Endoplasmic reticulum-mediated unfolded protein response and mitochondrial apoptosis in cancer. *Biochimica et Biophysica Acta (BBA)-Reviews on Cancer* 2016.

28. Wang B, Heath-Engel H, Zhang D, Nguyen N, Thomas DY, Hanrahan JW*, et al.* BAP31 interacts with Sec61 translocons and promotes retrotranslocation of CFTRΔF508 via the derlin-1 complex. *Cell* 2008; **133**(6)**:** 1080-1092.

29. Iwasawa R, Mahul-Mellier AL, Datler C, Pazarentzos E, Grimm S. Fis1 and Bap31 bridge the mitochondria–ER interface to establish a platform for apoptosis induction. *The EMBO journal* 2011; **30**(3)**:** 556-568.

30. Ng FW, Nguyen M, Kwan T, Branton PE, Nicholson DW, Cromlish JA*, et al.* p28 Bap31, a Bcl-2/Bcl-XL-and procaspase-8–associated protein in the endoplasmic reticulum. *The Journal of cell biology* 1997; **139**(2)**:** 327-338.

31. Breckenridge DG, Stojanovic M, Marcellus RC, Shore GC. Caspase cleavage product of BAP31 induces mitochondrial fission through endoplasmic reticulum calcium signals, enhancing cytochrome c release to the cytosol. *The Journal of cell biology* 2003; **160**(7)**:** 1115-1127.

32. Namba T, Tian F, Chu K, Hwang S-Y, Yoon KW, Byun S*, et al.* CDIP1-BAP31 complex transduces apoptotic signals from endoplasmic reticulum to mitochondria under endoplasmic reticulum stress. *Cell reports* 2013; **5**(2)**:** 331-339.

33. Rosati E, Sabatini R, Rampino G, De Falco F, Di Ianni M, Falzetti F*, et al.* Novel targets for endoplasmic reticulum stress-induced apoptosis in B-CLL. *Blood* 2010; **116**(15)**:** 2713-2723.

34. Ri M. Endoplasmic-reticulum stress pathway-associated mechanisms of action of proteasome inhibitors in multiple myeloma. *International journal of hematology* 2016; **104**(3)**:** 273-280.

35. Bertaina A, Vinti L, Strocchio L, Gaspari S, Caruso R, Algeri M*, et al.* The combination of bortezomib with chemotherapy to treat relapsed/refractory acute lymphoblastic leukaemia of childhood. *British Journal of Haematology* 2017; **176**(4)**:** 629-636.

36. Jhaveri K, Taldone T, Modi S, Chiosis G. Advances in the clinical development of heat shock protein 90 (Hsp90) inhibitors in cancers. *Biochimica et Biophysica Acta (BBA)-Molecular Cell Research* 2012; **1823**(3)**:** 742-755.

37. Lazenby M, Hills R, Burnett A, Zabkiewicz J. The HSP90 inhibitor ganetespib: A potential effective agent for Acute Myeloid Leukemia in combination with cytarabine. *Leukemia research* 2015; **39**(6)**:** 617-624.

38. Atkins C, Liu Q, Minthorn E, Zhang S-Y, Figueroa DJ, Moss K*, et al.* Characterization of a novel PERK kinase inhibitor with antitumor and antiangiogenic activity. *Cancer Research* 2013; **73**(6)**:** 1993-2002.

39. Tang C-HA, Ranatunga S, Kriss CL, Cubitt CL, Tao J, Pinilla-Ibarz JA*, et al.* Inhibition of ER stress–associated IRE-1/XBP-1 pathway reduces leukemic cell survival. *The Journal of clinical investigation* 2014; **124**(6)**:** 2585-2598.

40. Galligan JJ, Petersen DR. The human protein disulfide isomerase gene family. *Hum Genomics* 2012; **6**(Copyright (C) 2014 U.S. National Library of Medicine.)**:** 6.

41. Wang L, Wang X, Wang C-c. Protein disulfide–isomerase, a folding catalyst and a redox-regulated chaperone. *Free Radical Biology and Medicine* 2015; **83:** 305-313.

42. Xu S, Sankar S, Neamati N. Protein disulfide isomerase: a promising target for cancer therapy. *Drug Discovery Today* 2014; **19**(3)**:** 222-240.

43. Beesley AH, Firth MJ, Anderson D, Samuels AL, Ford J, Kees UR. Drug–Gene Modeling in Pediatric T-Cell Acute Lymphoblastic Leukemia Highlights Importance of 6-Mercaptopurine for Outcome. *Cancer Research* 2013; **73**(9)**:** 2749-2759.

44. Higa A, Taouji S, Lhomond S, Jensen D, Fernandez-Zapico ME, Simpson JC*, et al.* Endoplasmic Reticulum Stress-Activated Transcription Factor ATF6α Requires the Disulfide Isomerase PDIA5 To Modulate Chemoresistance. *Molecular and Cellular Biology* 2014 May 15, 2014; **34**(10)**:** 1839-1849.

45. Trivedi R, Müller G, Rathore M, Mishra D, Dihazi H. Anti-Leukemic Activity of Shikonin: Role of ERP57 in Shikonin Induced Apoptosis in Acute Myeloid Leukemia. *Cellular Physiology and Biochemistry* 2016; **39**(2)**:** 604-616.

46. Haefliger S, Klebig C, Schaubitzer K, Schardt J, Timchenko N, Mueller BU*, et al.* Protein disulfide isomerase blocks CEBPA translation and is up-regulated during the unfolded protein response in AML. *Blood* 2011 June 2, 2011; **117**(22)**:** 5931-5940.

47. Xu S, Butkevich AN, Yamada R, Zhou Y, Debnath B, Duncan R*, et al.* Discovery of an orally active small-molecule irreversible inhibitor of protein disulfide isomerase for ovarian cancer treatment. *Proceedings of the National Academy of Sciences* 2012 October 2, 2012; **109**(40)**:** 16348-16353.

48. Vatolin S, Phillips JG, Jha BK, Govindgari S, Hu J, Grabowski D*, et al.* Novel Protein Disulfide Isomerase Inhibitor with Anticancer Activity in Multiple Myeloma. *Cancer Research* 2016; **76**(11)**:** 3340-3350.

49. Eirich J, Braig S, Schyschka L, Servatius P, Hoffmann J, Hecht S*, et al.* A small molecule inhibits protein disulfide isomerase and triggers the chemosensitization of cancer cells. *Angewandte Chemie International Edition* 2014; **53**(47)**:** 12960-12965.

50. Jia J, Zhu F, Ma X, Cao ZW, Li YX, Chen YZ. Mechanisms of drug combinations: interaction and network perspectives. *Nature reviews Drug discovery* 2009; **8**(2)**:** 111-128.

51. Walczak H, Bouchon A, Stahl H, Krammer PH. Tumor necrosis factor-related apoptosis-inducing ligand retains its apoptosis-inducing capacity on Bcl-2-or Bcl-xL-overexpressing chemotherapy-resistant tumor cells. *Cancer Research* 2000; **60**(11)**:** 3051-3057.

52. Juo P, Kuo CJ, Yuan J, Blenis J. Essential requirement for caspase-8/FLICE in the initiation of the Fas-induced apoptotic cascade. *Current biology* 1998; **8**(18)**:** 1001-1008.

53. Haber M, Norris MD, Kavallaris M, Bell DR, Davey RA, White L*, et al.* Atypical Multidrug Resistance in a Therapy-induced Drug-resistant Human Leukemia Cell Line (LALW-2):

Resistance to Vinca Alkaloids Independent of P-Glycoprotein. *Cancer Research* 1989 October 1, 1989; **49**(19)**:** 5281-5287.

54. Kavallaris M, Tait AS, Walsh BJ, He L, Horwitz SB, Norris MD*, et al.* Multiple Microtubule Alterations Are Associated with Vinca Alkaloid Resistance in Human Leukemia Cells. *Cancer Research* 2001 August 1, 2001; **61**(15)**:** 5803-5809.

55. Verrills NM, Walsh BJ, Cobon GS, Hains PG, Kavallaris M. Proteome Analysis of Vinca Alkaloid Response and Resistance in Acute Lymphoblastic Leukemia Reveals Novel Cytoskeletal Alterations. *Journal of Biological Chemistry* 2003 November 14, 2003; **278**(46)**:** 45082-45093.

56. Terziyska N, Alves CC, Groiss V, Schneider K, Farkasova K, Ogris M*, et al.* In Vivo Imaging Enables High Resolution Preclinical Trials on Patients' Leukemia Cells Growing in Mice. *PLoS ONE* 2012; **7**(12)**:** e52798.

57. Vick B, Rothenberg M, Sandhöfer N, Carlet M, Finkenzeller C, Krupka C*, et al.* An advanced preclinical mouse model for acute myeloid leukemia using patients' cells of various genetic subgroups and in vivo bioluminescence imaging. *PLoS ONE* 2015; **10**(3)**:** e0120925.

58. Ou W, Silver J. Role of protein disulfide isomerase and other thiol-reactive proteins in HIV-1 envelope protein-mediated fusion. *Virology* 2006; **350**(2)**:** 406-417.

59. Nicoletti I, Migliorati G, Pagliacci M, Grignani F, Riccardi C. A rapid and simple method for measuring thymocyte apoptosis by propidium iodide staining and flow cytometry. *Journal of immunological methods* 1991; **139**(2)**:** 271-279.

60. Riccardi C, Nicoletti I. Analysis of apoptosis by propidium iodide staining and flow cytometry. *Nature protocols* 2006; **1**(3)**:** 1458-1461.

61. Ehrhardt H, Schrembs D, Moritz C, Wachter F, Haldar S, Graubner U*, et al.* Optimized anti–tumor effects of anthracyclines plus Vinca alkaloids using a novel, mechanism-based application schedule. *Blood* 2011; **118**(23)**:** 6123-6131.

62. Lock JT, Parker I, Smith IF. A comparison of fluorescent Ca 2+ indicators for imaging local Ca 2+ signals in cultured cells. *Cell calcium* 2015; **58**(6)**:** 638-648.

63. Cottet-Rousselle C, Ronot X, Leverve X, Mayol JF. Cytometric assessment of mitochondria using fluorescent probes. *Cytometry Part A* 2011; **79**(6)**:** 405-425.

64. Chen X, Zhong Z, Xu Z, Chen L, Wang Y. 2', 7'-Dichlorodihydrofluorescein as a fluorescent probe for reactive oxygen species measurement: forty years of application and controversy. *Free radical research* 2010; **44**(6)**:** 587-604.

65. Mosmann T. Rapid colorimetric assay for cellular growth and survival: application to proliferation and cytotoxicity assays. *Journal of immunological methods* 1983; **65**(1-2)**:** 55-63.

66. Smith PK, Krohn RI, Hermanson G, Mallia A, Gartner F, Provenzano M*, et al.* Measurement of protein using bicinchoninic acid. *Analytical biochemistry* 1985; **150**(1)**:** 76-85.

67. Ladner CL, Yang J, Turner RJ, Edwards RA. Visible fluorescent detection of proteins in polyacrylamide gels without staining. *Analytical biochemistry* 2004; **326**(1)**:** 13-20.

68. Vomacka J, Korotkov VS, Bauer B, Weinandy F, Kunzmann MH, Krysiak J*, et al.* An Aromatic Hydroxyamide Attenuates Multiresistant Staphylococcus aureus Toxin Expression. *Chemistry–A European Journal* 2016; **22**(5)**:** 1622-1630.

69. Szklarczyk D, Franceschini A, Wyder S, Forslund K, Heller D, Huerta-Cepas J*, et al.* STRING v10: protein–protein interaction networks, integrated over the tree of life. *Nucleic acids research* 2014**:** gku1003.

70. Consortium GO. Gene ontology consortium: going forward. *Nucleic acids research* 2015; **43**(D1)**:** D1049-D1056.

71. Tufo G, Jones A, Wang Z, Hamelin J, Tajeddine N, Esposti D*, et al.* The protein disulfide isomerases PDIA4 and PDIA6 mediate resistance to cisplatin-induced cell death in lung adenocarcinoma. *Cell Death & Differentiation* 2014.

72. Kaufmann SH, Earnshaw WC. Induction of apoptosis by cancer chemotherapy. *Experimental cell research* 2000; **256**(1)**:** 42-49.

73. Karpinich NO, Tafani M, Rothman RJ, Russo MA, Farber JL. The course of etoposide-induced apoptosis from damage to DNA and p53 activation to mitochondrial release of cytochromec. *Journal of Biological Chemistry* 2002; **277**(19)**:** 16547-16552.

74. Rovini A, Savry A, Braguer D, Carré M. Microtubule-targeted agents: when mitochondria become essential to chemotherapy. *Biochimica et Biophysica Acta (BBA)-Bioenergetics* 2011; **1807**(6)**:** 679-688.

75. Wang B, Nguyen M, Chang NC, Shore GC. Fis1, Bap31 and the kiss of death between mitochondria and endoplasmic reticulum. *The EMBO Journal* 2011; **30**(3)**:** 451-452.

76. Rizzuto R, De Stefani D, Raffaello A, Mammucari C. Mitochondria as sensors and regulators of calcium signalling. *Nature reviews Molecular cell biology* 2012; **13**(9)**:** 566-578.

77. Tait SW, Green DR. Mitochondria and cell death: outer membrane permeabilization and beyond. *Nature reviews Molecular cell biology* 2010; **11**(9)**:** 621-632.

78. Yadav N, Kumar S, Marlowe T, Chaudhary A, Kumar R, Wang J*, et al.* Oxidative phosphorylation-dependent regulation of cancer cell apoptosis in response to anticancer agents. *Cell death & disease* 2015; **6**(11)**:** e1969.

79. Ulrich M. Murine tumor models for the in vivo evaluation of natural compounds and their derivatives as new cancer therapeutics. lmu, 2016.

80. Chonghaile TN, Sarosiek KA, Vo T-T, Ryan JA, Tammareddi A, Moore VDG*, et al.* Pretreatment mitochondrial priming correlates with clinical response to cytotoxic chemotherapy. *Science* 2011; **334**(6059)**:** 1129-1133.

81. Sarosiek KA, Chonghaile TN, Letai A. Mitochondria: gatekeepers of response to chemotherapy. *Trends in cell biology* 2013; **23**(12)**:** 612-619.

82. Vo T-T, Ryan J, Carrasco R, Neuberg D, Rossi DJ, Stone RM*, et al.* Relative mitochondrial priming of myeloblasts and normal HSCs determines chemotherapeutic success in AML. *Cell* 2012; **151**(2)**:** 344-355.

83. Hashida T, Kotake Y, Ohta S. Protein disulfide isomerase knockdown-induced cell death is cell-line-dependent and involves apoptosis in MCF-7 cells. *The Journal of Toxicological Sciences* 2011; **36**(1)**:** 1-7.

84. Sun S, Lee D, Ho ASW, Pu JKS, Zhang XQ, Lee NP*, et al.* Inhibition of prolyl 4-hydroxylase, beta polypeptide (P4HB) attenuates temozolomide resistance in malignant glioma via the endoplasmic reticulum stress response (ERSR) pathways. *Neuro-Oncology (Cary, NC, U S)* 2013; **15**(Copyright (C) 2014 American Chemical Society (ACS). All Rights Reserved.)**:** 562-577.

85. Lovat PE, Corazzari M, Armstrong JL, Martin S, Pagliarini V, Hill D*, et al.* Increasing Melanoma Cell Death Using Inhibitors of Protein Disulfide Isomerases to Abrogate Survival Responses to Endoplasmic Reticulum Stress. *Cancer Research* 2008 July 1, 2008; **68**(13)**:** 5363-5369.

86. Eletto D, Eletto D, Dersh D, Gidalevitz T, Argon Y. Protein Disulfide Isomerase A6 Controls the Decay of IRE1α Signaling via Disulfide-Dependent Association. *Molecular Cell* 2014; **53**(4)**:** 562-576.

87. Barabási A-L, Gulbahce N, Loscalzo J. Network medicine: a network-based approach to human disease. *Nature Reviews Genetics* 2011; **12**(1)**:** 56-68.

88. Hopkins AL. Network pharmacology: the next paradigm in drug discovery. *Nature chemical biology* 2008; **4**(11)**:** 682-690.

89. Zimmermann GR, Lehar J, Keith CT. Multi-target therapeutics: when the whole is greater than the sum of the parts. *Drug discovery today* 2007; **12**(1)**:** 34-42.

90. Reed JC, Doctor KS, Godzik A. The domains of apoptosis: a genomics perspective. *Sci STkE* 2004; **239:** re9.

91. Lorkova L, Scigelova M, Arrey TN, Vit O, Pospisilova J, Doktorova E*, et al.* Detailed functional and proteomic characterization of fludarabine resistance in mantle cell lymphoma cells. *PLoS ONE* 2015; **10**(8)**:** e0135314.

92. Soriano G, Besse L, Li N, Kraus M, Besse A, Meeuwenoord N*, et al.* Proteasome inhibitor-adapted myeloma cells are largely independent from proteasome activity and show complex proteomic changes, in particular in redox and energy metabolism. *Leukemia* 2016; **30**(11)**:** 2198-2207.

93. Quistgaard EM, Löw C, Moberg P, Guettou F, Maddi K, Nordlund P. Structural and Biophysical Characterization of the Cytoplasmic Domains of Human BAP29 and BAP31. *PLoS ONE* 2013; **8**(8)**:** e71111.

94. Chatr-aryamontri A, Oughtred R, Boucher L, Rust J, Chang C, Kolas NK*, et al.* The BioGRID interaction database: 2017 update. *Nucleic acids research* 2016**:** gkw1102.

95. Keilhauer EC, Hein MY, Mann M. Accurate protein complex retrieval by affinity enrichment mass spectrometry (AE-MS) rather than affinity purification mass spectrometry (AP-MS). *Molecular & Cellular Proteomics* 2015; **14**(1)**:** 120-135.

96. Konopleva M, Pollyea DA, Potluri J, Chyla BJ, Busman T, McKeegan E*, et al.* A phase 2 study of ABT-199 (GDC-0199) in patients with acute myelogenous leukemia (AML). *Blood* 2014; **124**(21)**:** 118-118.

97. Röttgermann PJ, Dawson KA, Rädler JO. Time-Resolved Study of Nanoparticle Induced Apoptosis Using Microfabricated Single Cell Arrays. *Microarrays* 2016; **5**(2)**:** 8.

98. Schummer D, Höfle G, Forche E, Reichenbach H, Wray V, Domke T. Antibiotics from Gliding Bacteria, LXXVI. Vioprolides: New Antifungal and Cytotoxic Peptolides from Cystobacter violaceus. *Liebigs Annalen* 1996; **1996**(6)**:** 971-978.

99. Afonso-Grunz F, Hoffmeier K, Müller S, Westermann AJ, Rotter B, Vogel J*, et al.* Dual 3'Seq using deepSuperSAGE uncovers transcriptomes of interacting Salmonella enterica Typhimurium and human host cells. *BMC genomics* 2015; **16**(1)**:** 323.

100. Sass S, Buettner F, Mueller NS, Theis FJ. RAMONA: a Web application for gene set analysis on multilevel omics data. *Bioinformatics* 2014**:** btu610.

101. Horton JD, Goldstein JL, Brown MS. SREBPs: activators of the complete program of cholesterol and fatty acid synthesis in the liver. *The Journal of clinical investigation* 2002; **109**(9)**:** 1125-1131.

102. Banker DE, Mayer SJ, Li HY, Willman CL, Appelbaum FR, Zager RA. Cholesterol synthesis and import contribute to protective cholesterol increments in acute myeloid leukemia cells. *Blood* 2004; **104**(6)**:** 1816-1824.

103. Kornblau SM, Banker DE, Stirewalt D, Shen D, Lemker E, Verstovsek S*, et al.* Blockade of adaptive defensive changes in cholesterol uptake and synthesis in AML by the addition of pravastatin to idarubicin+ high-dose Ara-C: a phase 1 study. *Blood* 2007; **109**(7)**:** 2999-3006.

104. Bartel K, Winzi M, Ulrich M, Koeberle A, Menche D, Werz O*, et al.* V-ATPase inhibition increases cancer cell stiffness and blocks membrane related Ras signaling-a new option for HCC therapy. *Oncotarget* 2016; **5**.

105. Meier C, Steinhauer TN, Koczian F, Plitzko B, Jarolim K, Girreser U*, et al.* A Dual Topoisomerase Inhibitor of Intense Pro-Apoptotic and Antileukemic Nature for Cancer Treatment. *ChemMedChem* 2017; **12**(5)**:** 347-352.

8 Appendix

8.1 Abbreviations

ΔΨm	Mitochondrial membrane potential
ABPP	Activity-based protein profiling
ALL	Acute lymphoblastic leukemia
AML	Acute myeloid leukemia
AML1 = RUNX1	Runt-related transcription factor 1
Ara-C	Cytosine arabinoside, Cytarabine
BAP31	B-cell receptor-associated protein 31
BCA	Bicinchoninic acid
bp	Base pair
BSA	Bovine serum albumin
BSS	Balanced salt solution
CASP3	Caspase-3
CASP8	Caspase-8
CFU	Colony forming unit
CHOP	C/EBP-homologous protein
CTB	CellTiter Blue
Ctrl	Control
Cyt c	Cytochrome c
DHCR24	Delta(24)-sterol reductase
DMSO	Dimethyl sulfoxide
DNA	Deoxyribonucleic acid
DNR	Daunorubicin
EC_{50}	Half maximal effective concentration
ECL	Enhanced Chemiluminescence
Em	Emission
ER	Endoplasmic reticulum
ETO	Etoposide
Ex	Excitation
FACS	Fluorescence activated cell sorting
FDFT1	Squalene synthase
FLT3	Receptor-type tyrosine-protein kinase FLT3

GGPS1	Geranylgeranyl pyrophosphate synthase
GO	Gene Ontology
HMGCR	3-hydroxy-3-methylglutaryl-coenzyme A reductase
HMGCS1	Hydroxymethylglutaryl-CoA synthase
IC_{50}	Half maximal inhibitory concentration
INSIG1	Insulin-induced gene 1 protein
i. p.	Intraperitoneal
IRE1α	Inositol-requiring enzyme 1
KEGG	Kyoto Encyclopedia of Genes and Genomes
LSS	Lanosterol synthase
MACE	Massive analysis of cDNA ends
MC	Methylcellulose
MOMP	Mitochondrial outer membrane permeabilization
MPTP	Mitochondrial permeability transition pore
mRNA	Messenger ribonucleic acid
MSMO1	Methylsterol monooxygenase 1
MVD	Diphosphomevalonate decarboxylase
NGS	Next-generation sequencing
NOTCH1	Neurogenic locus notch homolog protein 1
NPM1	Nucleophosmin
NSG	NOD (Non-obese diabetic) scid gamma
PARP	Poly ADP ribose polymerase
PBMC	Peripheral blood mononuclear cell
PBS	Phosphate buffered saline
PDI	Protein disulfide isomerase
PDX	Patient derived xenograft
PE	Phycoerythrin
PERK	Protein kinase R (PKR)-like endoplasmic reticulum kinase
PI	Propidium iodide
qPCR	Quantitative polymerase chain reaction
RAMONA	Remotely Accessible Multilevel ONtology Analysis
ROS	Reactive oxygen species
RT	Room temperature
SCID	Severe combined immunodeficiency

SEM	Standard error of the mean
SQLE	Squalene monooxygenase
SREBF2	Sterol regulatory element binding transcription factor 2
STRING	Search Tool for the Retrieval of Interacting Genes/Proteins
TEL = ETV6	Transcription factor ETV6
UPR	Unfolded protein response
VCR	Vincristine
VCR-R	Vincristine resistant
VDAC	Voltage-dependent anion channel
VioA	Vioprolide A
VioD	Vioprolide D

8.2 Raw Data: ABPP Proteomics and MACE Transcriptomics

Raw data of ABPP and MACE screenings accompany this dissertation on the appended CD-ROM and the electronic thesis website of the LMU Munich:
https://edoc.ub.uni-muenchen.de

8.3 List of Publications and Conference Contributions

8.3.1 Articles

Targeting the ER-Mitochondrial Interface of Cell Death Sensitizes Leukemia Cells Towards Cytostatics
Koczian F, Vomacka A, Vick B, Hettich B, Kazmaier U, Sieber SA, Jeremias I, Vollmar AM, Braig S
In preparation

A Dual Topoisomerase Inhibitor of Intense Pro-Apoptotic and Antileukemic Nature for Cancer Treatment
Meier C, Steinhauer TN, Koczian F, Plitzko B, Jarolim K, Girreser U, Braig S, Marko D, Vollmar AM, Clement B. ChemMedChem. 2017 Mar 7; 12(5):347-352.

8.3.2 Scientific talks

7th FOR 1406 Meeting, July 5-6, 2016, Munich, Germany
Transcriptome Analysis of Vioprolide A Treated Leukemia Cells
Bischoff F, Besl C, Bischoff I, Braig S, Müller R, Fürst R, Vollmar AM

6th FOR 1406 Meeting, July 1-2, 2015, Saarbrücken, Germany
Antileukemic Effects of the Natural Compound Vioprolide A
Bischoff F, Braig S, Müller R, Vollmar AM

Interact 8th Munich Life Science Symposium., March 4-5, 2015, Munich, Germany
Chemosensitizing Effects of the Novel Compound PS89 on Leukemic Cells
Bischoff F, Braig S, Jeremias I, Kazmaier U, Vollmar AM

8.3.3 Poster presentations

ISAL XVI Acute Leukemias Symposium, February 19-22, 2017, Munich, Germany
Targeting the ER-Mitochondrial Interface of Cell Death Sensitizes Leukemia Cells Towards Cytostatics
Koczian F, Vomacka A, Vick B, Hettich B, Kazmaier U, Sieber SA, Jeremias I, Vollmar AM, Braig S

58th ASH Annual Meeting, December 3-6, 2016, San Diego, USA
Targeting the ER-Mitochondrial Interface of Cell Death Sensitizes Leukemia Cells Towards Cytostatics
Koczian F, Vomacka A, Vick B, Hettich B, Kazmaier U, Sieber SA, Jeremias I, Vollmar AM, Braig S

8.3.4 Awards

ASH Abstract Achievement Award for: Targeting the ER-Mitochondrial Interface of Cell Death Sensitizes Leukemia Cells Towards Cytostatics at the 58th ASH Annual Meeting, December 3-6, 2016, San Diego, USA

8.4 Acknowledgments

Mein herzlichster Dank geht an Frau Prof. Dr. Angelika Vollmar. Sie haben einen großartigen Rahmen geschaffen, um diese Arbeit in jeder Phase motiviert anzupacken. Das haben Sie nicht nur durch ein sehr gutes Gleichgewicht aus dem viel zitierten Fordern und Fördern erreicht, sondern auch durch Ihre bemerkenswert und ansteckend positive Art den Herausforderungen unserer Arbeit täglich zu begegnen.

Ein ganz besonderes Dankeschön gilt Dr. Simone Braig für die hervorragende Betreuung, den wissenschaftlichen Input und die vielen konstruktiven Diskussionen über die gesamte Arbeit hinweg. Vor allem aber bin ich dankbar, dass ich nicht nur fachlich, sondern auch auf einer so guten persönlichen Ebene mit Dir zusammen arbeiten durfte.

Ebenfalls möchte ich der Prüfungskommission danken, zuvorderst Prof. Dr. Irmela Jeremias für die Bereitschaft das Zweitgutachten für diese Dissertation anzufertigen, sowie Prof. Dr. Johanna Pachmayr, Prof. Dr. Wolfgang Frieß, Prof. Dr. Stefan Zahler und Prof. Dr. Gerhard Winter.

Für die finanziellen Mittel, die uns für das PS89 sowie das Vioprolid Projekt zur Verfügung gestellt wurden, gilt mein Dank der Dr. Robert Pfleger Stiftung und der DFG Forschergruppe 1406.

Zudem möchte ich mich für die produktive Zusammenarbeit im Rahmen unserer Kooperationen bedanken - bei Dr. Jan Vomacka für die PS89 Target ID, bei Dr. Binje Vick und Prof. Dr. Irmela Jeremias für die Bereitstellung der PDX Zellen und Eure eindrucksvolle Begeisterung für die Hämatologie, sowie bei Alexandra Murschhauser für die Motivation das Thema dieser Arbeit künftig weiter voran zu bringen.

Für die Möglichkeit die MACE Analyse an der Goethe-Universität Frankfurt durchzuführen gilt mein Dank Dr. Iris Bischoff sowie Prof. Dr. Robert Fürst. Zudem möchte ich Kerstin Loske und Silvia Schnegg für die Unterstützung rund um das PS89 Projekt danken. Ein besonderer Beitrag zum Erfolg dieser Arbeit wurde schließlich von

meinen Bachelor- und Masterstudenten geleistet. Daher vielen Dank an Britta Hettich, Patrick Spanner und Michaela Koburg für Eure Motivation und gute Mitarbeit.

Schließlich soll ein Höhepunkt der Promotion nicht unerwähnt bleiben, nämlich die Vorstellung des PS89 Projektes am 58th ASH Annual Meeting. Da dies ohne finanzielle Unterstützung nicht möglich gewesen wäre, geht diesbezüglich mein Dank an Prof. Dr. Angelika Vollmar, die Münchner Universitätsgesellschaft sowie die American Society of Hematology.

Dem gesamten AK Vollmar gilt an dieser Stelle noch ein ganz großes Dankeschön für den guten Austausch und Umgang miteinander, der Grundlage für die ausgesprochen gute Atmosphäre im Labor war. Insbesondere Christina, Karin, Meli, Flo und Max - ihr habt die Tage in der Uni, und auch darüber hinaus, immer mit Leben gefüllt und ich bin sehr glücklich zusammen mit Euch die letzten Jahre erlebt zu haben.

Zu guter Letzt möchte ich mich für den immer währenden Rückhalt meiner Freunde und Familie bedanken. Insbesondere meinen Eltern Andrea und Roland, ich schätze es wirklich sehr, dass Ihr mir stets die Freiheit gegeben habt meinen Weg zu gehen und diesen uneingeschränkt gefördert habt.